QC852
C6
no. 386
ARCHIVE

CHARACTERIZATION OF SILVER IODIDE–SODIUM IODIDE ICE NUCLEI USING CHEMICAL KINETIC METHODOLOGY

LIBRARIES
MAY 24 1985
COLORADO STATE UNIVERSITY

ROCHELLE R. BLUMENSTEIN

Atmospheric Science
PAPER NO.
386

US ISSN 0067-0340

DEPARTMENT OF ATMOSPHERIC SCIENCE
COLORADO STATE UNIVERSITY
FORT COLLINS, COLORADO

CHARACTERIZATION OF SILVER IODIDE-SODIUM IODIDE ICE NUCLEI USING CHEMICAL KINETIC METHODOLOGY

By

Rochelle Rose Blumenstein

This report was prepared with support provided by
National Science Foundation Grant ATM-8407543
Principal Investigator, Lewis O. Grant
and Colorado State Agricultural Experiment Station,
Hydrometeorology COL00113

Department of Atmospheric Science
Colorado State University
Fort Collins, Colorado

May 1985

Atmospheric Science Paper No. 386

ABSTRACT OF THESIS

CHARACTERIZATION OF SILVER IODIDE-SODIUM IODIDE ICE NUCLEI USING CHEMICAL KINETIC METHODOLOGY

Ice nucleation by aerosol particles generated from combustion of acetone solutions of silver iodide and sodium iodide has been characterized in the CSU Isothermal Cloud Chamber using the techniques of chemical kinetics. The mechanism of ice nucleation has been found to be primarily condensation-freezing ice nucleation. Two separate mechanisms of ice nucleation have been observed. One mechanism, identified as condensation to droplets followed by freezing, occurs at water saturation and is a characteristically slow process, with a half life on the order of 10-30 minutes. The other mechanism, identified as condensation to aqueous embryos followed by freezing, occurs at water supersaturated conditions, is characteristically fast, requiring less than a minute for completion, and results in a higher yield of ice crystals than the slow mechanism. The mechanisms are dependent on temperature and water vapor concentration, respectively, and are independent of the liquid water content of the cloud. Contact of the aerosol particles with cloud droplets has also been observed at high liquid water contents to be a mechanism of ice nucleation by silver iodide-sodium iodide aerosol particles.

The energy of activation for the slow mechanism of condensation to droplets followed by freezing, has been found to be three times the latent heat of condensation of water. This is believed to be related to the extent of hydration of the silver iodide-sodium iodide complex.

The mechanisms, rates, and yields observed in the laboratory are applied to a theoretical, physical and microphysical orographic cloud model to assess the ice nucleation characteristics of silver iodide-sodium iodide aerosol particles in the temporal and spatial scale of an orographic cloud. Three parameters have been found to control the extent and location of ice nucleation: 1) nucleation mechanism, 2) cloud temperature, and 3) wind speed. The slower mechanism of condensation to droplets followed by freezing, which occurs at slight water saturation, causes ice crystal production to be prolonged over time and space. Resulting precipitation can occur over large areas. The faster mechanism of condensation to aqueous embryos followed by freezing, which occurs in water supersaturated areas of the cloud, results in ice nucleation primarily within a zone of a few kilometers of the cloud. Precipitation would then occur in a limited area on the surface which would subsequently affect the targeting and analysis of seeding effects. Temperature influences the yield, or effectivity, and is most important for the fast mechanism. Wind speed controls the time available for nucleation. Application of laboratory determined rates and mechanisms to various cloud models can be an important tool in the development of the hypothesis, statistical design, and physical analysis of experiments and programs that utilize artificial ice nucleants for weather modification.

Rochelle Rose Blumenstein
Atmospheric Science Department
Colorado State Univeristy
Fort Collins, Colorado 80523
Spring, 1985

ACKNOWLEDGEMENTS

I would like to express my appreciation to the members of my committee, Lewis O. Grant, William G. Finnegan, Roger A. Pielke, and Branka M. Ladanyi, for their guidance in preparation of this thesis. I especially wish to express my gratitude to Dr. Finnegan for suggesting the question of effect of water supersaturation on ice nucleation as a topic for research and also for effectively teaching me about the aims of scientific research and writing. Special thanks are due to the following people: Randy Horn for technical assistance in the laboratory and many thought-provoking discussions; Cleon Swain for maintenance of equipment and assistance in testing procedures; Robert Rauber for patient explanation and guidance in the use of his model; Paul DeMott for assistance in testing and interpretation of methodology; Robert Rilling for assistance in testing; Brenda Thompson for teaching me how to use the word processor; Jan Davis for her support and guidance; Lucy McCall for dedicated drafting; and my parents for their encouragement of my goals.

This research was supported by National Science Foundation Grant No. ATM-8407543 and Colorado State Agricultural Experiment Station, Hydrometeorology Project No. COL00113.

TABLE OF CONTENTS

LIST OF TABLES

LIST OF FIGURES

I. INTRODUCTION

1.1 Background

Aerosol particles containing silver iodide have been known to effectively catalyze the phase change of water vapor and/or supercooled water to ice for about 35 years. These particles have been used in weather modification field programs to produce ice crystals in clouds in higher concentrations and at warmer temperatures than would occur naturally. Many weather modification research programs have used silver iodide ice nuclei, generated burning acetone solutions containing silver iodide for cloud seeding. Because of the insolubility of silver iodide in acetone, alkali iodides are used to solubilize the silver iodide. One such solubilizing compound that has been used is sodium iodide. The solution then contains a chemical complex containing silver iodide and sodium iodide. The aerosol particles generated from combustion of such solutions have been used in weather modification projects such as Climax (Grant, et al., 1979), the Israeli Rainfall Enhancement program (A. Gagin, personal communication), the Australian program (Smith, et al., 1966), and others.

In attempting to understand how ice nuclei which contain silver iodide behave in clouds, it is necessary to understand how the nuclei function, i.e., the mechanism of ice nucleation. This requires an understanding of the chemical and physical characteristics of the aerosol particles and how they influence the process of phase change of water to ice. The phase change process is controlled by cloud

parameters of temperature, water vapor concentration, and liquid water content as they interact with the aerosol particle prior to ice nucleation.

The methodology of chemical kinetics has been recently applied to the study of ice nucleation by silver iodide aerosol particles as the process occurs in an isothermal cloud environment (DeMott, 1982, and DeMott, et al., 1983). Chemical kinetic methodology can be used to define the physical mechanism of ice nucleation by interpreting the observed changes in rates and yields as functions of cloud parameters and aerosol composition. The temporal behavior of the processes observed is the integral element of the kinetic study. This methodology differs from past studies where the temporal characteristics of the ice nucleation process was not incorporated. Past studies have concentrated mostly on variations in effectivity (yield), particularly in the case of silver iodide-sodium iodide ice nuclei. Temporal rates of ice nucleation by silver iodide-sodium iodide aerosol particles have not been clearly determined. The effect of supersaturation with respect to liquid water on ice nucleation by these aerosol particles has not been fully explored. When encountered in experiments, the effects of supersaturations were noted. Attempts were usually made to eliminate the supersaturation rather than try to understand its effects.

1.2 Objectives

The primary goal of this study is to characterize the ice nucleating properties of silver iodide-sodium iodide aerosol particles produced by combustion of an acetone solution, using the methodology of chemical kinetics. The mechanism, temporal rate, and yield

(effectivity) of this ice nucleus is determined. The effect of water supersaturation is addressed to the extent possible.

The second goal of this study is to demonstrate how laboratory measurements of ice nucleation characteristics, ie, mechanisms, rates, and yields, can be applied to clouds that are seeded with silver iodide-sodium iodide aerosol particles. This is accomplished by incorporating laboratory data into a theoretical orographic cloud model. Past seeding hypotheses have assumed that when seeding with silver iodide-sodium iodide arosol particles, nucleation occurs instantaneously at the point of seeding and in numbers equal to the laboratory determined effectivity at that temperature (Plooster and Fukuta, 1975, Young, 1974b). Information about the rate and mechanism of an ice nucleant provides temporal and spacial resolution of the nucleation process in clouds. This should lead to better development of cloud seeding hypotheses and interpretation of results of weather modification projects.

The specific objectives of this study are to;

1) characterize ice nucleation by aerosol particles containing 2AgI-NaI using chemical kinetic methodology. This includes:
   a) determine the rates, yields (effectivity), and mechanisms of ice nucleation.
   b) determine the energy of activation of the mechanisms.
   c) demonstrate the effect of trasient supersaturation with respect to water on the nucleation process.
2) apply laboratory results of the kinetics of nucleation to a theoretical physical and microphysical orographic cloud model to assess the effectiveness of silver iodide-sodium iodide ice

nuclei as a seeding agent in winter, orographic weather modification.

1.3 Approach

The applicability of chemical kinetic methodology in the study of ice nucleation by artificial ice nuclei has been demonstrated by DeMott (1982) and DeMott, et al. (1983). By controlling reactant concentrations and temperature during the phase change process and observing shifts in temporal rate of ice nucleation with changes in cloud parameters, the mechanisms of ice nucleation can be deduced. Ice nucleation kinetics studied in the CSU isothermal cloud chamber are analogous to 'batch' reactions where temperature and cloud parameters are held constant throughout the length of the experiment. Ice nuclei aerosol particles are injected into the chamber at time zero and the decay of ice nuclei concentration with time is observed by monitoring ice crystal production rates. The total number of ice crystals produced in any experiment is used to assess the yield or effectivity. Yield is used here as a more accurate term for describing the total amount of ice nuclei which produce ice crystals in the given condition within the cloud chamber.

A series of experiments was performed where transitory water supersaturations were induced in the chamber to determine their effect on ice nucleation by AgI-NaI aerosol particles. A molar ratio of 2:1 AgI to NaI was used throughout the research program.

For the application of laboratory results of ice nucleation to cloud processes, a theoretical, two-dimensional, physical and microphysical, orographic cloud model (Rauber, 1981) was used. These clouds were 'seeded' with specific amounts of ice nuclei and the

mechanism of ice nucleation were assumed with corresponding rates and yields of ice crystal production. Nucleation was then followed spatially and temporally through the model predicted cloud. The model is also capable of predicting the location of precipitation reaching the ground as controlled by the predicted location of ice nucleation in cloud.

Application of chemical kinetic methodology to ice nucleation and the procedures for incorporating it into the theoretical orographic cloud model are presented in chapter three. Laboratory facilities, analysis and results are presented in chapters four and five. Results of the application of kinetics to the theoretical model are presented in chapter six. In the remainder of this paper, silver iodide is written in its chemical abreviation as AgI, and sodium iodide as NaI. AgI-NaI will refer to any mixture of AgI and NaI regardless of the proportions of the substances. Formulations, such as $2AgI \cdot NaI$ or $AgI \cdot NaI \cdot 4H_2O$ will refer to specific complex compounds.

II. LITERATURE REVIEW

2.1 Chemistry and Ice Nucleating Characteristics of AgI-NaI

2.1.1 Introduction of AgI-NaI Aerosol Ice Nucleants

Silver iodide was first discovered to be an effective ice nucleant in supercooled clouds by Vonnegut (1947). Vonnegut reasoned that the close similarity of crystal structure between AgI and ice was responsible for its ice nucleating ability. Attempts were made to generate smokes containing small sized (micron or less) AgI particles. Vonnegut (1949, 1950) introduced the technique of combustion of acetone solutions containing AgI. The heat of combustion vaporized the AgI which subsequently condensed into small, solid particles when quenched by the air. The problem of producing a solution of AgI, which is nearly insoluble in water or acetone alone, was remedied by adding NaI or other soluble alkali iodides to AgI-acetone suspensions. Laboratory experiments to determine the chemical composition of aerosol particles produced by combustion of acetone-AgI-NaI solutions showed that the aerosol was not pure AgI but was composed of a 'double salt' of AgI and NaI (Vonnegut, 1957). Further investigations have proven that the AgI and NaI in solution is actually in the form of a complex (Burkardt, et al., 1968, Burkardt and Finnegan, 1970, Davis, 1969, and St.-Amand, et al., 1971). Vonnegut (1957) also observed that the aerosol were 'strongly hygroscopic'. A two-step reaction was proposed wherein the aerosol particles first form solution droplets which, as they become larger and more dilute, '...reduces the concentration of the soluble

iodide [NaI] to the point that the silver iodide is no longer soluble and precipitates out' (Vonnegut, 1957). It is thus the solid precipitate that serves as the ice nucleus in the pre-formed droplet, a process known as condensation-freezing, or immersion ice nucleation. Later work by Tompkins, et al., (1963), Burkardt, et al., (1968), and Chang (1984) supports this proposed mechanism.

The AgI-NaI aerosol was distiguished from aerosol produced by combustion of acetone-AgI-ammonium iodide (NH_4I) solutions by Vonnegut (1949, 1957) where it was correctly noted that NH_4I is completely decomposed at high temperatures and so essentially pure AgI particles are produced. This was later confirmed by St.-Amand, et al. (1971) and DeMott, et al. (1983).

2.1.2 Chemical and Physical Properties of AgI-NaI Aerosol Particles

The solubility of AgI in either water is low (eg. $3x10^{-9}$g AgI/g H_2O). By adding an alkali iodide to the system, such as NaI or KI (potassium iodide), both of which dissolve readily in water or acetone, the solubility of the AgI <u>appears</u> to increase. For instance, the amount of AgI which will dissolve in water increases three orders of magnitude when 0.01 g NaI per gram of water is added (Davis, 1972). This is not due to the common ion effect, as is often supposed. The common ion effect causes precipitation of the least soluble compound in solution. Solubility is an equilibrium condition between a solid compound and its ionic components (eg. $AgI(s) \rightleftarrows Ag^+ + I^-$) Addition of the ion in common, I^- ions from NaI in this case, would increase the I^- concentration and cause a shift in the equilibrium away from dissolution and toward production of solid AgI precipitate (a shift to the left in the above equation). Instead, the Ag^+ and I^- complexes with the alkali

iodide to form a new compound ($Na^+Ag_2I_3^-$) which reduces the Ag^+ and I^- concentrations. The new compound effectively removes the ions because the stable AgI·NaI complex readily dissolves in water or acetone and does not dissociate into its component ions. Thus the equilibrium is shifted toward more dissolution of AgI (St.-Amand, et al., 1971).

The earliest study of the chemical composition complexes of AgI-alkali iodides was made by Mason and Hallett (1956). They analysed electron diffraction patterns of vaporized AgI-KI and AgI-NaI mixtures and concluded that AgI alone was not being produced when these aerosols were generated and that mixed crystals of both substances, AgI and the solubilizing salt, were formed. Several workers then concentrated their efforts on studying the AgI-KI system. Because of the similarity of AgI-NaI and AgI-KI in nucleating behavior (Rilling, et al., 1984) a brief discussion of the chemistry of the AgI-KI system follows.

Electron diffraction studies by dePena and Caimi (1967) and Burkardt, et al., (1968) demonstrated that simple mixtures of AgI and KI were not formed by combustion of acetone solutions containing these materials. DePena and Caimi (1967) concluded that a solid solution of AgI and KI in a 2:1 mole ratio was formed. Burkardt, et al. (1968) lists the known AgI-alkali iodide-water complexes and presents X-ray diffraction results which support the existence of these complexes.

The complex formed by AgI and KI is hygroscopic due to the presence of KI, in contrast to AgI alone, which is hydrophobic. AgI-KI samples collected from a field burner, similar to that used in this research, begin to adsorb water vapor at 53% relative humidity (Tompkins, et al., 1963). Similar aerosol particles were shown to form droplets at 95% relative humidity (dePena and Caimi, 1967).

The chemistry of the AgI-NaI-water system has been studied by Burkardt, et al. (1968), Mossop and Tuck-Lee (1968), Davis (1969), Burkardt and Finnegan (1970), St.-Amand, et al., (1971), Chen et al. (1972), and Johnson and Davis (1972). X-ray diffraction analysis of samples prepared by evaporating AgI-NaI solutions of various ratios indicated AgI-NaI was always complexed and hydrated. Formation of the hydrated complex appeared to be preceeded by hydration of the NaI (Burkardt, et al., 1968). Mossop and Tuck-Lee (1968) performed more detailed X-ray diffraction analysis and concluded that aerosol particles of AgI-NaI greater than 0.05 diameter produced by combustion of an 2.5AgI-NaI-acetone solution are composed of β-AgI and $NaI \cdot 2H_2O$.

By using the sample chamber of the X-ray diffractometer as an environmental chamber Davis (1969) determined the phase diagram for a 2.5:1 mole ratio of AgI to NaI, produced by acetone solution combustion, as a function of temperature and water vapor pressure. At room temperature, in an initially dry mixture of AgI and NaI crystals, the NaI forms the two mole hydrate, $NaI \cdot 2H_2O$, at approximately 16% relative humidity. At about 28.5% relative humidity a three or four mole hydrate of $AgI \cdot NaI$ forms. At 42% relative humidity solid AgI and a water solution of AgI and NaI results. Similar sequences of hydration and complexing occur at 10°C and 0°C with somewhat higher relative humidities required for transitions.

The three mole hydrated complex, $2AgI \cdot NaI \cdot 3H_2O$, was observed by Burkardt and Finnegan (1970) when water was evaporated from bulk samples of AgI-NaI solutions in X-ray diffraction analysis. They present several mechanisms for the formation of this complex in the presence of excess water vapor, all of which include or begin with $NaI \cdot 2H_2O$, as

observed by Davis (1969). Later work (Chen, et al., 1972 and Johnson and Davis, 1972) favored the existence of the 4 mole hydrate, $AgI \cdot NaI \cdot 4H_2O$. The 4 mole hydrated phase (Johnson and Davis, 1972) was particularly difficult to examine at subzero temperatures and near water saturation. Experimental error in the technique of measuring the extent of hydration was estimated to be 25% for compounds at subzero temperatures. It was proposed that water was physically, rather than chemically adsorbing on the surface of the compound. In water supersaturated environments $AgI \cdot NaI \cdot 4H_2O$ broke down to NaI solution and solid AgI (Johnson and Davis, 1972). A similar sequence of hydration was observed by St.-Amand, et al. (1971) for the $2AgI \cdot NaI$ compound.

A distinction can be made between the time required for hydrate formation and the rate of supply of water vapor to the compound as the controlling factor in chemical transformation in the AgI-NaI-water system. Chen, et al. (1972) estimated diffusion of water vapor through pores and over surfaces of $2AgI \cdot NaI$ complexes in a water supersaturated environment. Hygroscopicity of the material was neglected but was noted to speed the process. Diffusion was estimated to require less than six seconds. Measured rates of transformation of the chemical compounds studied (hydrates of AgI-NaI) required between 5 and 20 minutes time. It was concluded that the rate, or kinetics, of the chemical reaction is the contolling factor in hydrate formation and breakup, not the supply of water vapor.

Using the phase diagram in St.-Amand, et al. (1971) and solubility tables for $2.5AgI \cdot NaI$ Mossop and Jayaweera (1969) found the proportion of AgI dissolved in water reaches a maximum of 21% when the particle has taken up 10% by weight of water. Considering a particle of 0.01 μm

diameter in an equilibrium droplet only 18% of the AgI will be in solution. Davis (1972) examined the effect small particle size has on the solubility of AgI in AgI-NaI-water systems. Small particle size is known to enhance the solubilty of various salts (Dundon and Mack, 1923 and Pruppacher and Klett, 1978, p. 160). For a AgI particle of 0.05μm diameter (a realistic size for most acetone generators burning a 2AgI·NaI solution) in water alone, solubility is increased about 1% due to size alone. In a saturated solution of NaI, approximately 30% of the AgI in the particle dissolves.

The fact that AgI-NaI aerosol particles are hygroscopic was established by Mossop and Tuck-Lee (1968). Electron micrographs of particles with mean diameter of 0.085μm show growth of all the particles between 40 and 80% relative humidity. These particles are about an order of magnitude more effective as condensation nuclei than are pure AgI particles (Mossop, 1968).

2.1.3 General Ice Nucleation Characteristics of AgI-NaI Aerosol

Yield of ice nucleation has been referred to as effectivity or activity and has been measured as the number of ice crystals per gram of AgI produced by the generator used. Effectivity of ice nucleation by aerosol particles produced by the combustion of AgI, NaI, and acetone has been studied using a variety of techniques (Smith and Heffernan, 1954, Edwards and Evans, 1960, Warburton and Heffernan, 1964, Grant and Steele, 1966, Davis and Steele, 1968, Mossop, 1968, Mossop and Jayaweera, 1969, Donnan, et al., 1970, St.-Amand, et al., 1971, Blair, et al., 1973, and Garvey, 1975). Reported values of yield or effectivity are strongly dependent on temperature, chemical composition of the aerosol particles tested, type of generator, and device used for

detecting ice nucleation. Figure 1 summarizes the effectivity measurements of some past efforts. The threshold of nucleation (the warmest temperature at which ice production can be detected) varies from $-6^{o}C$ to $-9^{o}C$ and the effectivity at cold temperatures ($-20^{o}C$) spans three orders of magnitude.

Smith and Heffernan (1954) used a small cloud chamber, 76 liters in volume. The walls of the chamber were cooled. No mechanism for cooling the air within the chamber other than conduction of heat from the air to the walls was provided. Fog was maintained by introduction of steam at the bottom of the chamber. The fog volume was reported to be 10 liters. Temperature variations within this system were probably quite large in the verticle. Aerosol samples were introduced at the top of the chamber. Only a small proportion of aerosol particles at the bottom of the chamber were subjected to the correct temperature and water conditions of the experiment.

Warburton and Heffernan (1964) found the threshold to be $2^{o}C$ warmer and effectivity at $-20^{o}C$ two orders of magnitude greater than reported in Smith and Heffernan (1954) (Fig. 1). Warburton and Heffernan (1964), also used a mixing cloud chamber. The smaller size, 10 liters, allowed faster heat conduction from the air to the walls. Temperature and relative humidity was uniform in the lower 75% of the chamber (Warner, 1957). Fog was produced by inserting a semipermeable membrane containing water at a temperature of $20^{o}C$. This membrane had to be changed at five minute intervals. The warm water vapor in a sub-zero environment produced large supersaturations that reoccured every five minutes as each membrane was replaced with a fresh one. Mossop (1968) showed, by varying the humidifier temperature, that greater

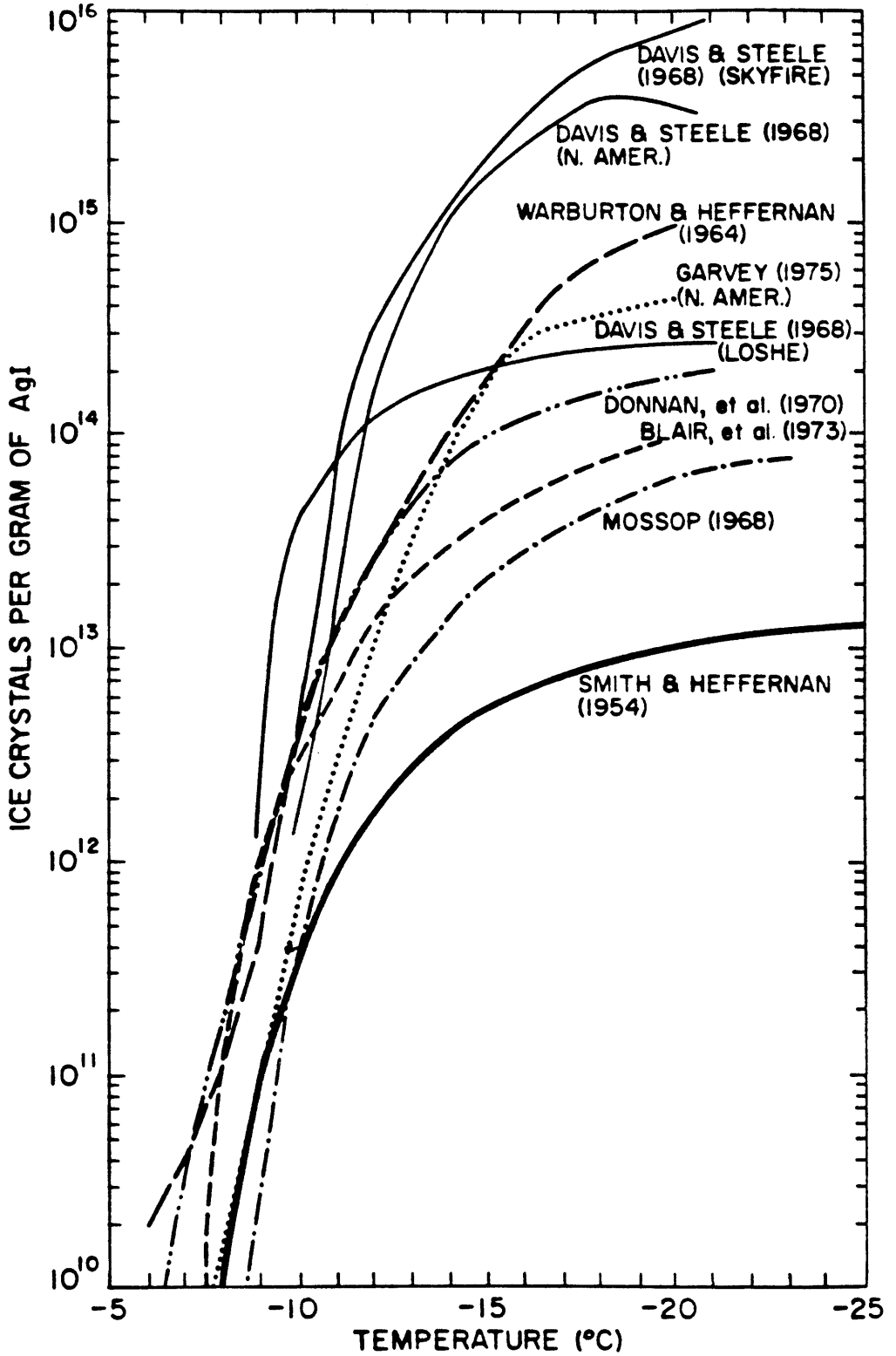

Figure 1: Ice nucleation effectiveness of AgI-NaI aerosol particles produced from combustion of acetone solutions as reported in various sources.

supersaturations resulted in higher yields for both hygroscopic and hydrophobic AgI aerosol particles.

The results of Davis and Steele (1968) should be compared to those of Garvey (1975) (Fig. 1). Both investigators used the isothermal cloud chamber at Colorado State University. The 960 liter chamber was subjected to major alterations to improve its performance in about 1970. The most important of these changes was the provision for supplying pre-cooled cloud air near the top of the chamber. This assured temperature and cloud density uniformity throughout the chamber volume. Prior to 1970, warm cloud air was introduced into the subzero degree chamber and large water supersaturations and temperature gradients resulted. As in the work of Warburton and Heffernan (1964) yield measured by Davis and Steele (1968) was high at cold temperatures. Subsequent elimination of supersaturations and temperature gradients greatly reduced the yield for a given generator (Garvey, 1975). The yield at $-20^{o}C$ for the North American generator burning AgI-NaI-acetone, was reduced from $3X10^{16}gm^{-1}$ to $3X10^{15}gm^{-1}$ (Fig. 1).

Edwards and Evans (1960) assumed that the ice nuclei they examined was pure, hydrophobic AgI. In semi-quantitative tests where their aerosol was compared with aerosol containing AgI-NaI produced from acetone solution combustion, Edwards and Evans (1960) found both aerosols functioned in the same manner. It is questionable that the AgI used in their tests was hydrophobic due to possible contamination of the AgI. The number of sublimation (deposition) nuclei which functioned at 98% relative humidity at any temperature was less than 0.5% of the number which functioned at water saturation, indicating that water saturation and hence droplet formation was a necessary step in the

mechanism of ice formation. Effectivity was increased in water supersaturated environments, further supporting the conclusion that their nucleant functioned by a condensation-freezing mechanism.

The temporal rate of ice formation has been shown to be a vital element in the deduction of nucleation mechanisms (DeMott, et al., 1983, Horn, et al., 1982, and Reiss, 1982). The interpretation of observed rates of nucleation in past studies has been inadequate and, at times, have been ignored in spite of gross shifts in rates with slight changes in conditions. Such is the case when AgI first became known as an ice nucleant. The rate of ice crystal production by AgI aerosol produced by combustion of an AgI-NH_4I-acetone solution in a small cloud chamber was observed to decrease exponentially with time and required about 55 minutes (Vonnegut, 1949). The rate of AgI nucleation was compared to the rate of ice formation due to the use of a pop gun. When a pop gun is used in a cloud chamber containing supercooled cloud, the rapid expansion of air from the gun causes spontaneous (homogeneous) nucleation. The rate of ice crystal formation by the pop gun was reported as non-exponential with time (actually, the rate is linear with time), and ice crystal fallout was complete in about 8 minutes. Vonnegut attempted to explain the phenomenon by asserting that ice embryo formation on the AgI particle is a random process that depends on chance. He reasoned that because of certain energy requirements, surface energy relative to free energy, the probability of ice embryo formation increases with decreasing temperature. Thus, nuclei which normally function instantaneously at colder temperatures require more time to function at warmer temperatures. This hypothesis conflicts with Vonnegut's statement that the rate of ice nucleation by AgI did not

significantly change with temperature. The AgI aerosol Vonnegut used was later shown to nucleate ice primarily by a mechanism controlled by Brownian coalescence of aerosol particles with cloud droplets (DeMott, et al., 1983).

The rate of ice crystal production by 2AgI·NaI aerosol particles was measured by Smith and Heffernan (1954). The observed rate was exponential with time and required about 12 minutes for complete nucleation at -16°C. A conversion factor was defined as the ratio of the total number of ice crystals produced at the end of a run to the number of ice crystals observed in the first minute. The conversion factor approaches one as the rate increases. Conversion factors from -8°C to -28°C indicate that the rate of ice nucleation increased with decreasing temperature. No explanation was given by the authors for this behavior. Variation of rate with temperature was presented indirectly by Davis and Steele (1968). They introduced the parameter 'effective nuclei per minute' for several nucleants at different temperatures. For AgI-NaI aerosol particles from acetone solution combustion, the effective nuclei per minute, or rate, increases exponentially with decreasing temperature, in agreement with Warburton and Heffernan (1964).

The half life (time required for ice crystal fallout rate to decrease to 1/e of its initial value) for AgI aerosol particles produced from the NEI TB-1 pyrotechnic flare at temperatures above -20°C is given by Garvey, et al. (1976). These aerosol particles are hygroscopic (W. Finnegan, personal communication) and are similar to AgI-NaI aerosol. The half lives reported decrease with decreasing temperature, indicating the rate of ice nucleation increases with decreasing temperature. Other

flares tested, which produced hydrophobic AgI particles, showed no clear temperature dependence for the half lives. Hydrophobic nuclei generally function by a contact mechanism (DeMott, et al., 1983).

The nuclei particles used by Edwards and Evans (1960), apparently functioned at two different rates depending on the initial environmental conditions in the mixing cloud chamber used. The cloud chamber was maintained at constant temperature and at water saturation. In one set of experiments, the aerosol sample was at room temperature and 100% relative humidity. Injection of the sample into the bottom of the cold chamber temporarily produced significant supersaturation with respect to water. Ice crystal production and fallout was observed to be rapid, being complete within one minute. The aerosol was also introduced into the chamber with dry air (relative humidity not stated). Ice crystal production in this case was observed to be 'prolonged', requiring more than five minutes to complete. Experiments conducted in a small rapid expansion chamber, where supersaturations were estimated, support the above observations. Edwards and Evans suggested that additional mechanisms involved in the 'prolonged' nucleation were movement, by convection, of the aerosol to more humid regions of the chamber and contact of aerosol particles with droplets.

Experiments were conducted in a 'dynamic', slow expansion cloud chamber, which simulates the temperature and pressure changes of adiabatic and pseudo-adiabatic expansion of an air parcel (Garvey, et al., 1976). AgI-NaI aerosol particles from acetone combustion appeared to exhibit different rates of ice nucleation depending on the initial conditions of the aerosol. When AgI-NaI aerosol was introduced into chamber air that was warmer than that of the lifting condensation level

(LCL), ice crystal production was prolonged, achieving a maximum at a temperature of $-30^{o}C$. When the aerosol are introduced into cloudy air, cooler than the LCL, nucleation occured more rapidly, achieving a maximum at a temperature of $-22^{o}C$, for the same rate of cooling of the previous experiment.

The work of Chen, et al. (1972) has shown that the rate of chemical reaction is the controlling process in the transformations that occur in the AgI-NaI-H_2O system. The rates of chemical reaction (hydration and break up of the AgI-NaI-water complex) observed are comparable in scale to many of the rates of ice crystal production observed by Smith and Heffernan (1954), Edwards and Evans (1960), Warburton and Heffernan (1964), Davis and Steele (1968), and Garvey, et al. (1976).

2.1.4 Effect of Water Supersaturation on Ice Nucleation by AgI-NaI

The effect of excess water vapor concentration or supersaturation with respect to a plane water surface on the properties of condensation nuclei has been investigated (see, for example, Pruppacher and Klett, 1978, p. 225-241). Comparatively little work, however, has been done on the relationship of water supersaturation and ice nucleating properties of hygroscopic ice nuclei such as 2AgI·NaI containing aerosol particles. A full spectrum of number of ice nuclei or yield versus supersaturation for any aerosol which contains AgI is lacking. The type of data available that describes trends in the ice nucleating behavior of hygroscopic ice nuclei are those in which qualitatively high water supersaturations were used in mixing cloud chamber tests (Edwards and Evans, 1960, and Mossop, 1968). Other research dealt with the effect of preconditioning the aerosol with high water vapor concentrations prior to making ice nucleation observations (St. Louis and Steele, 1968).

Two sampling procedures were used by Edwards and Evans (1960) in their examination of hygroscopic aerosol particles. In one procedure, aerosol at 100% relative humidity at room temperature was injected into a cloud chamber which was approximately water saturated. This aerosol was termed 'wet'. The other procedure involved injection of aerosol from a significantly drier environment into the cloud chamber. The extent of supersaturation caused by the 'wet' aerosol was not determined. Results indicated that the yield of ice nucleation by 'wet' aerosol was approximately an order of magnitude greater than the yield of ice nucleation by 'dry' aerosol at all temperatures. Additionally, 'wet' aerosol was observed to nucleate rapidly, within one minute, while 'dry' aerosol was observed to nucleate for prolonged amounts of time. They attributed the difference in ice nucleation behavior to a combination of factors including location of sample injection, convection in the chamber and subsequent migration of nuclei to zones of water supersaturation and high liquid water, and overseeding.

Water supersaturations were induced in the cloud chamber used by Mossop (1968) where a semi-permeable membrane containing warm water was used for humidification and cloud formation in the cold box. Two humidifier temperatures were used, 35°C and 45°C, to produce two relatively different water vapor conditions. Increases in yield were noted for AgI-NaI ice nuclei of about a half order of magnitude at temperatures warmer than -16°C.

Preconditioning AgI-NaI ice nuclei in a moist environment resulted in similar ice nucleation behavior. St. Louis and Steele (1968) allowed AgI-NaI aerosol particles produced from acetone combustion to equilibrate in environments of varying relative humidities before

injecting them into a mixing cloud chamber. No drying of the sample was done before introduction into the chamber, so water supersaturation can be expected to occur which is proportional to the relative humidity of the sample. Results indicate that when the aerosol is preconditioned above a water vapor pressure of 12mm Hg, yield of ice crystals increased in direct proportion to the vapor pressure. Yield increased by a factor of three when the sample was conditioned at 25mm Hg.

The possibile existence of transient water supersaturations was generally not considered in most research involving ice nucleation by AgI and AgI-NaI. Mossop (1968) recognized it in his work and recommended that future researchers should avoid supersaturations. Garvey (1975) made a conscious effort to avoid supersaturations, by modifying the cloud chamber and carefully diluting aerosol samples with clean, dry ($-30^{o}C$ dew point temperature) air.

The chemical nature of AgI-NaI particles as affected by high water supersaturation was briefly examined by Johnson and Davis (1972). They noted the temporary, metastable existence of the hydrated AgI·NaI complex in high, non-equilibrium humidities. After a time, which is governed by the kinetic rate of chemical transformation, these complexes were observed to break down, resulting in the appearence of solid AgI particles in NaI solution envelopes. Solid AgI appeared more quickly when the dry particle became embedded into a cloud droplet.

Adiabatic and pseudo-adiabatic temperature and humidity changes can create water supersaturated environments. Chen, et al. (1972) noted that when temperature and humidity changes are sufficiently rapid, certain complex phases of the AgI-NaI-H_2O system can effectively be bypassed. This may have been demonstrated by Garvey, et al. (1976) in

tests in the 'dynamic' cloud chamber at CSU. More ice crystals appeared at a faster rate when an initially dry (-30°C dewpoint), room temperature sample was injected into a cold, cloudy environment than when a similar sample was injected into a warmer, subsaturated environment.

2.2 Chemical Kinetic Methodology in the Study of Phase Change

The incorporation of chemical kinetic methodology in the study of heterogeneous ice nucleation has been introduced only recently (DeMott, 1982, DeMott, et al., 1983, and Reiss, 1982). The thermodynamic approach to ice nucleation research, often referred to as the 'classical model' (Turnbull and Vonnegut, 1952, Fletcher, 1958, 1959, 1968, 1969, Fukuta and Schaller, 1982, Pruppacher and Klett, 1978, p. 268-281), has received the most attention. These two approaches differ markedly in their respective starting assumptions and lines of reasoning. Certain properties, most importantly the temporal nature of the physical process of phase change, can be determined only via chemical kinetics and not by a thermodynamic approach.

General principles of chemical kinetics as an emperical discipline can be found in most textbooks of physical chemistry (eg. Moore, 1972, and Berry, et al., 1980). Chemical kinetics addresses the evolution in time of a chemical or physical process or reaction. It is based on the Law of Mass Action which states that the dynamic rate of a reaction or process is dependent on the concentration of the reactants. An example of the information kinetics provides about phase change in a chemically homogeneous system is given in Berry, et al. (1980, p. 1025). Water in a container open to the atmosphere will evaporate. Changes in thermodynamic state functions depend only on the initial and final

states of the water, not on the path by which evaporation occurs nor on the time required to achieve the final state. Thermodynamics can predict what the final state will be. The two properties of path and required time, corresponding to mechanism and rate, can be addressed emperically using chemical kinetics. The dynamic action of evaporation, including the approach to equilibrium, or how evaporation occurs, is the subject of chemical kinetics.

Reiss (1982) outlines how homogeneous nucleation to a denser phase can be interpreted kinetically. He draws an analogy to the Lindemann mechanism (eg. Moore, 1972) which involves two steps; the establishment of a dynamic equilibrium where a critical substance is formed, followed by an irreversible step where the critical substance is removed. In the case of ice nucleation, the critical substance is the critically sized ice embryo. The embryo can be removed from the system either by decomposition in the reverse reaction of the equilibrium, or by irreversibly growing to become an ice crystal. In a series of sequential steps, the slowest step of the series is, kinetically, the rate determining step (eg. Berry, et al., 1980). In Reiss's interpretation of the Lindemann mechanism, the equilibrium of the first step is quickly established and the rate at which the second step proceeds, embryo growth, determines the rate of nucleation. The rate can be expressed as a first-order reaction, dependent exponentially on the concentration of the reactants and the rate constants of the individual steps. Additionally, Reiss states that heterogeneous nucleation is 'an example of catalysis' which constitutes an important branch of chemical kinetics. A catalyst can be defined as a substance which effectivley changes the rate, or kinetics, of a reaction without

changing the final equilibrium or product and is not destroyed (Berry, et al., 1980).

The chemical kinetic methodology in the study of heterogeneous ice nucleation was demonstrated by DeMott (1982) and DeMott, et al. (1983). They utilized hydrophobic AgI and AgI-AgCl aerosol particles and observed the decay of the aerosol particle population with time after injection into a large mixing cloud chamber.

DeMott (1982) and DeMott, et al. (1983) present a full outline of the possible mechanisms of heterogeneous ice nucleation by aerosol particles, including vapor deposition, condensation to embryos followed by freezing, condensation to droplets followed by freezing, and contact freezing. Each process is described with a chemical reaction equation of the form $A+B \rightarrow C \rightarrow D$. Rate expressions are given for the slowest, or rate determining step which they assess is the nucleation process itself. Two basic equations are given. The rate of disappearence of ice nuclei is proportional to the concentrations of nuclei and water vapor for the case of vapor deposition and condensation freezing. For contact ice nucleation, the rate is proportional to the concentrations of nuclei and cloud droplets. The authors proceed to demonstrate that for hydrophobic ice nuclei, functioning by the contact mechanism, the rate significantly shifted as the concentration of cloud droplets was altered. The proportionality constant for the rate was determined. The measured values agreed favorably with theoretical values for Brownian coagulation of aerosol particles to cloud droplets.

Chemical kinetics in the study of ice nucleation differs in a number of ways from past methods used. The time factor in ice nucleation was first noted by Vonnegut (1949) when he observed the

exponential decrease of ice crystal production with time. He interpreted this behavior as a probabilistic phenomenon, based on the chance formation of stable nuclei which would grow to ice crystals. Fletcher (1958, 1959) interpreted the temporal behavior of ice nucleation themodynamically using Gibbs free energy of formation. In his theory, ice nuclei were 'active' only at a particular temperature which was dependent on the the particle size. Ice nuclei of the proper size, and at the proper temperature or colder, nucleate ice instantaneously. Ice nuclei too small in size may nucleate the ice phase after a time, referred to as the 'time lag'. This theory implies that there is a unique size for each nucleation temperature. Such a relationship was refuted by Edwards, et al. (1962) and Mossop and Jayaweera (1969) for the case of hygroscopic ice nuclei and Langer, et al, (1978) for the case of AgI aerosol particles greater than 0.02μm radius. Fletcher (1968, 1969) later modified his model to account for aerosol particles containing a soluble component and for particles with localized active sites. However, laboratory results continued to be difficult to interpret using the thermodynamic model (Davis and Steele, 1968, Blair, et al., 1973, and Garvey, et al., 1976).

2.3 Ice Nucleation in Orographic Cloud Modeling

Numerical simulations of microphysical cloud and precipitation processes in cold orographic cloud systems have been carried out by Hobbs, et al. (1973), Young (1974 a,b), Plooster and Fukuta (1975), and Rauber (1981). These models were applied to steady-state flow normal to the modeled barrier in two dimensions, using an upwind atmospheric sounding as input. Airflow dynamics were similar in all models. Model predicted airflow streamlines were used together with model calculated

growth and subsequent fall velocity of cloud and precipitation particles to predict the extent and location of precipitation reaching the ground. Cloud particle growth processes include growth by vapor deposition, accreation (Plooster and Fukuta, 1975 and Rauber, 1981), and aggregation (Hobbs, et al., 1973 and Young, 1974a).

Of importance to the research presented in this study is the method of initiation, or nucleation of the ice phase in the models. Hobbs, et al. (1973) and Rauber (1981) arbitrarily specified a concentration of ice particles at a location within the cloud. Young (1974a) modeled contact and sorption ice nucleation. The contact process, collection of aerosol particles by cloud droplets, included Brownian coagulation, thermophoresis, and diffusiophoresis, modified at each time step by the effectivity (yield) spectrum of the natural or artificial nuclei used. Sorption nucleation in Young's model was assumed to be condensation-freezing nucleation in the case of natural ice nuclei, modified by temperature effects on effectivity. Sorption nucleation could also be vapor deposition in the case of modeled AgI cloud seeding, modified by an effectivity spectrum dependent on supersaturation with respect to ice. Both sorption nucleation modes were assumed to function instantaneously in the time step. Unfortunately, in the application of the model to an orographic cloud in Young (1974b) only contact nucleation was used.

Modeled ice nucleation by Plooster and Fukuta (1975) was similar to Young's (1974a) sorption nucleation, where ice nucleation occured intantaneously in any time step and was controlled by the temperature dependence of effectivity imposed on it. Plooster and Fukuta (1975)

were generally more interested in the effect of seeding rate, or initial concentration of ice nuclei, on modeled precipitation.

Similar results were achieved in both models. It was concluded that the impact of ice nucleation, ie. amount and location of precipitation at the surface and precipitation efficiency, strongly depend on the location of ice initiation and the initial concentration of ice embryos.

2.4 Use of AgI-NaI in Weather Modification Projects

A comprehensive explaination of the concepts and methods of weather modification for precipitation enhancement can be found in Dennis (1980). Basically, when clouds are seeded with ice nuclei, increased conversion of water vapor or liquid water to ice is sought. Weather modification projects, for the most part, used 2AgI·NaI aerosol particles until approximately 1970. At that time AgI-NH_4I-acetone solutions became more widely used in an effort to optimize the effectivity/cost ratio of AgI in weather modification and to improve the likelihood of cloud response at warmer temperatures (W. G. Finnegan, personal communication). Only one major weather modification project, the Israeli program, continues to use 2AgI·NaI seeding material from acetone combustion generators (A. Gagin, personal communication).

Aerosols of 2AgI·NaI particles have been used for both orographic and convective cloud seeding in countries worldwide (Dennis, 1980). The most notable of these programs are the Climax experiments and the Israeli program. Climax was a wintertime, orographic snowfall enhancement project conducted in the Colorado Rocky Mountains from 1960 to 1970. The Israeli program, still in progress, is a convective rainfall enhancement project which began in 1961. Seeding in both

projects was randomized and precipitation measured in snow and rain gage networks was analyzed statistically. Results indicated statistically significant increases in precipitation were acheived due to seeding in Climax (Mielke, et al., 1981) and Israel (Gagin and Neumann, 1981). The indicated precipitation increases from these two experiements, both of which used 2AgI·NaI as a seeding material, probably have higher statistical significance than any other long term randomized weather modification experiments.

III. THEORETICAL CONSIDERATIONS

3.1 Principles of Chemical Kinetics

The discipline of chemical kinetics is the study of the rates of chemical reactions and physical processes. A related study is the deduction of the mechanism(s) of the reaction or process from the observed rates. Chemical kinetics differs from other branches of physical chemistry in that it is an empirical study where observations of the progress of a reaction through time are made. The discussion in this section is referenced in Espenson (1981).

Kinetics begins with a knowledge of the reactants and products of a chemical reaction or physical process in the form of a chemical or physical reaction equation,

$$A + B + \cdots \xrightarrow{k} Y + Z + \cdots \qquad (3.1.1)$$

where letters denote chemical or physical species and k is the empirical reaction rate constant. From the chemical equation, a differential rate expression can be given as,

$$\frac{-dA}{dt} = \frac{-dB}{dt} = \frac{+dY}{dt} = \frac{+dZ}{dt} = k[A]^a[B]^b \cdots [N]^n \qquad (3.1.2)$$

where brackets denote concentrations and lower case letters represent the empirical order of the reaction with respect to the corresponding reaction species.

A common method of chemical kinetics methodology is to observe the reaction in a constant-volume, batch reactor where all reactant

concentrations are held constant except one. Either the concentration of the non-constant reactant or a product is monitored through time. In the above example, if reactant B is held constant and the concentration of A or Y could be monitored, then eq. 3.1.2 could be expressed as

$$\frac{d[A]}{dt} = -k'[A]^a \qquad (3.1.3)$$

$$\frac{d[Y]}{dt} = k'[A]^a \qquad (3.1.4)$$

where

$$k' = k[B]^b \qquad (3.1.5)$$

If eq. 3.1.1 represents an elementary reaction, that is, a single microscopic process, then eq. 3.1.3 and 3.1.4 will describe the mechanism of that process. The total of the exponents, a + b in eq. 3.1.2, determine the order of the reaction. Often, reaction equations such as eq. 3.1.1 describe an overall, or net, process in which several intervening steps occur. These steps can occur in parallel to each other or in consecutive order. Also, equilibria can be established within the process in which reverse reactions can become important to the overall rate. The rate constants, k' in eqs. 3.1.3 and 3.1.4, would not be equivalent in a net process and may be expressed as k'_1 and k'_2, respectively.

In the laboratory, when a net process is being studied, typically, the concentration of either a reactant or a product is monitored through time. If the concentration of Y is to be monitored, eq. 3.1.4 must be solved using the integrated form of eq. 3.1.3. Integration of eq. 3.1.3 yields several solutions, depending on the value of the exponent, a.

The general solution for a=n (n≠1) is

$$[A]_t^{n-1} = [A]_o^{n-1} - (k'_1[A]_o^{n-1})(n-1)([A]_t^{n-1}t) \qquad (3.1.6)$$

where subscripts t and o represent concentrations at time t and initial concentrations respectivley. For physical processes, the exponent, a, is often zero or one, giving the simple solutions

$$[A]_t = [A]_o - k'_1 t \qquad (3.1.7)$$

$$[A]_t = [A]_o \exp(-k'_1 t) \qquad (3.1.8)$$

If a=0 and y=1, then eq. 3.1.4 becomes $\frac{d[Y]}{dt} = k'_2$ for which the solution is

$$[Y]_t = k'_2 t \qquad (3.1.9)$$

where the initial concentration of product Y is zero. Substitution of the first order rate, eq 3.1.8, into eq. 3.1.4 and subsequent integration yields

$$[Y]_t = \frac{k'_2}{k'_1}[A]_o\,(1 - \exp(-k'_1 t)) \qquad (3.1.10)$$

for the first order reaction.

For the zero order reaction, eq. 3.1.9, a plot can be constructed of $[Y]_t$ versus time which will yield a straight line with a slope corresponding to rate constant k'_2. Obtaining the rate constants for the first order reaction, eq. 3.1.10, is more complicated. At the effective end of the reaction, t=∞,

$$[Y]_\infty = \frac{k'_2}{k'_1}[A]_o. \qquad (3.1.11)$$

Subtracting eq. 3.1.10 from eq. 3.1.11 and taking the logarithm,

$$\ln([Y]_\infty - [Y]_t) = \ln\frac{k'_2[A]_o}{k'_1} - k'_1 t. \qquad (3.1.12)$$

A plot of $\ln([Y]_\infty - [Y]_t)$ versus time will yield a straight line of slope equal to k'_1 and intercept $\ln \frac{k'_2[A]_o}{k'_1}$ $(=\ln \frac{k'_2[A]_o}{\text{slope}})$. It is the object of the chemical kinetic methodology to obtain straight line plots in order to determine the order of reaction and rate constants.

After the proper rate relationship and constants have been determined, the mechanism of the process can be deduced. This is somewhat of an intuitive process but there are certain guidelines. For instance, the concentration dependences in the rate law establish the species that are involved in the mechanism of the reaction or process. Rate laws for complex reactions can take on various forms. The number of additive terms in a rate law indicate the number of parallel pathways in the mechanism. A rate law with a denominator indicate successive and reversible pathways. The most important concept is that of the rate-limiting, or rate-determining step. In sequential steps of a mechanism this is the slowest step with the lowest valued rate constant, k. It controls the progress of the entire reaction since faster subsequent steps cannot proceed until the rate limiting step has occurred. A final rule is that any given mechanistic interpretation of a rate law is not unique to that rate. Alternative mechanisms leading to a given rate law are kinetically indistinguishable and cannot be ruled out.

Chemical reactions and physical processes often display a temperature dependence. Typically the rate constant is logarithmically dependent on the inverse of temperature. Three theories have made use

of this relation. First, the Arrhenius relation,

$$k = A \exp(\frac{-E_a}{RT}) \qquad (3.1.13)$$

is simply an empirical relationship where k is the measured rate constant at any temperature, A is the pre-exponential factor, independent of temperature, E_a is the energy of activation, R is the gas constant, and T is temperature in Kelvin. A plot of ln k versus T^{-1} yields the intercept A and a slope equal to E_a/R. Second, collision theory presents a similar relation for bimolecular reactions in the gas phase. Third, the Eyring or activated complex or absolute rate theory expresses the rate constant as

$$k = K \frac{RT}{Nh} \exp(\frac{\Delta S^{\dagger}}{R}) \exp(-\frac{\Delta H^{\dagger}}{RT}) \qquad (3.1.14)$$

where K is a transmission coeffecient, usually taken as unity, N is Avagadro's number, h is Planck's constant, and $\Delta S^{\dagger}$ and $\Delta H^{\dagger}$ are the entropy and enthalpy, respectively, of activation. The activated complex is a hybrid species, usually a combination of two molecules, in quasi-equilibrium with the reactants. A plot of the Eyring relation, ln k/T versus T^{-1}, yields a straight line with slope equal to $\Delta H^{\dagger}/R$ and an intercept of $\frac{RT}{Nh} \exp(\frac{\Delta S^{\dagger}}{R})$ from which $\Delta S^{\dagger}$ can be determined.

The use of one reaction energetics relation as opposed to another, with the exception of the collision theory which applies only to gases, is not of critical importance. This is because the exponential term containing T is dominant in the relation. It is often the case that plots of ln k and ln k/T versus T^{-1} are both linear within experimental

error of the data. Furthermore, activation energy, E_a, of the Arrhenius equation is related to $\Delta H^{\dagger}$ of the activated complex theory;

$$\Delta H^{\dagger} = E_a - RT. \qquad (3.1.15)$$

3.2 Kinetic Reaction Mechanisms of Ice Nucleation

A chemical kinetic interpretation of heterogeneous ice nucleation via four modes, or mechanisms is discussed in DeMott (1982) and DeMott, et al. (1983). The four modes are 1) vapor deposition, 2) condensation to aqueous embryos followed by freezing, 3) condensation to droplets followed by freezing, and 4) contact freezing. Experimental evidence of the contact freezing and vapor deposition modes of ice nucleation by hydrophobic aerosol particles given in these papers indicate the applicability of the kinetic methodology to phase change processes. The second and third forms of ice nucleation above, generically termed condensation-freezing processes, will be emphasized here.

Reaction equations for the condensation-freezing processes can be expressed as follows;

condensation to embryos followed by freezing:

$$N + V \xrightarrow{k_1} AE \xrightarrow{k_2} IE + V \xrightarrow{k_3} IC \qquad (3.2.1)$$

condensation to droplets followed by freezing

$$N + V \xrightarrow{k_4} DSD \xrightarrow{k_5} FD + V \xrightarrow{k_6} IC \qquad (3.2.2)$$

Specific species are as follows: N is an ice nucleus, V is water vapor, IC is ice crystal, AE is aqueous embryo, IE is ice embryo, DSD is dilute solution droplet, and FD is frozen droplet. Each arrow or step in the processes has a rate constant, k_n, unique to that step. Both processes individually are examples of consecutive reactions. Both processes can also occur simultaneously.

Differential rate expressions can be written for each component of the process. From eq. 3.2.1:

$$\frac{dC_N}{dt} = -k_1 C_N^n C_V^v$$

$$\frac{dC_{AE}}{dt} = k_1 C_N^n C_V^v - k_2 C_{AE}^a$$

$$\frac{dC_{IE}}{dt} = k_2 C_{AE}^a - k_3 C_{IE}^i C_V^v \qquad (3.2.3)$$

$$\frac{dC_{IC}}{dt} = k_3 C_{IE}^i C_V^v$$

$$\frac{dC_V}{dt} = -k_1 C_N^n C_V^v - k_3 C_{IE}^i C_V^v$$

These form a system of related equations. Likewise, from eq. 3.2.2

$$\frac{dC_N}{dt} = -k_4 C_N^n C_V^v$$

$$\frac{dC_{DSD}}{dt} = k_4 C_N^n C_V^v - k_5 C_{DSD}^d$$

$$\frac{dC_{FD}}{dt} = k_5 C_{DSD}^d - k_6 C_{FD}^f C_V^v \qquad (3.2.4)$$

$$\frac{dC_{IC}}{dt} = k_6 C_{FD}^f C_V^v$$

$$\frac{dC_V}{dt} = -k_4 C_N^n C_V^v - k_6 C_{FD}^f C_V^v$$

Two simplifications can immediately be made. The concentration of water vapor can be held constant, as it is in the experiments to be described below, in which case $\frac{dC_V}{dt} = 0$ and

$$k'_x = k_x C_V^v, \qquad (x=1,2,3\ldots). \qquad (3.2.5)$$

Secondly, all exponents expressing reaction orders can be assumed to be equal to one. There is no physical reason why more than one nucleus

should serve to form an embryo or droplet. Also, only one embryo or droplet should form an ice crystal. The occurrence of ice multiplication, where one ice nucleus may produce more than one ice crystal, is not considered because laboratory cloud chamber conditions in this study are not conducive to such processes. Equations 3.2.3 and 3.2.4 can now be written as,

$$\frac{dC_N}{dt} = -k_1' C_N$$

$$\frac{dC_{AE}}{dt} = k_1' C_N - k_2 C_{AE} \qquad (3.2.6)$$

$$\frac{dC_{IE}}{dt} = k_2 C_{AE} - k_3' C_{IE}$$

$$\frac{dC_{IC}}{dt} = k_3' C_{IE}$$

and

$$\frac{dC_N}{dt} = -k_4' C_N$$

$$\frac{dC_{DSD}}{dt} = k_4' C_N - k_5 C_{DSD} \qquad (3.2.7)$$

$$\frac{dC_{FD}}{dt} = k_5 C_{DSD} - k_6' C_{FD}$$

$$\frac{dC_{IC}}{dt} = k_6' C_{FD}$$

In the experiments that follow, a final step, common to both mechanisms of eq. 3.2.1 and 3.2.2, must be included. Ice nucleation is monitored in this research when ice crystals have fallen to the bottom of the 1 m^3 chamber. The process of fallout of the ice crystals after growth is a kinetic process that must be included in the net process. This step can be expressed as

$$IC \xrightarrow{k_F} IC(COLLECTED). \qquad (3.2.8)$$

The differential rate expression can be written as

$$\frac{dC_{IC}}{dt} = \frac{dC_{IC}}{dy}\frac{dy}{dt} \qquad (3.2.9)$$

where $\frac{dC_{IC}}{dy}$ is the vertical distribution of ice crystals and $\frac{dy}{dt}$ is the fall velocity of the crystals. The terms of eq. 3.2.9 may be assumed to be constant if at some initial time the well-mixed chamber contains only ice crystals of uniform size and hence uniform fall speed. Eq. 3.2.9 then becomes a zero order rate process where

$$\frac{dC_{IC}}{dt} = k_F. \qquad (3.2.10)$$

If the two mechanisms of eq. 3.2.1 and 3.2.2 occur simultaneously, or in parallel, the rate constants must be added in the solution. From eq. 3.2.6 and 3.2.7, $\frac{dC_N}{dt} = -(k_1' + k_4')C_N$ and

$$C_N - C_{N,o} = \exp(-(k_1' + k_4')t) \qquad (3.2.11)$$

where $C_{N,o}$ is the initial concentration of nuclei which form ice crystals.

If only one process occurs, there remains the fact that the reaction involves consecutive steps. In this case, the controlling factor in the overall rate is the slowest rate, the step with the smallest k. This is termed the rate-determining or rate-limiting step. The overall, observed rate will then be the same as that of the rate-determining step. A possible rate determining step can be the second step, freezing of aqueous embryos or droplets. If the freezing process is much slower than the condensation process, particles would have the opportunity to grow to their equilibrium size and become dilute solution

drops. In this case, the mechanims of condensation to embryos followed by freezing, eq. 3.2.1, can be eliminated. The concentration of nuclei can be assumed to be zero since the first step, condensation, quickly converts all nuclei to droplets. Eq. 3.2.2 can be simplified to become $C_{DSD} \xrightarrow{k_5} C_{IC}$ which reduces eq. 3.2.7 to

$$\frac{dC_{DSD}}{dt} = -k_5 C_{DSD}$$
$$\frac{dC_{IC}}{dt} = k_5 C_{DSD}. \qquad (3.2.12)$$

The solution to this system of equations in terms of ice crystal production is

$$\ln(C_{IC,\infty} - C_{IC,t}) = \ln C_{N,o} - k_5 t \qquad (3.2.13)$$

where $C_{N,o}$ is substituted for $C_{DSD,o}$ and represents the nuclei which form droplets that freeze. A plot of $\ln(C_{IC,\infty} - C_{IC,t})$ versus time will yield a straight line with slope equal to the rate of the freezing process, k_5.

Temperature dependencies of observed rate constants are used in determining energies of activation as in Eq. 3.1.13 and 3.1.14 and may provide additional information on the mechanism. Reactant concentration dependencies are used to determine the species which influence the process and so tells something directly about the mechanism. For instance, in DeMott, et al. (1983) contact nucleation was established as the primary mechanism of ice nucleation by the aerosol used because rates shifted in proportion to shifts in cloud droplet concentrations. However, caution should be used in the case of parallel reactions where a shift in rate with changes in a reactant concentration above certain levels can actually increase the rate of a parallel reaction to observable levels.

3.3 Incorporation of Kinetic Rates and Mechanisms into an Orograhic Cloud Model

As part of the research effort to describe the process of condensation-freezing ice nucleation by aerosol particles, a numerical model of microphysical cloud processes was utilized in order to assess how rate and mechanism of ice nucleation influence precipitation patterns. The model is a two-dimensional orographic cloud model, developed by Rauber (1981), consisting of two parts. The first part of the model calculates streamlines, potential condensate production, and condensate production rates under steady-state conditions as air passes over a mountain barrier. The second part estimates ice crystal growth and fall velocity to calculate ice crystal trajectories (Rauber, 1981). Figure 2 shows the mountain profile used for the simulation.

The first part of the model incorporates rawinsonde data of wind speed and direction, temperature, and humidity obtained in the Colorado Orographic Seeding Experiment (COSE III) conducted in the Park Range of northeastern Colorado in the winter of 1981-82. Air parcel streamlines are calculated by considering input horizontal wind speeds and model predicted vertical velocity. Vertical velocities were calculated assuming adiabatic, steady state conditions and neglecting friction and Coriolis accelerations. The governing equations were vertical and horizontal momentum, continuity, and the thermodynamic energy relation with Boussinesq approximations. Temperature, saturation mixing ratio, and cloud condensate content of the parcel were calculated adiabatically assuming the equivalent potential temperature of the parcel was conserved from the point of origin (the upwind sounding). Condensation

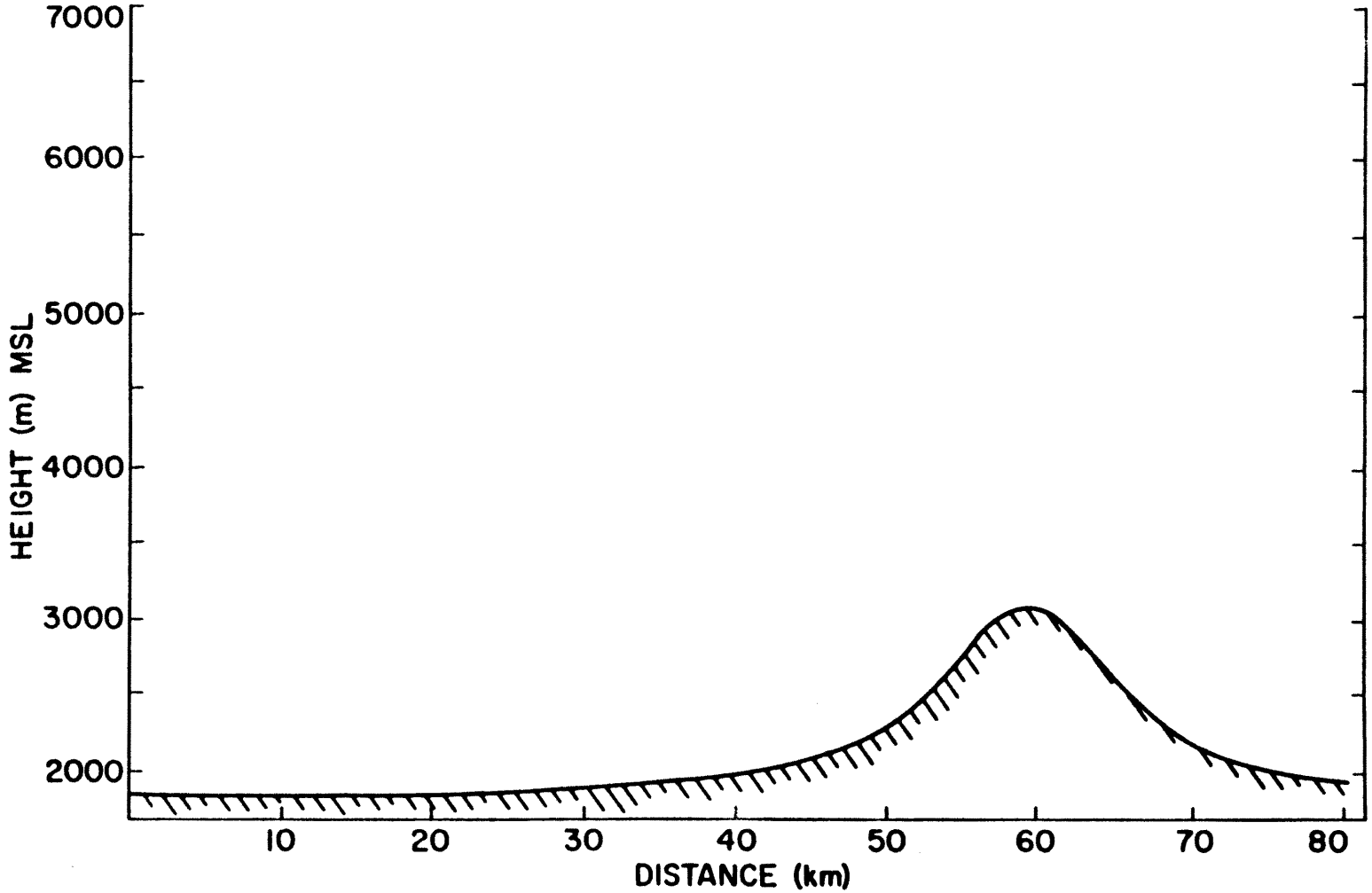

Figure 2: Mountain barrier profile used in orographic cloud model.

was assumed to occur when a parcel was lifted beyond its lifting condensation level.

Ice crystal trajectories in the second part of the model are determined as follows. Nucleated ice crystals are initiated as ice spheres of 10μm diameter. Habit is assumed to be that expected for ice crystals growing at observed temperatures. Single crystals grow continuously in the model by the vapor diffusion process, assuming equilibrium between latent heat production due to mass growth and molecular diffusion of heat away from the crystal. Ice crystal terminal velocity is parameterized. Some calculations are made where riming processes are included in the calculation of crystal terminal velocity. A weighted transition from the terminal velocity equation for unrimed to rimed crystals is performed where riming is assumed to occur. Aggregation processes were not included. Ice crystal fallspeed is balanced by the vertical velocities, calculated in the first part of the model, while advecting the crystal with the horizontal wind field.

The model used in this study is subject to limitations and is used only for qualitative comparison of possible cloud seeding situations. The model can only be applied to stably-stratified flow with no significant blocking. Entrainment and the effect of latent heat release are neglected. Diffusion and spreading of the air parcel are assumed not to occur. This would affect the kinetics of nucleation since it is dependent on the concentration of particles in the air parcel. Model terrain is idealized. Ice crystal habit and fall speed parameterization is based on simple, ideal crystals, rarely observed in mountain precipitation. However, the purpose of using the model is a) to demonstrate how chemical kinetic information can be incorporated into a

theoretical cloud model and b) to show how rates and mechanisms of ice nucleation influence cloud ice crystal and precipitation patterns. These objectivess can be achieved, at least in a relative sense, with the model.

Kinetic ice nucleation processes have been incorporated into the first part of the model. Nucleation begins when the condensate production rate is positive, assumed to correspond to water saturated conditions. Condensate production rates greater than zero, assumed to correspond to relative values of water supersaturation, generally increased in value as the barrier crest was approached. Clouds in the model are 'seeded' at their upwind edge with an air parcel containing a population of 1000 ice nucleating 2AgI·NaI aerosol particles per liter. This seeding rate was observed in the Bridger Range Experiment (Super and Heimbach, 1983). The air parcel was assumed to remain coherent as it traversed the model domain. Ice nuclei remain in the parcel while nucleated ice crystals may leave the parcel as they grow and fallout. Time used in the kinetics is calculated across the horizontal domain at 1km intervals by dividing the horizontal distance by the wind speed.

The first order rate expression used is

$$C_{N,t} = C_{N,t-\Delta t}\exp(-k_n \Delta t) \qquad (3.3.1)$$

where k_n is the empirical rate constant of ice nucleation and Δt is the increment of time from the previous calculation point. The number of aerosol particles that nucleate ice is also controlled by the yield, Y, of the nucleant, or effectivity, which is temperature dependent. The relationship

$$Y = c_1\exp(c_2 T) \qquad (3.3.2)$$

is used where c_1 and c_2 are empirical constants determined from yield measurements. An upper limit is imposed where, at temperatures less than -18.0°C, the yield of ice crystals is 100%. The upper limit is used to calculate percentages (Y_T/Y_{-18}) of ice nuclei that can function within the time interval.

The number of ice crystals in the parcel is calculated as the difference between the number of nuclei at the beginning of the time step and the number of nuclei remaining at the end of the time step. The difference is multiplied by the yield percentage. The ice nuclei not nucleated due to yield considerations are brought foward to the next time step. Knowing the number of ice crystals produced along a streamline across the model domain, ice crystal trajectories at selected points are calculated using the second part of the model.

IV. INSTRUMENTATION AND ANALYSIS PROCEDURES

4.1 Instrumentation

4.1.1 CSU Standard Aerosol Generator

The CSU standard test generator used for this study is similar in design to the spray-nozzle type generator presented by Vonnegut (1950). An acetone solution containing silver iodide and sodium iodide is atomized in a commercial atomizing kerosene furnace spray nozzle. A propane flame just above the nozzle ignites and vaporizes the sprayed acetone solution. The AgI-NaI rapidly condenses to form aerosol particles as the smoke rises and cools.

The acetone solution was made by dissolving 10g AgI and 3.19g NaI in 0.633 liters of acetone producing a solution 2% by weight AgI. The mole ratio of AgI to NaI was 2:1. The burn rate of the generator was measured periodically and ranged from 23 to 25 ml/min. The aerosol size spectrum was not measured in this study but was assumed to be approximately the same as that measured by DeMott (1982) for AgI and AgI-AgCl particles generated from 2% AgI solutions in the same generator.

4.1.2 Vertical Dilution Tunnel and Sample Procedure

The aerosol generator was operated below a vertical wind tunnel described in Garvey (1975) and DeMott (1982). The aerosol sample was collected with a 4.25 liter syringe at the first rooftop platform. Mixing of the aerosol, controlled by the airflow in the tunnel, was

assumed to be uniform. Experiments were conducted with either natural draft or increased airflow induced by a fan operated at maximum speed.

The sample collected at rooftop could be further diluted by repeatedly expelling a portion of the aerosol sample in the syringe and drawing AgI aerosol free dilution air as often as necessary. Two types of dilution air were used. In one set of experiments the dilution air was filtered and dry (-30°C dewpoint). In another set of experiments dilution air was drawn from a 1000 liter tank at room temperaure. The interior of the tank was lined with blotting paper and contained several gallons of water. The air in the tank was assumed to be saturated or nearly saturated with water vapor due to evaporation from the water surface and the blotting paper. A small fan placed in the tank was used to assure uniformity of water vapor pressure. Estimates of the amount of water vapor, in grams, drawn in the sampling syringe was made to facilitate analysis. Dilution air tested in the isotermal cloud chamber was found to be free of ice nuclei.

4.1.3 Isothermal Cloud Chamber

The CSU isothermal cloud chamber (ICC) used in this research is described by Garvey (1975), DeMott (1982), and DeMott, et al. (1983). Calibrations of dewpoint (liquid water content) and airflow was made by DeMott (1982). One modification has been made for the present study. The ultrasonic nebulizer has been lowered about 2 feet below the chamber in order to install a plenum (Fig. 3). The plenum allows the the larger drops produced by the nebulizer to settle out while the smallest droplets can enter the chamber. The precooled airflow rate was greatly reduced because less cooling of the smaller droplets was necessary as they move moved up the stand tube. The new droplet size spectrum was

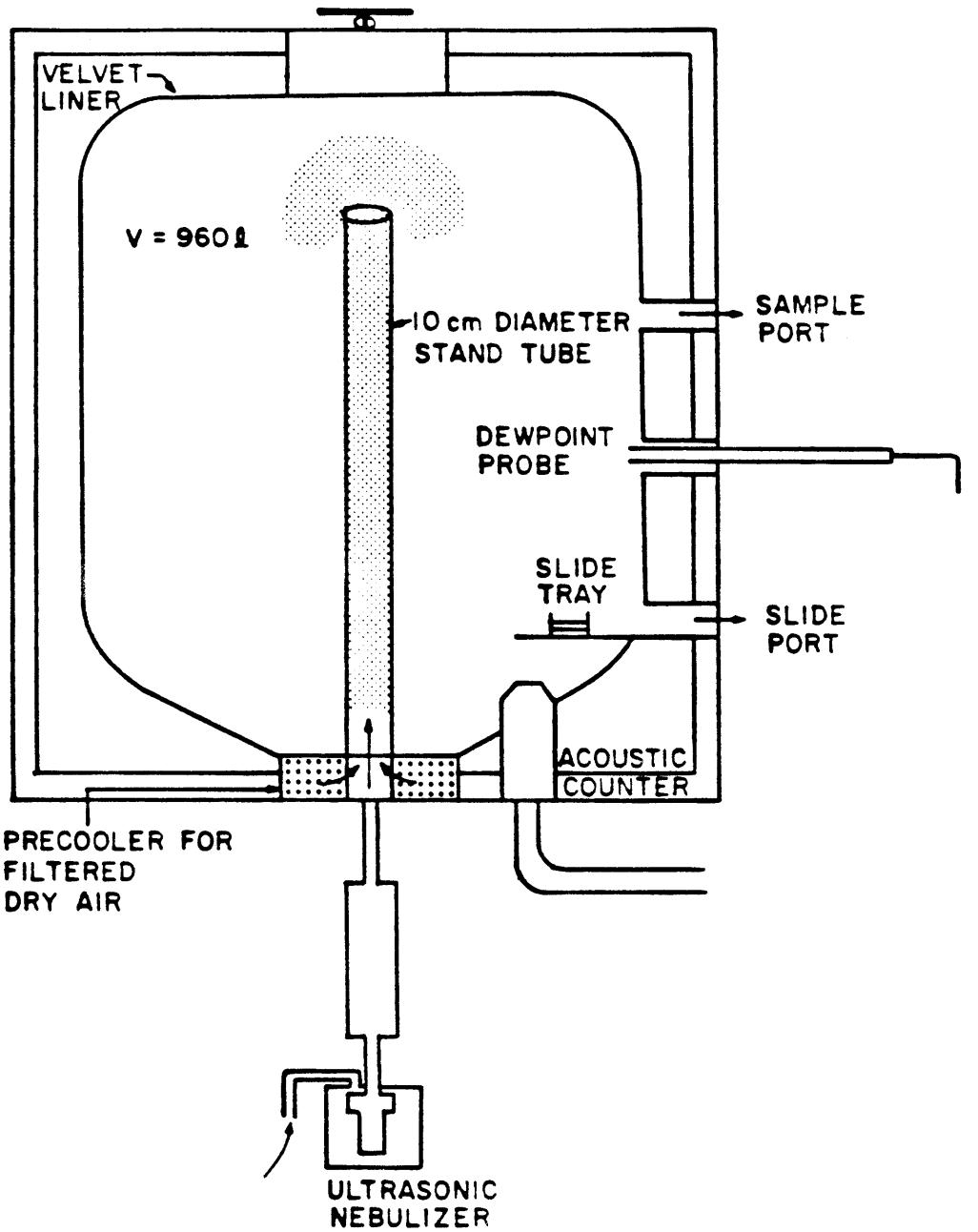

Figure 3: Schematic diagram of the CSU Isothermal Cloud Chamber.

not measured but is not expected to effect the condensation-freezing process. Liquid water content can be varied from 0.3 to 3.0 gm^{-3}. Maximum error is ± 0.2 gm^{-3} at the coldest temperatures

4.2 Experimental Procedures

The kinetic characterization of 2AgI·NaI ice nuclei was conducted by measuring the rates and yields of ice crystal production. A single chamber or aerosol variable was changed with each experiment to determine that variable's effect on ice nucleation. The variable of primary concern in this study is water vapor concentration, controlled in a qualitative manner. In one set of experiments, water saturation was maintained in the ICC by injecting the sample diluted with dry, $-30^{o}C$ dewpoint air. The alternate experiment involved injecting the sample diluted with moist, room temperature air into the ICC which is assumed to induce transitory water supersaturations. Both sets of experiments, saturated and supersaturated, or dry and moist, were tested at several chamber temperatures ranging from $-8^{o}C$ to $-20^{o}C$. At one temperature, $-12^{o}C$, seperate tests were made to determine the effect of liquid water content (cloud droplet concentration) and aerosol size on ice nucleation by both dry and moist aerosol samples.

The testing procedure and ice crystal monitoring technique used in this study is outlined in Garvey (1975).

4.3 Analysis of Laboratory Data

4.3.1 Determination of Rates

Kinetic reaction rate equations were derived in sections 3.1 and 3.2. Ice nucleation rates are expected to be characteristic of a first order process (DeMott, et al., 1983). Ice crystal production rates obtained in this research, assumed to be first order, were plotted

according to eq. 3.2.13, repeated here,

$$\ln(C_{IC,\infty} - C_{IC,t}) = \ln C_{N,o} - k_a t. \qquad (4.3.1)$$

where C_{IC} represents cumulative number of ice crystals counted on slides at the bottom of the chamber and k_a is the apparent or measured rate constant. The use of number rather than the concentrations of ice crystals does not affect the determination of first order rate constants. In the plot of natural log of ice crystals versus time, the slope is equal to the apparent rate constant, k_a , and the intercept is equal to the yield, $C_{N,o}$, or total number of ice crystals counted. This plot differs from those presented by DeMott (1982) and DeMott, et al. (1983) in that plots are not normalized. Determination of rates and yields are not affected by this method. In some cases, visualization of shifts in rate and yield with parameter changes can be improved.

If obvious curvature resulted from plotting data according to eq. 4.3.1, a first order, single step rate process for the observed production of ice crystals was ruled out. Data was then replotted assuming a zero order and second order rate process. The zero order process, following eq. 3.1.7, can be written as

$$C_{IC,t} = k_a t \qquad (4.3.2)$$

where the slope equals the apparent rate constant. The second order process follows from eq. 3.1.6;

$$\frac{1}{C_{IC,\infty} - C_{IC,t}} = \frac{1}{C_{IC,o}} - k_a t. \qquad (4.3.3)$$

If the data forms a straight line when either of the two equations above are applied, then the apparent order of ice crystal production can be defined.

4.3.2 Data Correction

Two factors that influence the ice nuclei population in the ICC other than ice nucleation have been discussed in DeMott (1982) and DeMott, et al. (1983). Diffusion of aerosol pariticles to the walls of the chamber, estimated to be of small magnitude, was neglected. The exponential rate of loss of nuclei due to airflow into and out of the chamber was given as

$$\frac{dC_N}{dt} = -\alpha C_N V^{-1} \qquad (4.3.4)$$

where α is the airflow dilution rate, constant at any temperature and liquid water content, and V is the chamber volume, equal to 960 liters. A constant airflow through the chamber is necessary to continuously supply and cool the cloud particles. Airflow was monitored during the experiments by recording the back pressure on the precooler. Figure 4, from DeMott (1982), shows the airflow dilution rate, α, versus precooler pressure. A check was made which proved that airflow versus pressure had not been altered in the time following the original calibration.

The value $-\alpha/V$ is the first order rate constant for the parallel or simultaneous airflow process. As described in section 3.2, rate constants of parallel processes are summed. The apparent rate constant, k_a of eq. 4.3.1 is the sum of the nucleation and airflow rates:

$$k_a = k_n + \frac{\alpha}{V}. \qquad (4.3.5)$$

As outlined in Chapter III, solving for the two processes of nucleation and airflow, the observed kinetic process is

$$\ln(C_{IC,\infty} - C_{IC,t}) = \frac{k_n \ln C_{N,o}}{k_n + \frac{\alpha}{V}} - (k_n + \frac{\alpha}{V})t. \qquad (4.3.6)$$

Rate constants of nucleation, k_n, were determined by subtracting airflow

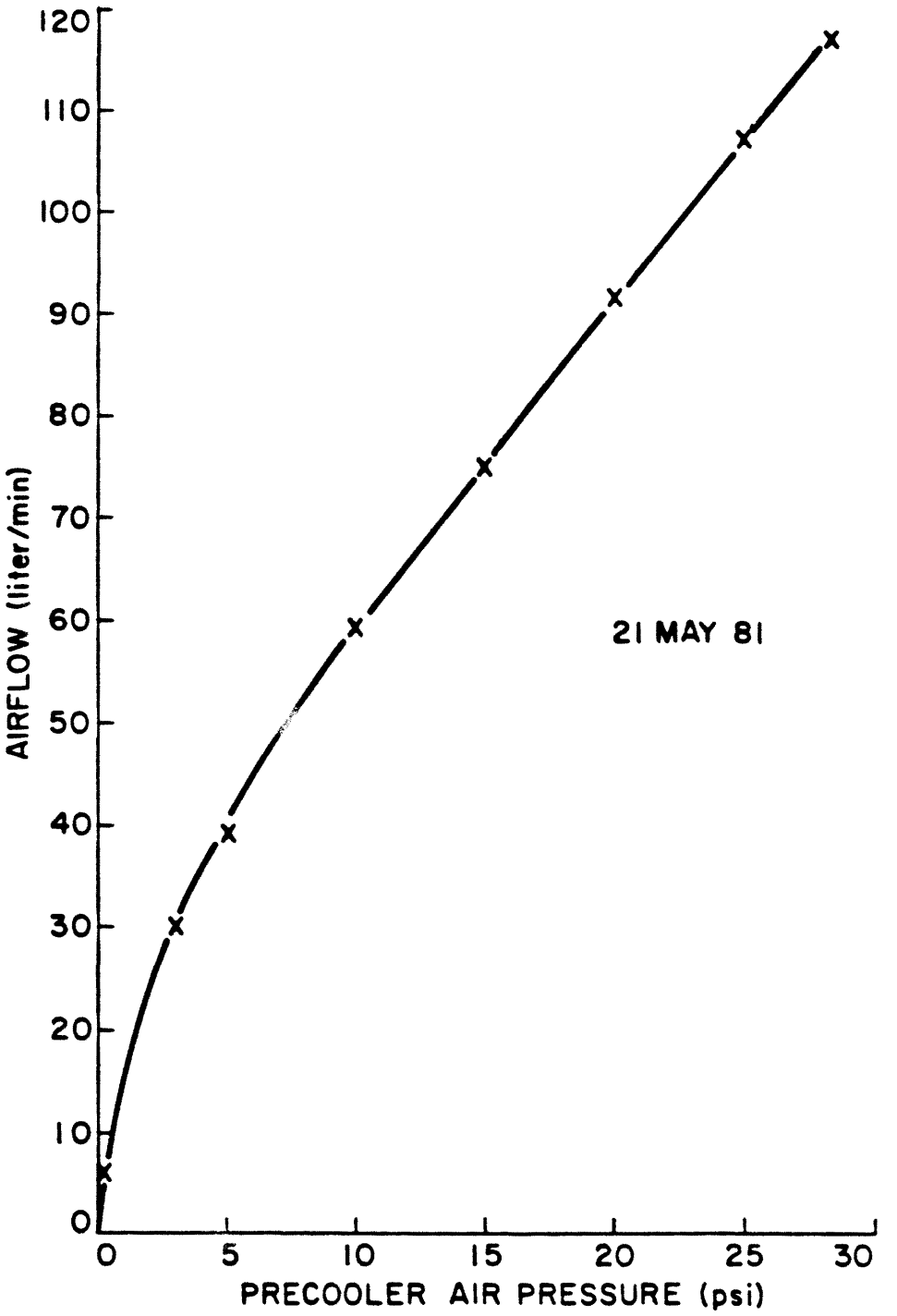

Figure 4: Rate of airflow through the ICC as a function of precooler pressure. From DeMott (1982).

rates from the observed rates, or slopes, of ice crystal formation. The initial number of ice nuclei which function to produce ice, $C_{N,o}$, was determined by solving eq. (4.3.6) for t=0,

$$\ln(C_{IC,\infty}) = \frac{k_n \ln C_{N,o}}{k_n + \frac{a}{V}} \qquad (4.3.7)$$

which corresponds to the intercept of the kinetic plots. After corrections for airflow dilution by subtracting $\frac{a}{V}$ from the slope and from the denominator of the intercept, the kinetic nucleation equation becomes

$$\ln(C_{IC,\infty} - C_{IC,t}) = \ln C_{N,o} - k_n t. \qquad (4.3.8)$$

Corrected kinetic plots can then be constructed knowing the new intercept and slope.

4.3.3 Determination of Yield (Effectiveness)

Ice nucleation yield has traditionally been referred to as effectiveness and defined as the number of ice crystals produced per gram of AgI. Ice nucleation effectiveness from 2AgI·NaI aerosol particles were determined by the method outlined in DeMott (1982) and DeMott, et al. (1983) using the equation:

$$E = N_{IC} \times \frac{A_C}{A_V} \times \frac{R_D}{R_G} \times \frac{D_S}{V_S} \qquad (4.3.9)$$

E: effectivity (yield) (#/g AgI)
N_{IC}: total number of ice crystals collected per slide viewing area (corrected for dilution)
A_C: chamber cross sectional area (cm^2)
A_V: microscope viewing area (cm^2)
R_D: wind tunnel dilution rate ($l\ min^{-1}$)
R_G: AgI generation (burn) rate ($g\ min^{-1}$)
D_S: syringe dilution factor
V_S: syringe volume (l)

Values of constants used in the effectivity equation were identical to that reported in DeMott (1982). The number of ice crystals collected

had to be corrected for the airflow which carries potential ice nuclei out of the chamber before they form ice crystals.

4.3.4 Determination of Energy of Activation

In section 3.1, the relation between kinetic rates and temperature was discussed. In general, a temperature dependence indicates an energy requirement for the process. Where applicable, the Arrhenius relation and the Eyring or activated complex relation, equations 3.1.13 and 3.1.14, were applied to the data. Energy of activation, and entropy and enthalpy of activation were thus determined as well as a general relation of ice nucleation rate versus temperature.

4.4 Theoretical Model Experiments

Calculations using the cloud model were made as case studies. Input data was obtained from the Colorado Orographic Seeding Experiment (COSE) III, conducted in the Park Range of northern Colorado. The mountain barrier profile of the model approximates that of the Park Range. Rawinsonde data obtained 60 km upwind of the barrier crest initiated model runs. Air parcel trajectories were plotted on the mountain profile of Fig. 2. At intervals along the trajectory the air parcel time and the total number of ice nuclei which have formed ice crystals were noted. Ice crystal trajectories calculated at intervals along the path of nucleation indicate the portion of the air parcel trajectory in which nucleation events may result in precipitation and where along the mountain barrier the crystals reach the surface. This implicitly gives the number or proportion of nucleation events which forms precipitation as a function of the spatial and temporal distribution of nucleation events.

V. LABORATORY RESULTS

5.1 Ice Nucleation Rates

The kinetics of ice nucleation by 2AgI·NaI aerosol particles measured in the ICC was assumed to be first order with respect to nuclei and were plotted using eq. 4.3.1. The first set of experiments to be discussed are those in which the aerosol sample was diluted with dry air. These experiments include the effect of temperature, liquid water content (LWC), and aerosol size on the nucleation rate and are illustrated in figs. 5-7. The next set of experiments presented are those in which the aerosol sample was diluted with varying amounts of moist air. It is assumed that moist air dilution and subsequent injection into the water saturated ICC creates a transitory water supersaturation. The effect of temperature, liquid water content, and aerosol size were also investigated. Results of experiments involving water supersaturations are shown in figs. 8-11.

5.1.1 Rates at Water Saturation

The solid lines on fig. 5 show the observed kinetic rate of decay of ice crystal production by 2AgI·NaI aerosol particles as a fuction of temperatures from -8 to -14°C. All aerosol samples were diluted with dry air, so that chamber moisture was assumed to be held at water saturation. Liquid water content was constant at 0.5 gm^{-3} for these experiments. Aerosol size was assumed to be constant based on a constant generating method. Experiments were triplicated to check for

Figure 5: First order kinetic plot of decay of ice crystal production at the indicated temperatures, dry dilution. LWC=0.5 gm^{-3}. Natural wind tunnel draft. Solid line indicates observed kinetic rate. Dashed line indicates rate and yield corrected for airflow dilution.

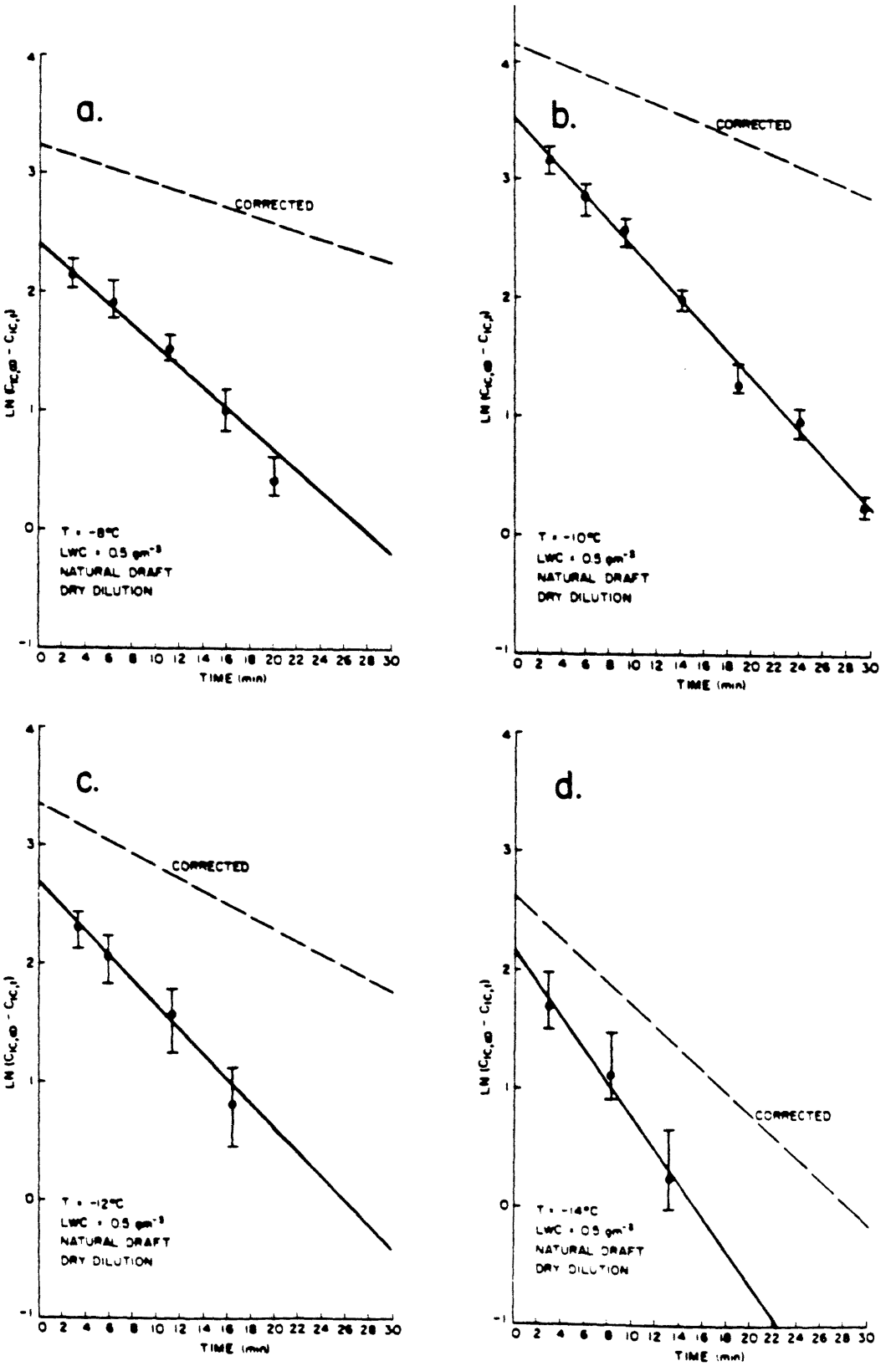
a.
CORRECTED
T = -8°C
LWC = 0.5 gm⁻³
NATURAL DRAFT
DRY DILUTION
TIME (min)
b.
CORRECTED
T = -10°C
LWC = 0.5 gm⁻³
NATURAL DRAFT
DRY DILUTION
TIME (min)
c.
CORRECTED
T = -12°C
LWC = 0.5 gm⁻³
NATURAL DRAFT
DRY DILUTION
TIME (min)
d.
CORRECTED
T = -14°C
LWC = 0.5 gm⁻³
NATURAL DRAFT
DRY DILUTION
TIME (min)

repeatability and results were averaged. Rate constants (slopes) of the observed rates as a function of temperature are listed in table 1.

Table 1
RATE CONSTANTS AS FUNCTIONS
OF TEMPERATURE (DRY DILUTIONS)

TEMP(C)	LWC(g/m3)	DRAFT	OBS.RATE(/min)	(NUCL.RATE) COR.RATE(/min)
-8	0.5	nat	0.0874	0.0327
-10	0.5	nat	0.1058	0.0441
-12	0.5	nat	0.1042	0.0535
-14	0.5	nat	0.1433	0.0926

Observed rates were corrected for the effect of airflow dilution as described in section 4.3.2 by subtracting the dilution rate. Resulting corrected rate constants, which are actual rate constants of ice nucleation by the aerosol, are listed in the last column of table 1. Values of the nucleation rate constants clearly increase, or become faster, at water saturation as the temperature decreases for any constant set of cloud conditions and aerosol characteristics at water saturation.

The initial number of ice nuclei used in each experiment was corrected for airflow dilution by using eq. 4.3.7. The resulting corrected kinetic rate plots, or rates of nucleation, are indicated by the dashed line in fig. 5.

A problem was encountered as experiments were attempted at temperatures colder than $-14^{o}C$. After correcting for airflow dilution, which becomes large as temperatures decrease (fig. 4), corrected rate constant values were near zero and in a few cases, were slightly positive. From eq. 4.3.5, this would indicate that airflow dilution was approximately equal to or greater than the rate of nucleation. The depletion of ice nuclei then became dominated by the parallel process of

dilution. Since dilution removes potential ice nuclei from the chamber, an accurate assessment of nucleation rates could not be made.

Nucleation rates as a function of liquid water content of the ICC cloud are illustrated in fig. 5c and fig. 6. These experiments were conducted at -12°C with natural draft wind tunnel conditions. Rate constants of the observed and corrected rates of ice crystal production are listed in table 2. A raise in LWC corresponds, approximately, to a proportionate raise in cloud droplet concentration (DeMott, 1982). Within the limits of experimental error, the corrected rate of nucleation was observed not to change when the LWC was raised form 0.5 to 1.5 gm^{-3}. When the LWC was raised again to 3.0 gm^{-3}, the rate of nucleation increased by 0.02 min^{-1}. This indicates that when the droplet concentration of a cloud raises over a certain threshold level the rate of contact of droplets by nuclei increases to an observable value and the droplet population begins to influence the nucleation rate in a parallel process. In this case, the increase in rate associated with the increased LWC implies that contact nucleation is possible for 2AgI·NaI aerosol particles. The rate of contact, however, is not large even at liquid water contents as high as 3.0 gm^{-3}.

Table 2
RATE CONSTANTS AS FUNCTIONS
OF LWC (DRY DILUTIONS)

TEMP(C)	LWC(g/m3)	DRAFT	OBS.RATE(/min)	(NUCL.RATE) COR.RATE(/min)
-12	0.5	nat	0.1042	0.0535
-12	1.5	nat	0.1088	0.0482
-12	3.0	nat	0.1316	0.0710

The effect of aerosol size on nucleation rate by 2AgI·NaI particles is presented in table 3 and in figs. 5c, 6, and 7. DeMott (1982) has

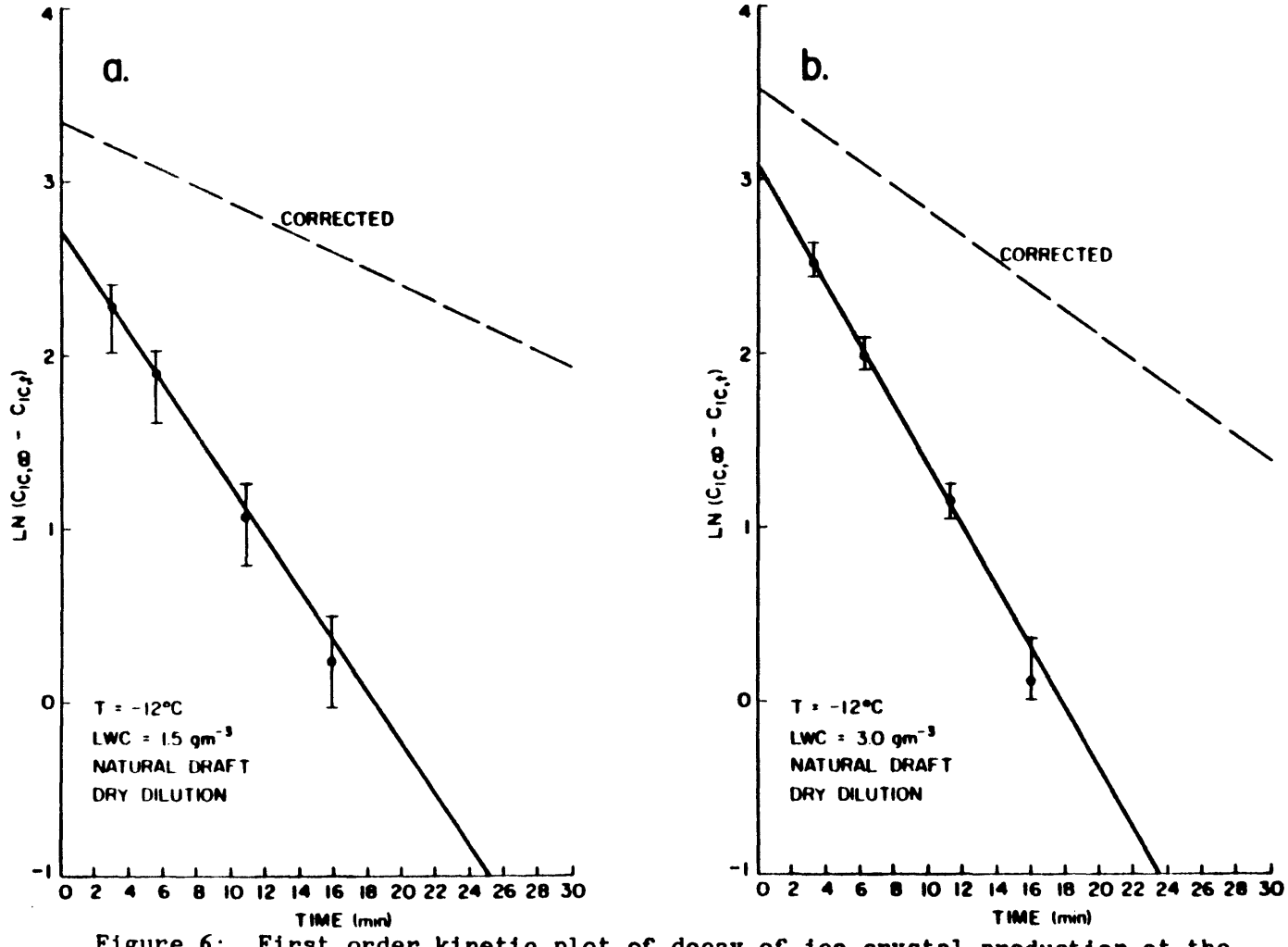

Figure 6: First order kinetic plot of decay of ice crystal production at the indicated LWC, dry dilution. Temperature -12°C. Natural wind tunnel draft. Solid line indicates observed kinetic rate. Dashed line indicates rate and yield corrected for airflow dilution.

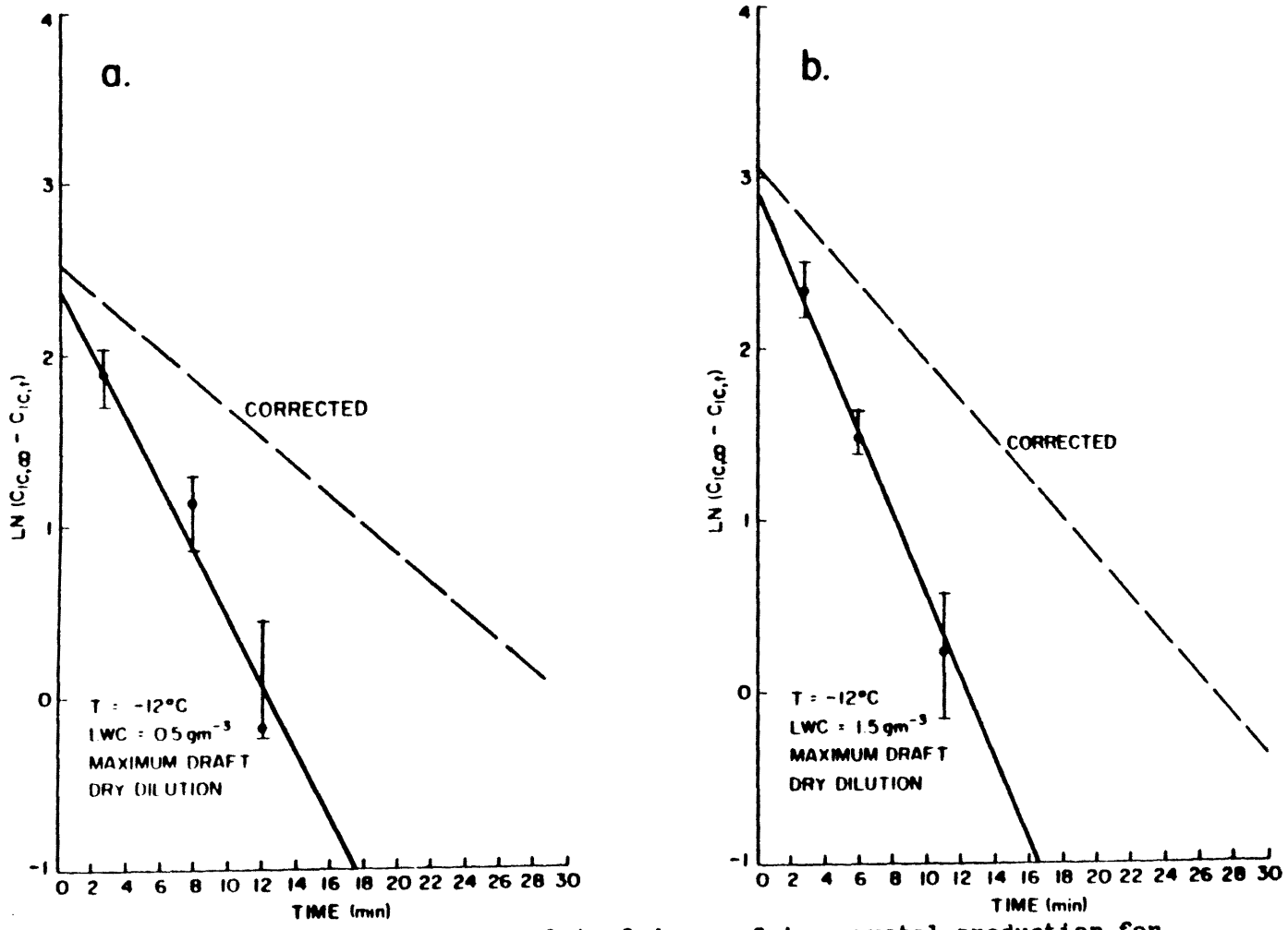

Figure 7: First order kinetic plot of decay of ice crystal production for particles generated at maximum fan speed, dry dilution. Temperature -12°C. LWC as indicated. Solid line indicates observed kinetic rate. Dashed line indicates rate and yield corrected for airflow dilution.

shown that when the wind tunnel draft is increased from natural to maximum, or approximately $1x10^5$ l/min to $3x10^6$ l/min, the mean particle diameter of aerosol generated from 2% AgI solutions decreases from 521.8 Å to 289.6 Å. When both the LWC was raised to 1.5 gm^{-3} and the particle size was decreased, the rate constant increased by 0.06 min^{-1}. Rate also increased at 0.5 gm^{-3} LWC when the aerosol particle size was reduced. The increased droplet concentration and the decreased particle size made conditions more conducive for an increased rate of contact nucleation to occur concurrently with the primary mode of condensation-freezing ice nucleaion.

Table 3
RATE CONSTANTS AS FUNCTIONS
OF PARTICLE SIZE (DRY DILUTIONS)

TEMP(C)	LWC(g/m3)	DRAFT	OBS.RATE(/min)	(NUCL.RATE) COR.RATE(/min)
-12	0.5	nat	0.1042	0.0535
-12	0.5	MAX	0.1363	0.0856
-12	1.5	nat	0.1088	0.0482
-12	1.5	MAX	0.1759	0.1153

5.1.2 Rates at Transitory Water Supersaturation

Experiments were conducted in which the aerosol sample was diluted, either in part or fully, with moist air from the holding tank. The amount of water vapor drawn into the syringe before injection into the ICC was estimated in grams H_2O_v. These are maximum values since water saturation in the tank was not assured. The exact magnitude of the amount of water vapor in the syringe was concluded to be unimportant in an absolute sense because the consequence of injecting the water vapor into the water saturated ICC could not be measured. Calculations of the extent of supersaturation produced also could not be made since the

response of the droplet population was not measured and could not be estimated. Water supersaturation produced from water vapor from the syringe became evident upon examination of the kinetics and yield of nucleation which significantly differed from that at water saturation. The presence of water supersaturation in the ICC was assumed to be transitory, both in space and time, because of the operation of the chamber which would quickly reestablish steady-state conditions. The values of amount of water vapor in the syringe reported below were used in a relative sense only, to compare different sets of conditions.

Experiments were conducted at -8, through -20°C, 0.5 gm^{-3} LWC, and natural draft wind tunnel conditions in which the final syringe dilution was made with moist air from the holding tank. Temperature in the tank varied from 18 to 22°C. The amount of water vapor drawn into the syringe before injection into the ICC was estimated to have a maximum value of 0.06 to 0.07 g H_2O_v. Ice crystal production rates were observed to be very rapid. Ice crystal fallout was complete within 2 to 4 minutes. At all temperatures, an average of 94% of the ice crystals were counted on slides after the first minute after injection, 99% were counted after the second minute, and 100% were counted after 4 minutes.

Because much of the process of ice crystal production occurs within the first minute after ice nuclei injection, visual counts of ice crystals were made primarily for yield measurements. The CSU acoustic ice crystal counter was used for a more detailed determination of ice crystal production rates. The counter, still being tested and calibrated at the time of this research, did not give accurate or consistent values of total ice crystals but is believed to report accurate temporal rates of ice crystal counts (Morrison, 1983).

Figure 8 shows the rates of ice crystal production at -10°C for a sample diluted with wet air plotted as a first order process. The plot is curved, indicating the process is not exponential. Curvature of the first order rate plots was observed for all experiments in which a wet dilution was made. Similarly, plotting the data as a second order process also resulted in a curve. Figure 9 shows the rate of ice crystal production plotted as a zero order, or linear rate process according to eq. 4.3.2. These plots resulted in straight lines for at least 80% of the observed reaction. The remaining 20% is not critical to the determination of the kinetics. Comparison of figs. 8 and 9b indicate that the linear plot is more appropriate in assessing the rate constant from the slope of the plotted data. (Data from the acoustic ice particle counter for experiments conducted at -12°C and wet dilutions was not available at the time this report was being written.)

The slope of the zero order rate plots give the apparent rate constant, k_a. In general, the values of k_a were very large. The half-life of the zero order ice crystal production rate was less than 30 seconds, compared to the half-life of dilution which ranges from five to 25 minutes. Corrections for air flow dilution were therfore not made. Table 4 shows the measured rate constants for these fast reactions at various temperatures, 0.5 gm^{-3}, and natural draft. There is no consistent variation of rate constant with temperature. Instead, rate constants roughly vary with the terminal velocity of the predominate crystal habit. Dendritic crystals at -16°C were counted at the slowest rate, plates at -10°C were counted twice as fast, and columns at -8°C had the largest rate constant. The large rate observed at -20°C is due to high ice crystal concentrations and will be explained in the next

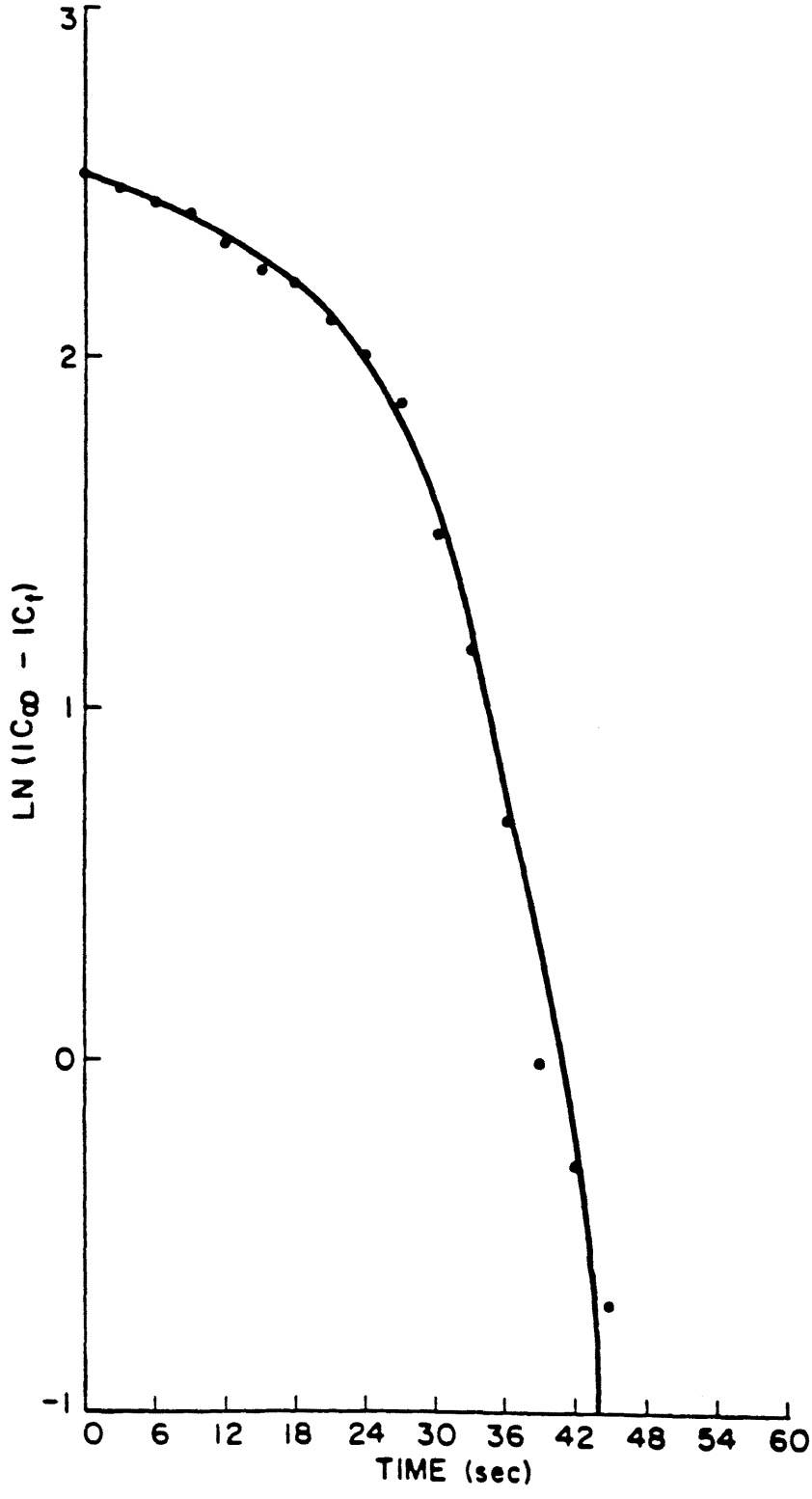

Figure 8: First order kinetic plot for wet dilution experiment at -10°C, 0.5 gm^{-3} LWC, and natural wind tunnel draft.

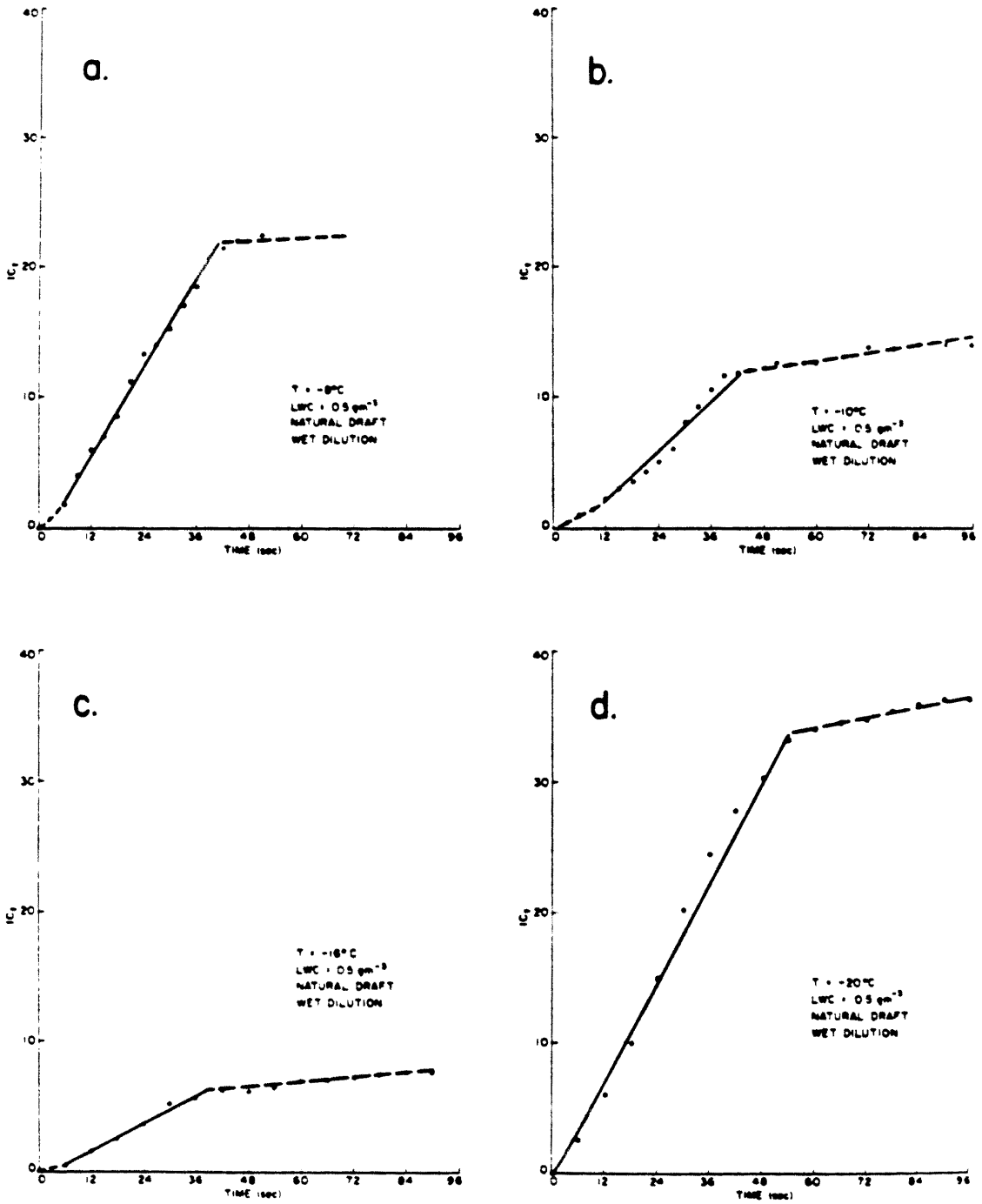

Figure 9: Zero order kinetic plot of ice crystal production at the indicated temperatures, wet dilution. LWC=0.5 gm^{-3}. Natural wind tunnel draft. Solid line indicates raw rate used to determine rate constant.

section. Since crystals of different habits have different terminal velocities, it is apparent that fallout of ice crystals was the rate determining, slowest step when water supersaturated conditions existed in the ICC.

Table 4
RATE CONSTANTS AS FUNCTIONS
OF TEMPERATURE (WET DILUTIONS)

TEMP(C)	OBS.RATE(#/min)
-8	34.09
-10	20.11
-16	10.25
-20	37.83

The rate of ice crystal production increased when the LWC was raised. At $-10^{o}C$, 1.5 gm^{-3} LWC, and natural draft the measured rate constant was 29.67 crystals/min as compared to 20.11 crystals/min at 0.5 gm^{-3} LWC. Acoustic ice particle counter data of runs done with aerosol of decreased size was not available at the time this report was being written. Slide count data at $-12^{o}C$, 0.5 gm^{-3} LWC, and maximum fan wind tunnel conditions indicate ice crystal production was rapid and complete within 2 minutes.

Another set of experiments done at water supersaturation were those in which partial moist air syringe dilutions were made. In these runs the first fraction of the final dilution was made with dry, filtered air, and the remaining portion was made with air from the holding tank containing moist air. Fractions used were 1/2, 3/8, and 1/4, each representing decreasing amounts of water vapor drawn into the syringe. The effect of varying the amount of water vapor injected into the ICC was assumed to vary the extent of water supersaturation produced in the chamber in a proportional manner. Table 5 lists the percentage of the

total crystals counted on slides after one minute as a function of various amounts of wet air dilution, temperature, LWC, and aerosol size. The percentage of crystals produced in one minute consistently decreases as the amount of water vapor injected into the ICC, or water supersaturation is decreased except at -16°C, within experimental error. This relation is graphically shown in fig. 10. Temperature and other cloud and aerosol variables do not appear to influence the effect of decreasing supersaturation.

Table 5
PERCENTAGE OF TOTAL ICE CRYSTALS COUNTED IN ONE MINUTE FOR VARIOUS WET AIR SYRINGE DILUTIONS

TEMP(C)	LWC(g/m3)	DRAFT	FRACTION OF WET DILUTIONS	SYRINGE H_2O_v(g)	% CRYSTALS IN 1 MIN
-10	0.5	nat	1	0.06	98
-10	0.5	nat	1/2	0.03	74
-12	0.5	nat	1	0.065	97
-12	0.5	nat	1/2	0.04	76
-12	0.5	nat	3/8	0.03	45
-12	0.5	nat	1/4	0.02	14
-12	1.5	nat	1	0.07	91
-12	1.5	nat	1/2	0.03	88
-12	1.5	nat	3/8	0.025	22
-12	1.5	nat	1/4	0.02	4
-12	1.5	MAX	1	0.065	92
-12	1.5	MAX	1/2	0.03	92
-12	1.5	MAX	1/4	0.015	21
-16	0.5	nat	1	0.06	84
-16	0.5	nat	1/2	0.03	97
-16	0.5	nat	3/8	0.02	53
-16	0.5	nat	1/4	0.015	23
-20	0.5	nat	1	0.065	95
-20	0.5	nat	1/2	0.03	99
-20	0.5	nat	3/8	0.025	88
-20	0.5	nat	1/4	0.01	34

Following the first minute of ice crystal production, shown above to be a linear process, any remaining nucleation processes are observed

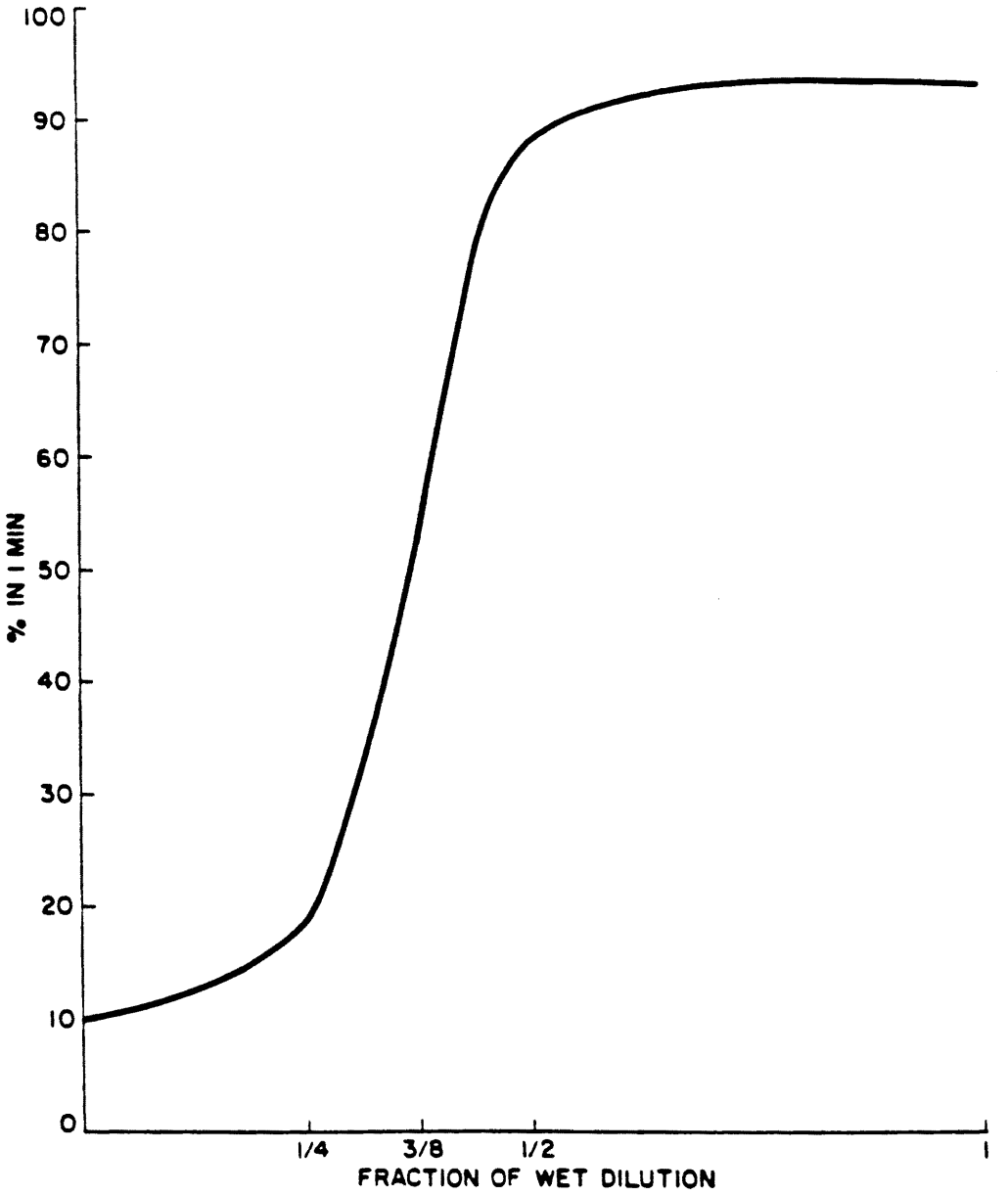

Figure 10: Percentage of total yeild produced in the first minute after injection of aerosol into the ICC as a function of amount of wet air dilution.

to occur at an exponential rate. To illustrate, data from experiments conducted at $-12^{o}C$, $0.5gm^{-3}$ LWC, natural draft, and wet dilutions from 1/4 to 1 is shown in fig. 11 as first order, exponential processes. Data from the first minute, which was observed to be zero order, was estimated with a straight line on the first order plot for illustrative purposes. After the initial burst of rapid ice nucleation due to supersaturations induced by the water vapor in the syringe, continued nucleation proceeded at an exponential rate nearly equal to the rate of ice crystal production at water saturation. Similar results were obtained at other temperatures. Table 5 and fig. 11 indicates that reduced transient water supersaturations affect proportionately smaller amounts of the total ice nuclei population without affecting the remaining ice nuclei, which continue to nucleate at an exponential rate. This indicates that two separate ice nucleation processes occur simultaneously on what can essentially be considered to be two separate nucleating species. The aerosol population used range in size from approximately 0.01 to 0.30 μm diameter. Increasing water vapor concentration, or supersaturation, would affect increasingly smaller sized aerosol particles and thus increasingly larger proportions of the aerosol population. A similar phenomenon was observed by DeMott (1982) and DeMott, et al. (1983) for the case of contact ice nucleation occurring concurrently with vapor deposition nucleation. Additionally, the amount of water vapor in the syringe required to have 50% of the aerosol particles nucleate via the fast mechanism and 50% by the slow mechanism is about 3/8 wet dilution or 0.02 to 0.03 g excess H_2O_v for all chamber and aerosol conditions (fig. 10).

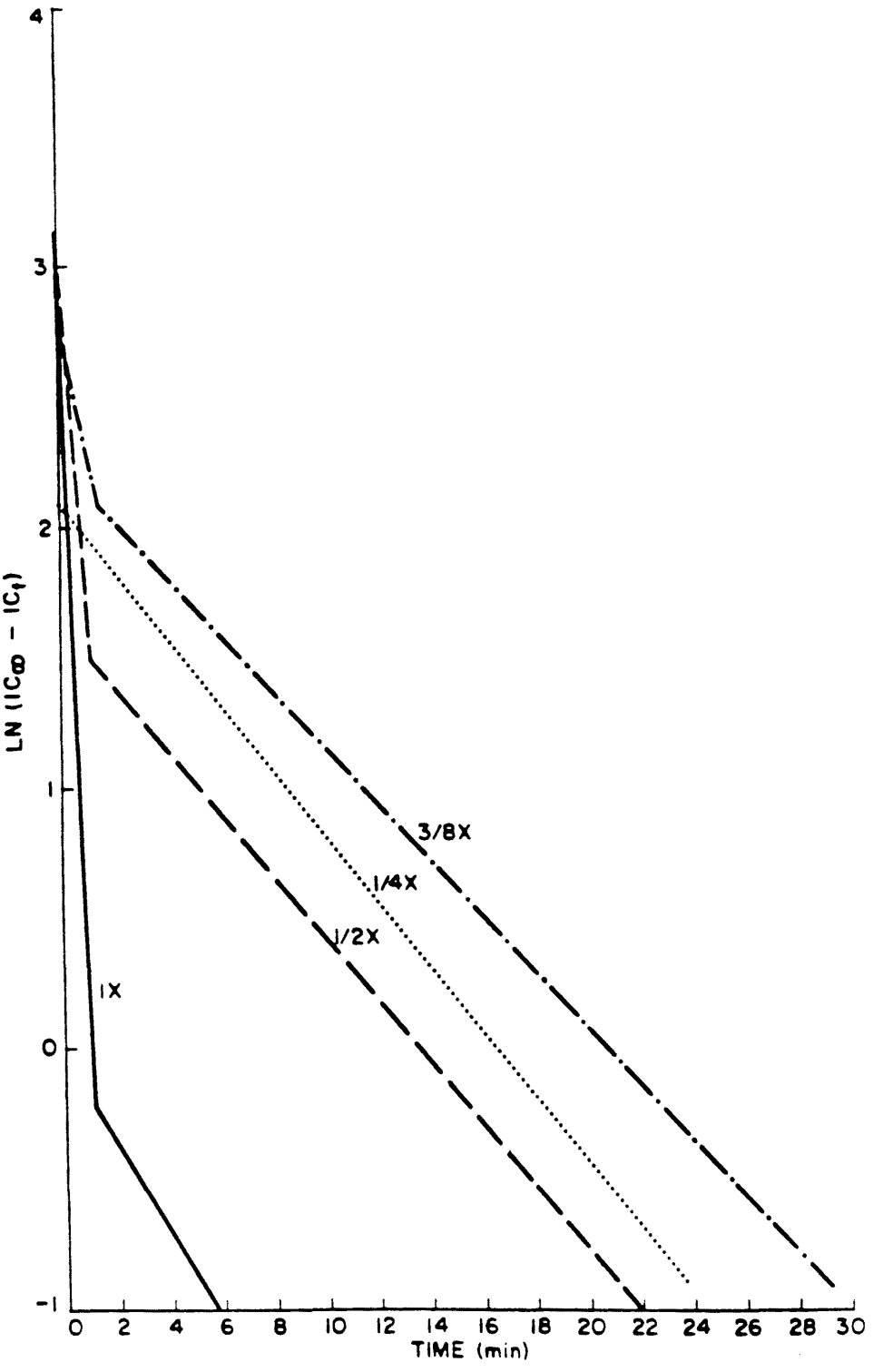

Figure 11: First order kinetic plot of decay of ice crystal production at -12°C, 0.5 gm^{-3} LWC, natural wind tunnel draft, for indicated amounts of wet air dilution.

5.2 Ice Nucleation Yield (Effectivity)

Yield of ice nucleation by 2AgI·NaI aerosol particles was measured as ice nucleation effectivity or number of ice crystals per gram of AgI as calculated using eq. 4.3.8. Results are shown in figs. 12-13. All figures show averaged results, corrected for air flow dilution as determined by eq. 4.3.7.

Yield from -8 to -14°C in experiments where aerosol samples were diluted with dry air and the slow mechanism was observed is shown in fig. 12. At temperatures below -14°C, yield measurements were not possible for reasons stated above, ie. airflow dilution became comparable or greater than the rate of nucleation so that corrections could not be made to the observed kinetics. At temperatures above -8°C, the aerosol sample could no longer be diluted before injection into the ICC. Moisture conditions inside the wind tunnel at the time of sampling could not be assesed. The amount of H_2O_v in the syringe was unknown in this case and experiments could not be distinguished as water saturated or supersaturated. At -7°C yield was measured as $2.21X10^{11}(g\ AgI)^{-1}$ and at -6°C yield was $1.67X10^{10}(g\ AgI)^{-1}$ which is the threshold of nucleation in the ICC.

Fig. 12 also shows the yield of ice nucleation for the fast mechanism when samples were diluted with moist air which induced water supersaturations in the ICC. The yield of ice nucleation at water saturation is shown for comparison. Beginning at -9°C, supersaturation enhances the yield of ice nucleation. The effectivity of wet samples closely follows that of Davis and Steele (1968) in fig. 1 for the same nucleant generated by the North American generator tested in the CSU ICC, whereas the effectivity of samples diluted with dry air resembles

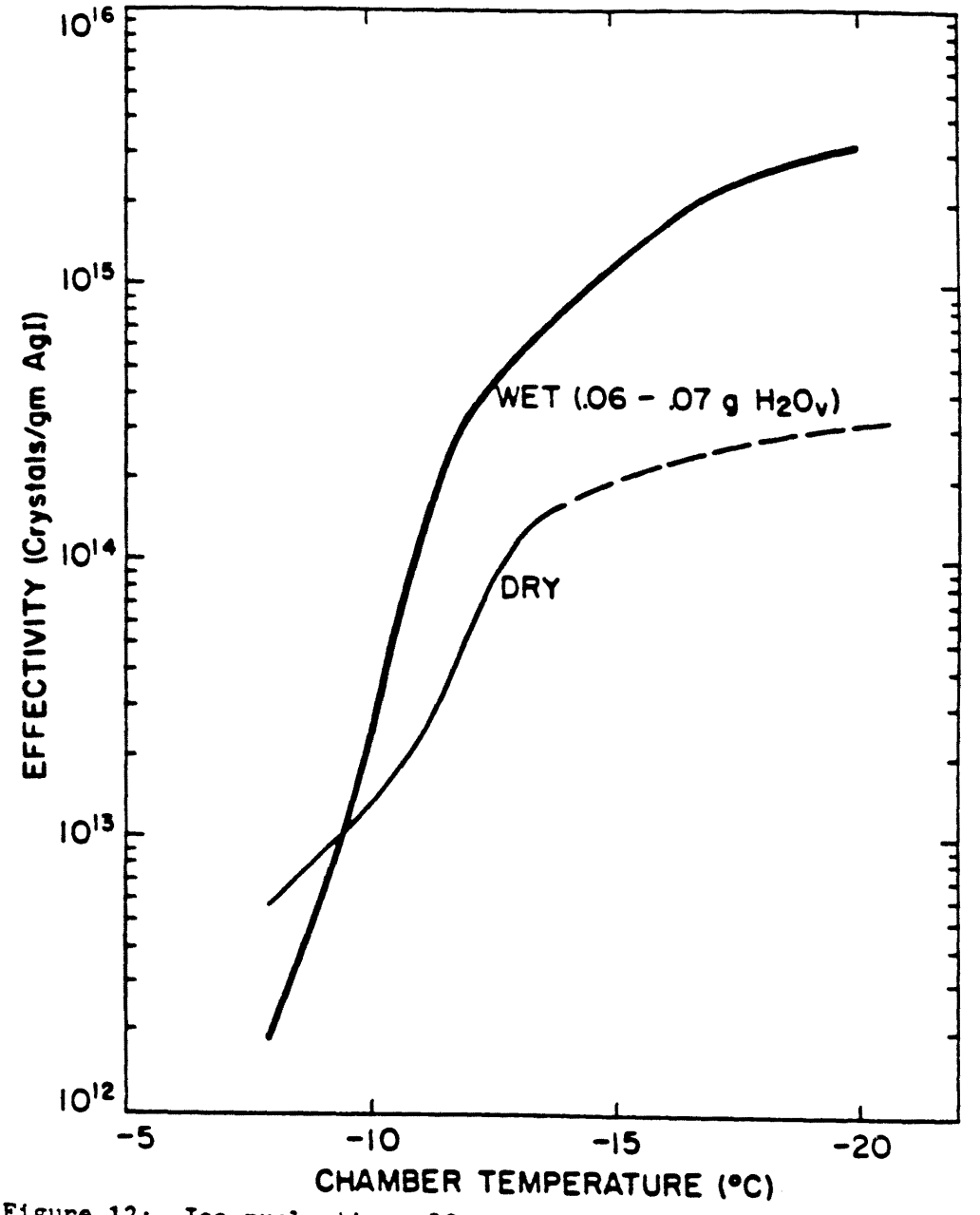

Figure 12: Ice nucleation effectivity, corrected for airflow dilution, as a function of temperature for 0.5 gm^{-3} LWC, natural draft. Dry indicates results obtained at water saturation. Wet indicates results at maximum water supersaturation. Dashed line shows estimate of effectivity at temperatures below -14°C.

that of Garvey (1975) for the same chamber and generator. As noted in Chapter II, prior to 1968, cloud droplets introduced into the chamber were not equilibrated to chamber temperature and large supersaturations were likely to have existed.

The results of varying the extent of water supersaturation in the ICC by making partial moist air dilutions is shown in fig. 13. In general, yield decreases as supersaturation is decreased. An exception is noted at $-16^{\circ}C$ where the yield increased between 1 and 1/2 moist dilution. Table 5 also indicates that the rate of nucleation increased at $-16^{\circ}C$ between 1 and 1/2 moist dilution. It is probable that experimental conditions could have caused the increase, such as a temporary drying of the moist dilution air in the holding tank or uncontrolled wind tunnel conditions resulting in an unknown dilution rate.

For experiments at $-12^{\circ}C$ the yield of ice nucleation increases in the following sequence. The lowest yields were observed at 0.5 and 1.5 gm^{-3} LWC, natural draft, and dry sample dilutions. Yield is slightly increased when LWC is raised to 3.0 gm^{-3} due to contact nucleation occuring simultaneously with the primary mechanism of condensation to droplets followed by freezing. Yield then increases at water saturation by a half order of magnitude when particle size is decreased by maximum wind tunnel draft. Higher yields occur when samples are diluted with moist air and the mechanism changes to the fast process. Yield is highest for moist air dilutions of aerosol of decreased particle size.

5.3 Energy of Activation of Ice Nucleation

The rate of nucleation at water saturation was shown above to be a function of temperature. Using the data in table 1 and the Arrhenius

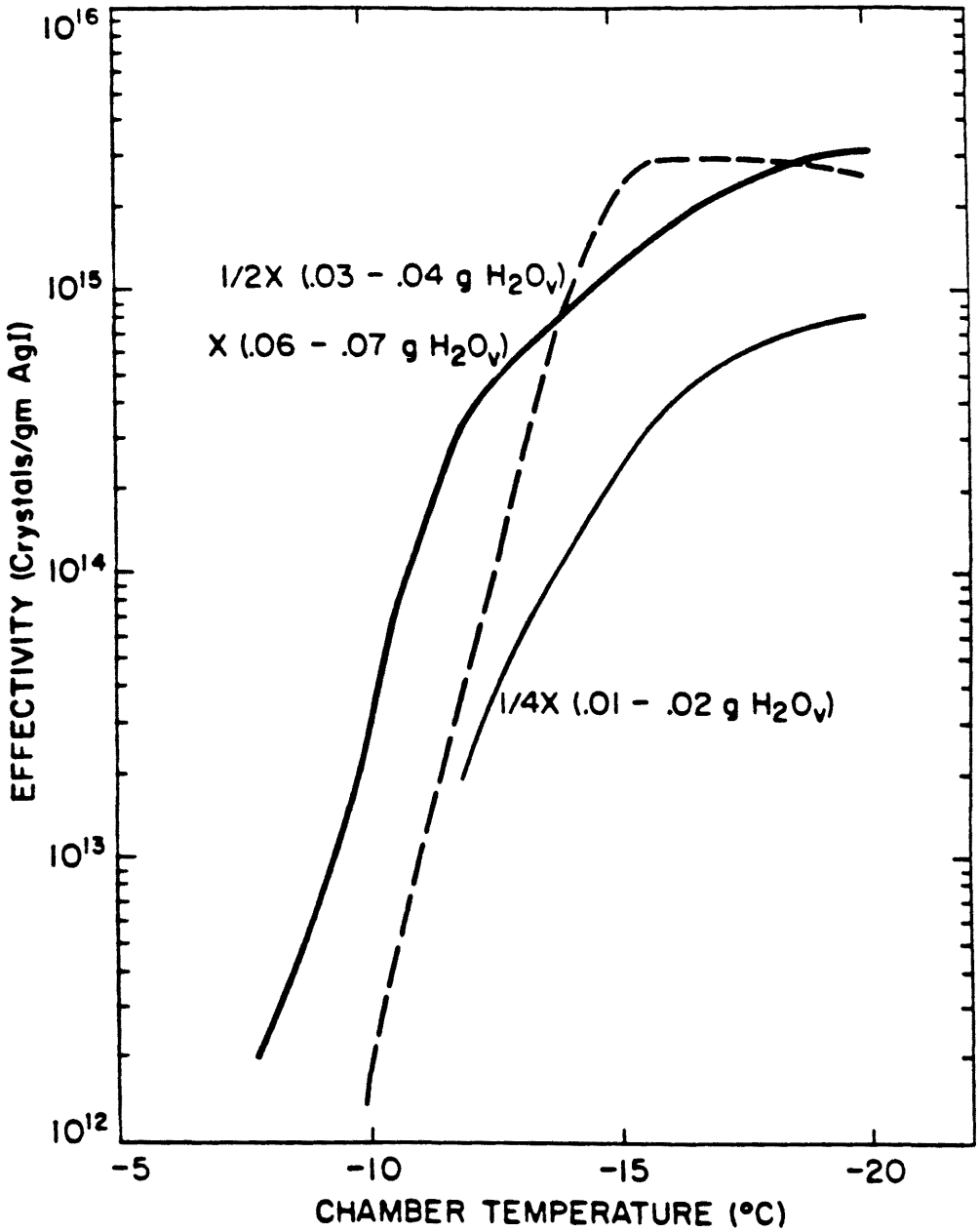

Figure 13: Ice nucleation effectivity as a function of temperature for 0.5 gm^{-3} LWC, natural draft, at the indicated amount of wet air dilution.

equation (eq. 3.1.14), the energy of activation of the nucleation process at water saturation was determined. Fig. 14 shows the plot of ln k_n versus T^{-1}. The intercept was extrapolated to determine the pre-exponential factor, A, and is equal to $8.77X10^{-30}$ s^{-1}. The slope of the line is equal to $-E_a/R$. The energy of activation, E_a was found to be -130 $kJmol^{-1}$ which is the amount of energy released upon nucleation. It is approximately 3 times larger than the latent heat of condensation of water and 22 times larger than the latent heat of fusion of water. From a plot of the Eyring or activated complex theory the enthalpy of activation was determined to be -88 $kJmol^{-1}$ and the entropy of activation was -638 $Jmol^{-1}{}^{o}K^{-1}$.

The assumption presented in section 3.2 of a constant concentration of water vapor in the ICC at water saturation, $k_n' = k_n C_V^v$, was used in the kinetic analysis of these experiments. If the rate constants of table 1 are divided by the concentration of water vapor, which varies with temperature, (assuming the exponent, v=1) and the data replotted, the pre-exponential factor changes to $2.89X10^{-28}$ sec^{-1} but the energy of activation, E_a, remains at -130 $kJmol^{-1}$. This is significant in that it implies that the concentration of water vapor does not influence the rate of nucleation and the exponent, v, is equal to 0.

Energy of activation could not be determined from an Arrhenius plot for nucleation at water supersaturation since a trend of rate with temperature was not evident and the concentration of water vapor could not be assessed.

5.4 Ice Nucleation Mechanisms

From the results of laboratory experiments discussed above, the mechanisms of ice crystal production by 2AgI·NaI aerosol particles in

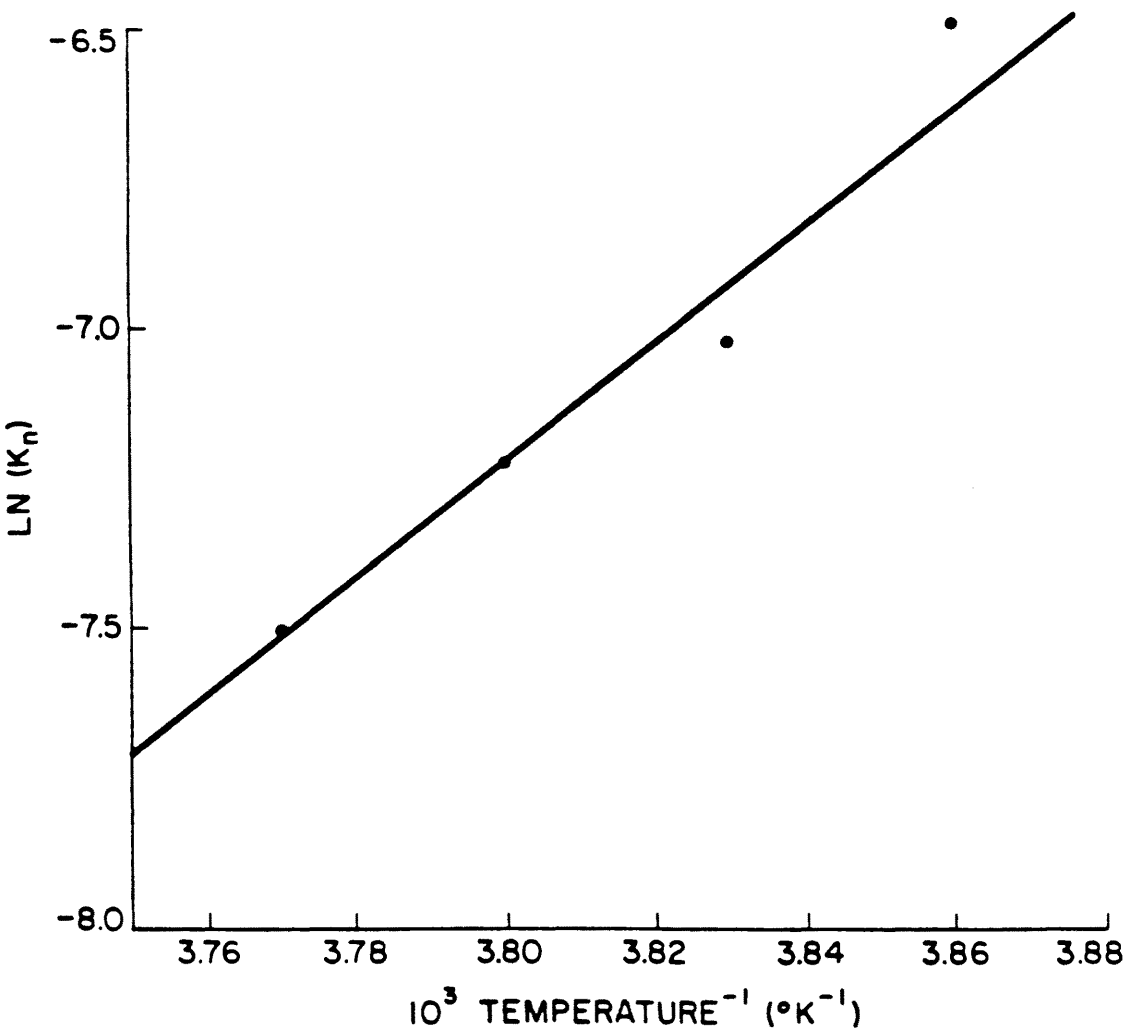

Figure 14: Arrhenius plot of corrected nucleation rates, dry dilution.

the ICC can be determined. Three mechanisms can be identified. One occurs at or slightly above water saturation, is slow, has a moderate yield, and has a large energy of activation. The second mechanism requires an unknown amount of water supersaturation, is very rapid, and has a higher yield than the slow mechanism. The third mechanism is contact nucleation.

The slow mechanism was shown to be a first order, or exponential rate process, dependent only on temperature. The rate law for this process can be expressed as

$$\frac{dC_N}{dt} = k_{n,s}C_N. \qquad (5.4.1)$$

The rate constant, $k_{n,s}$, is on the order of 0.1 min^{-1}. This rate is much slower than the predicted rate of growth and fallout of crystals in the ICC. The nuclei are strongly hygroscopic (Mossop, 1968, and Mossop and Tuck-Lee, 1968) and are assumed to form dilute solution droplets. Growth of a distribution of aerosol particles to eqilibrium sized droplets requires approximately five minutes to complete (Fukuta and Walter, 1970). Ice nucleation for the slow mechanism was observed to continue past this time for 20 to 40 minutes. Observed ice nucleation is independent of the concentration of water vapor or size of the aerosol particles. Therefore, drop growth is not rate determining. The process of ice formation by 2AgI·NaI occurs <u>after</u> the formation and growth of droplets. Another indication that ice nucleation occurs within the preformed droplet is the temperature dependence and related release of energy of activation associated with the process. Chang (1984) observed a two step process in individual drops where growth of droplets nucleated by AgI-NaI preceeds ice formation in the interior of

the drop. The mechanism of ice nucleation is condensation to droplets followed by freezing.

The energetics of ice nucleation at water saturation indicates that the process which occurs within the droplet is a chemical reaction. Large activation energy associated with processes involving particles, insoluble AgI in this case, is characteristic of chemical adsorption where chemical bonds are being broken and/or formed. Values for chemisorption are typically about 200 $kJmol^{-1}$. Physical adsorption activation energies are generally on the order of 20 $kJmol^{-1}$ (Atkins, 1982, p.1015). The activation energy of ice nucleation by 2AgI·NaI by condensation to droplets followed by freezing is -130 $kJmol^{-1}$, or three times the latent heat of condensation. The 2AgI·NaI forms a hydrated complex at relative humidities near 100% with either 3 or 4 moles water (Mossop and Tuck-Lee, 1968, Davis, 1969, Burkardt and Finnegan, 1970, Chen, et al., 1972, and Johnson and Davis, 1972). The energy of activation reported here indicates that the three mole hydrate ($2AgI \cdot NaI \cdot 3H_2O$) is the chemical form of the nucleant. The release of energy may be the result of destruction of the hydrogen bonds of the three water molecules in the 2AgI·NaI complex. Alternatively, three moles of water molecules may attach themselves to the hydrated water of the complex. The chemical reaction would be the the rate limiting step, after which ice nucleation can proceed rapidly.

The mechanism which functions above water saturation occurs at a faster rate. The rate of production of ice crystals was shown to be linear, or

$$\frac{dC_{IC}}{dt} = k_F. \qquad (5.4.2)$$

Fig. 15 shows a comparison of the ice crystal fallout rate by 2AgI·NaI

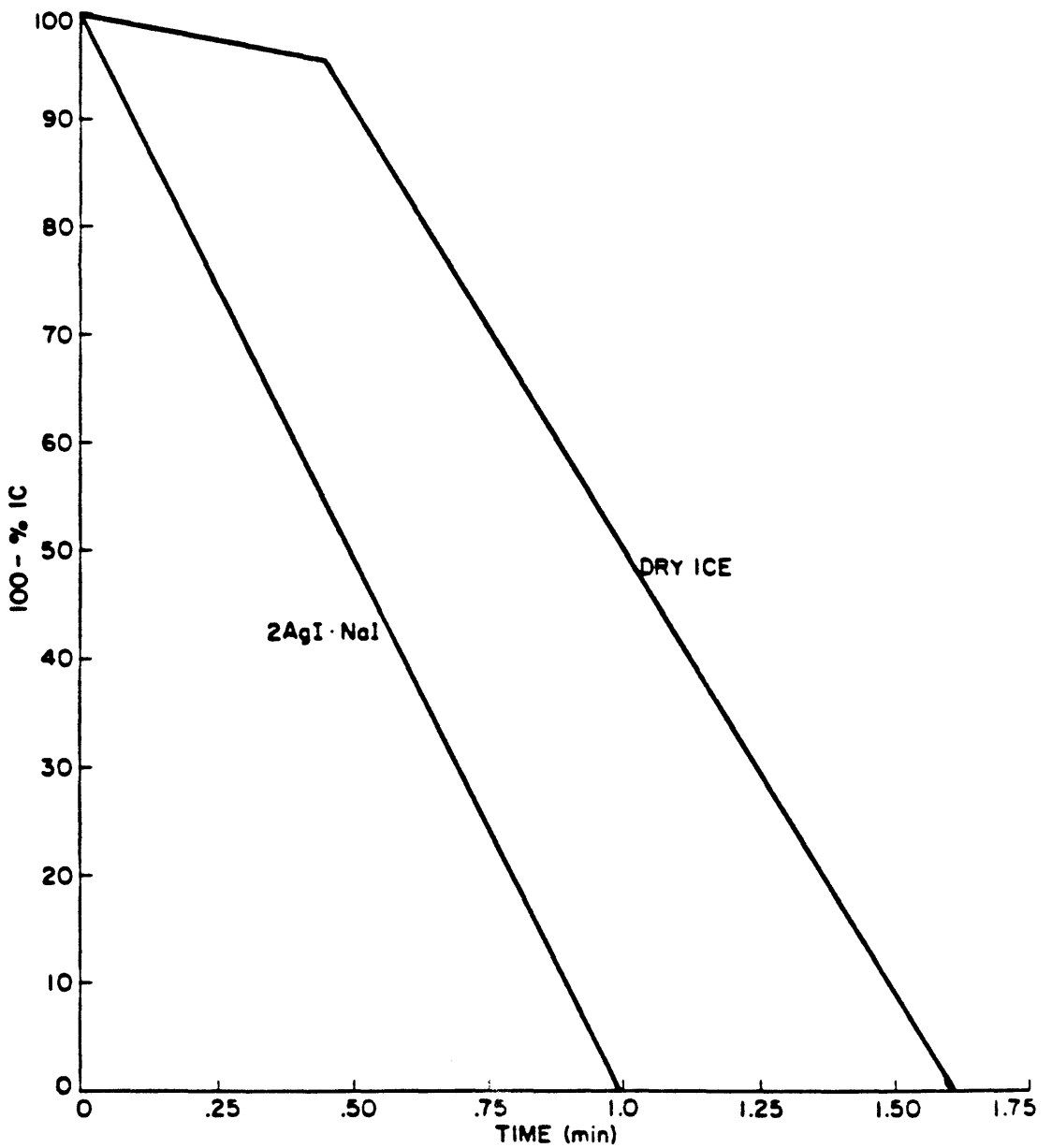

Figure 15: Ice crystal fallout rates for the fast nucleation process. The 2AgI·NaI plot is taken form this study, -10°C, 0.5 gm^{-3} LWC, natural draft, wet dilution. The dry ice plot is taken from Morrison (1983), -10°C, 0.5 gm^{-3}. Both plots were normalized.

aerosol with that obtained by Morrison, et al. (1983) for ice production by dry ice pellets at -10°C in the ICC. The slopes, or rates of ice crystal production are nearly equal. Comparisons at other temperatures also showed agreement. Morrison concluded dry ice induced homogeneous nucleation which is a very fast process. The first part of the dry ice plot is controlled by diffusional growth of ice embryos to a size large enough to commence fallout (Morrison, 1983). (In the rate plots of the fast mechanism above, the first phase was observed but not included in the kinetics.) The second phase appears to be dominated by the fallout rate of the crystals.

Ice nuclei are assumed to be uniformly distributed within the ICC upon injection. If nucleation of ice particles occurs at a faster rate and hence prior to growth and subsequent fallout of the crystals, the resulting ice embryos would be uniformly distributed within the chamber. The vertical distribution of crystals over the ice crystal detector or glass slides, $\frac{dC_{IC}}{dy}$, would be constant. The embryos would grow simultaneously to a size large enough to fall. Observations of crystals as they are counted in the cold stage microscope indicated they are roughly of uniform size (Blair, et al., 1973). Growth of the crystal as it falls can be neglected because of the short fall distance in the chamber, about one meter. The fall velocity, $\frac{dy}{dt}$, can be approximated as being constant. Multiplication of vertical distribution and fall speed gives $\frac{dC_{IC}}{dt}$ (eq. 3.2.9). As an example, the fall speed of 50 μm plates, a common observation at -10°C, is about 4 cms^{-1} (Pruppacher and Klett, 1978, Fukuta, 1969). At -10°C, the average number of ice crystals counted on a 0.02 cm^2 view area of the slides corresponds to 4.5 crystals cm^{-3} or 0.09 cm^{-1} in a column over the slide. Multiplying the

vertical distribution with the fall speed, the theoretical rate at which ice crystals appear is equal to 0.36 s^{-1} or 21.6 min^{-1}. The observed rate at -10°C at water supersaturation is 20.1 min^{-1}. The rate at which ice crystals are detected in the ICC in water supersaturated conditions is controlled by crystal fallout.

Fallout of the ice crystals was the only process that could be observed for the fast process and is the rate limiting step in the ICC for fast nucleation. Information about the mechanism of ice nucleation could not be obtained directly from the rates. The mechanism would however have to be a form of condensation-freezing nucleation because of the hygroscopicity of the aerosol particles. The increased concentration of water vapor in the supersaturated environment may have greatly increased the rate of condensation of liquid water onto the nuclei. Chemically, this would imply that the transformation proposed for the slower condensation to droplets followed by freezing mechanims may be bypassed. Chen, et al. (1972) suggested that the formation of some intermediate complex phases of AgI-NaI-H_2O are indeed bypassed if temperature and humidity changes are sufficiently rapid. The embryos would freeze without the need to break and/or form any bonds in the AgI-NaI-H_2O complex. The process is likely to be condensation freezing to frozen embryos followed by freezing or sorption nucleation. The rate expression for this mechanism is

$$\frac{dC_N}{dt} = k_{n,f} C_V^v C_N. \qquad (5.4.3)$$

The exponent, v, for this mechanism may be greater than one which implies that slight increases in supersaturation (water vapor concentration) can account for the large increases in rate. The very large nucleation rate increase may be a manifestation of a large

exponent. Formation of aqueous embyros, of probably a few microns in size, is likely to be the rate determining step for this mechanism.

The sorption mechanism is dependent on particle size. Yield of the fast mechanism increases as the concentration of water vapor increases. It is likely that lower values of water supersaturation affect only the largest particles. As the concentration of water vapor increases, particles of decreasing size can form embryos that freeze by the fast process.

The 2AgI·NaI ice nucleant also operates by a third mechanism, contact ice nucleation as reported by DeMott, et al. (1983). When the cloud droplet concentration was increased, or when both LWC was increased and particles size was decreased, the rate of contact nucleation was increased to observable levels. Yields also increased when contact nucleation occured. Contact nucleation was observed only at water saturation and high liquid water contents.

Rates of contact were considerably slower for 2AgI·NaI particles than for AgI particles reported by DeMott (1982). At $-12^{o}C$, 1.5 gm^{-3} LWC, maximum draft, the contact rate constant for AgI aerosol is 0.22 min^{-1}. The rate of the parallel process of contact for 2AgI·NaI for the same chamber conditions is 0.06 min^{-1}. There are two possible explanations for the occurrance of contact. The hygroscopic particles would quickly grow to sizes large enough to effectivley slow the rate of contact nucleation. However, extreme cloud conditions, 6000 droplets cm^{-3}, can increase the rate of contact of droplets to particles to observable levels. Alternatively, the smallest particles in the aerosol population may not act as condensation nuclei. When generated in slower natural draft, the concentration of these small particles would be too

low for contact to be observable. Increasing the concentration of small particles which do not form droplets would increase the rate of contact to observable levels.

VI. APPLICATION OF LABORATORY RESULTS IN A THEORETICAL CLOUD MODEL

6.1 Ice Nucleation Kinetics and Yield Parameterization

Results from the laboratory characterization of ice nucleation by 2AgI·NaI aerosol particles were incorporated into the two dimensional orographic cloud model described in section 3.3 (Rauber, 1981). Condensation to droplets followed by freezing (slow) and sorption (fast) ice nucleation rates were modeled. Contact nucleation was not included because the cloud model does not predict droplet concentrations.

Model predicted air parcel temperature was used to determine rate constants for the slow mechanism according to the Arrhenius equation,

$$k_{n,S} = 8.77X10^{-30}\exp(1.57x10^{4}T^{-1}), \qquad (6.1.1)$$

where the subscript S denotes the slow mechanism and T is temperature in degrees Kelvin. The rate of sorption nucleation was estimated by assuming $k_{n,F}=0.05\ s^{-1}$, where the subscript F denotes the fast mechanism. The actual rate of nucleation by this mechanism is known to be faster. The parameterization represents a minimum rate of sorption nucleation. In the model, the number of nucleation events predicted are minimum values. Both nucleation mechanisms were assumed to be first order processes. Eq. 3.3.1 was used to predict the number of possible nucleation events at intervals along the air parcel trajectory.

Yield was determined according to eq. 3.3.2. For condensation to droplets followed by freezing (slow nucleation) the empirical

constants, c_1 and c_2, were such that

$$Y_S = 4.83X10^{10}\exp(-0.59T) \qquad (6.1.2)$$

and for sorption nucleation,

$$Y_F = 1.78X10^{10}\exp(-0.71T) \qquad (6.1.3)$$

where T is temperature in degrees Celsius. The maximum yield of ice nucleation used was $1X10^{15}$ $(g\ AgI)^{-1}$ for the slow mechanism and $4X10^{15}$ $(g\ AgI)^{-1}$ for the fast mechanism. Temperature changes within each time step were small, less than two degrees.

Condensation to droplets followed by freezing occured when the model predicted condensate production rate was positive. The cloud at this time was assumed to be water saturated. Arbitrary values of rate of condensate production were used to predict proportionate values of water supersaturation for sorption ice nucleation. Rates of condensate production increased as the crest of the mountain barrier was approached where updrafts due to orography increased in the modeled cloud. These relative values of cloud water production rates were used to encompass the span of slight to strong supersaturations which may trigger the fast nucleation mode. Field observations of orographic clouds show the formation of new, small cloud droplets at locations of increased orographic lift, indicating water supersaturation (DeMott, et al., 1985). The situation where a portion of the nuclei population was affected by water supersaturation, as was observed in the ICC with partial moist dilutions, was not modeled.

6.2 Model Results

Three case studies are presented using input data from COSE III to determine the influence of ice nucleation rate and mechanism on ice

crystal production in orographic clouds. The 15 December 1981, 15GMT case study was a warm cloud with high total cloud condensate values. The temperature at the crest of the barrier was -4.5°C and wind speeds were moderate. The 5 January 1982, 12GMT model simulation resulted in a cloud which had lower temperatures and cloud condensate values. In this case the barrier temperature was -10°C. Wind speeds were high. A cold and shallow cloud with low wind speeds, the 12 January 1982, 6GMT study, was used for the third study. The barrier crest temperature was -14°C.

6.2.1 15 December Case Study

Results of the 15 December study are shown on fig. 16-24. Fig. 16 shows the model predicted cloud and the air parcel trajectories used in this analysis. The initial temperature of the trajectories are -5, -10, and -15°C. Clouds were 'seeded' in all cases at the windward edge. Numbers written over the trajectories in the following figures are cumulative counts of nucleated ice crystals of the initial 1000 ice nuclei.

Ice nucleation along the -5°C trajectory, slightly above cloud base, is shown in figs. 17-19. In fig. 17, it was assumed that supersaturation with respect to water never reaches a high enough level to initate fast nucleation. Only nucleation by condensation to droplets followed by freezing is shown. The first observable ice nucleation event was predicted by the model to occur 40 minutes, or 34 km downwind from the point of seeding. Less than one percent of the ice nuclei function in cloud while the remaning ice nuclei leave the area unaffected. Model predicted ice crystal trajectories indicate that 0.02% of the ice nuclei form precipitation which reaches the ground on the lee side of the barrier. In fig. 18, it is assumed that a large

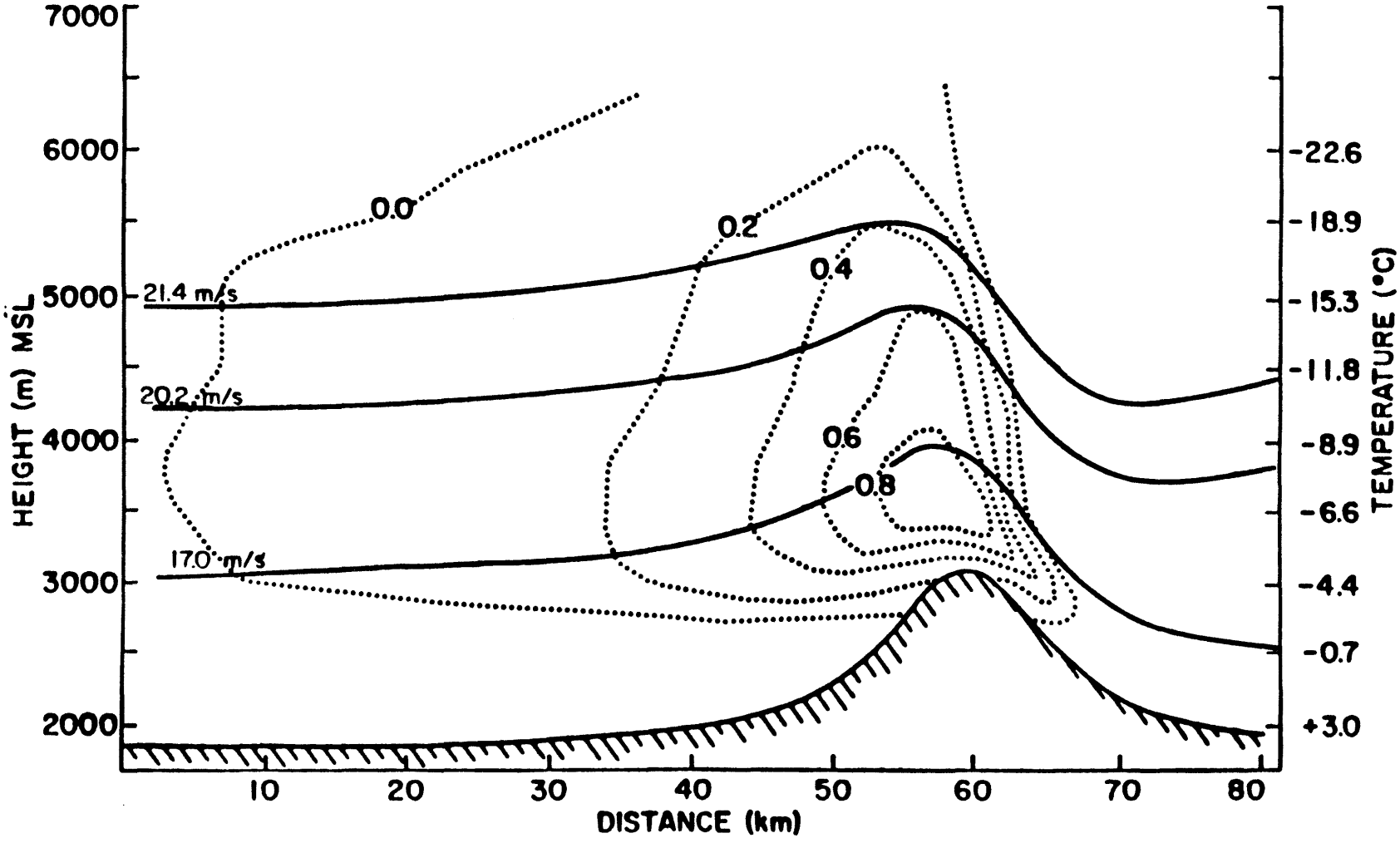

Figure 16: December 15 air parcel trajectories (heavy solid lines) and cloud water contents in gm^{-3} (dotted lines) as predicted by the orographic cloud model. Initial wind speeds are indicated on the upwind (left) side of the trajectories.

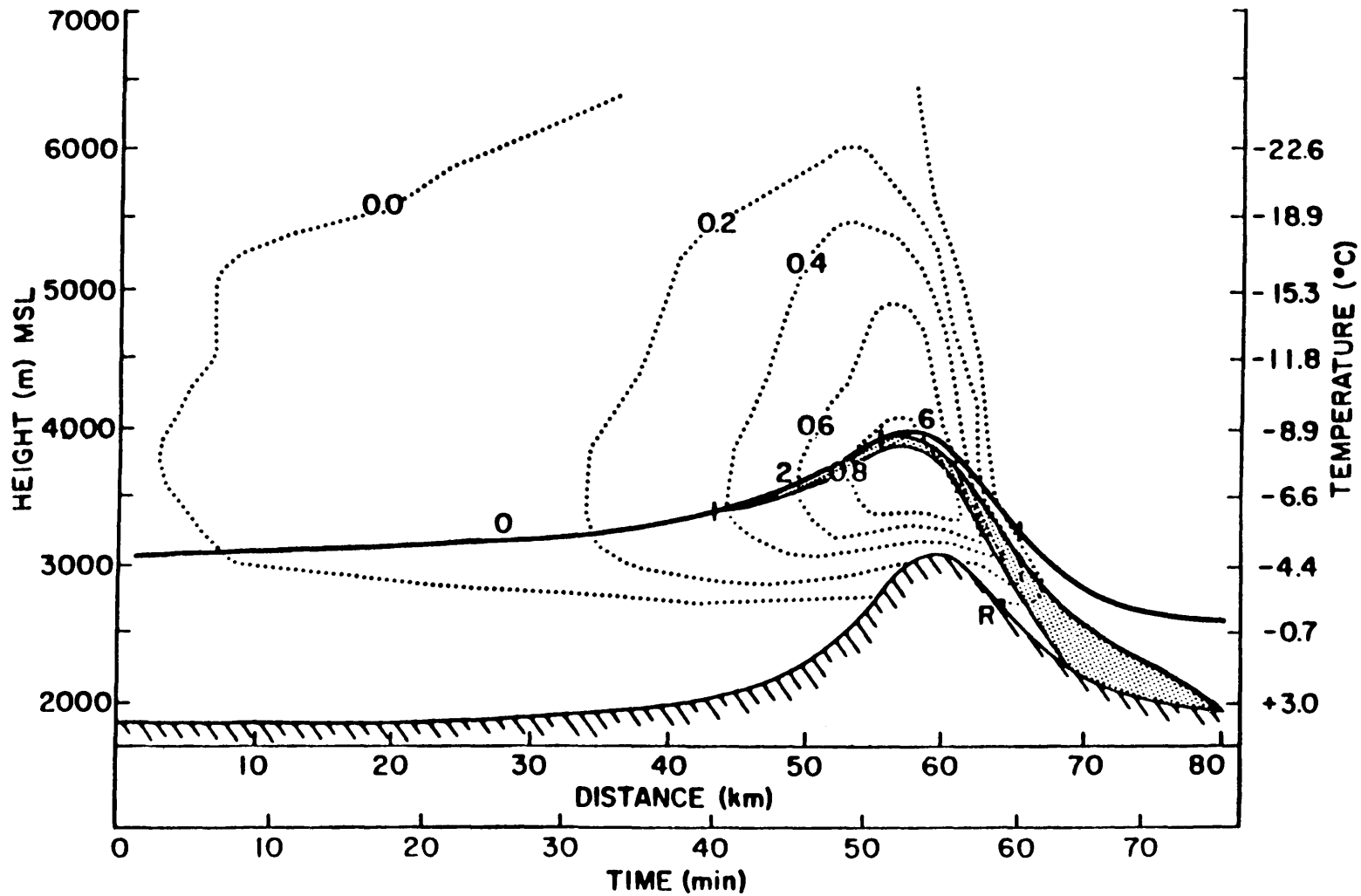

Figure 17: December 15. Slow ice nucleation at -5°C. Numbers over trajectory indicate cumulative number of nucleation events. Stipled area shows model predicted ice crystal fallout due to nucleation. R indictes location of precipitation when riming processes are included.

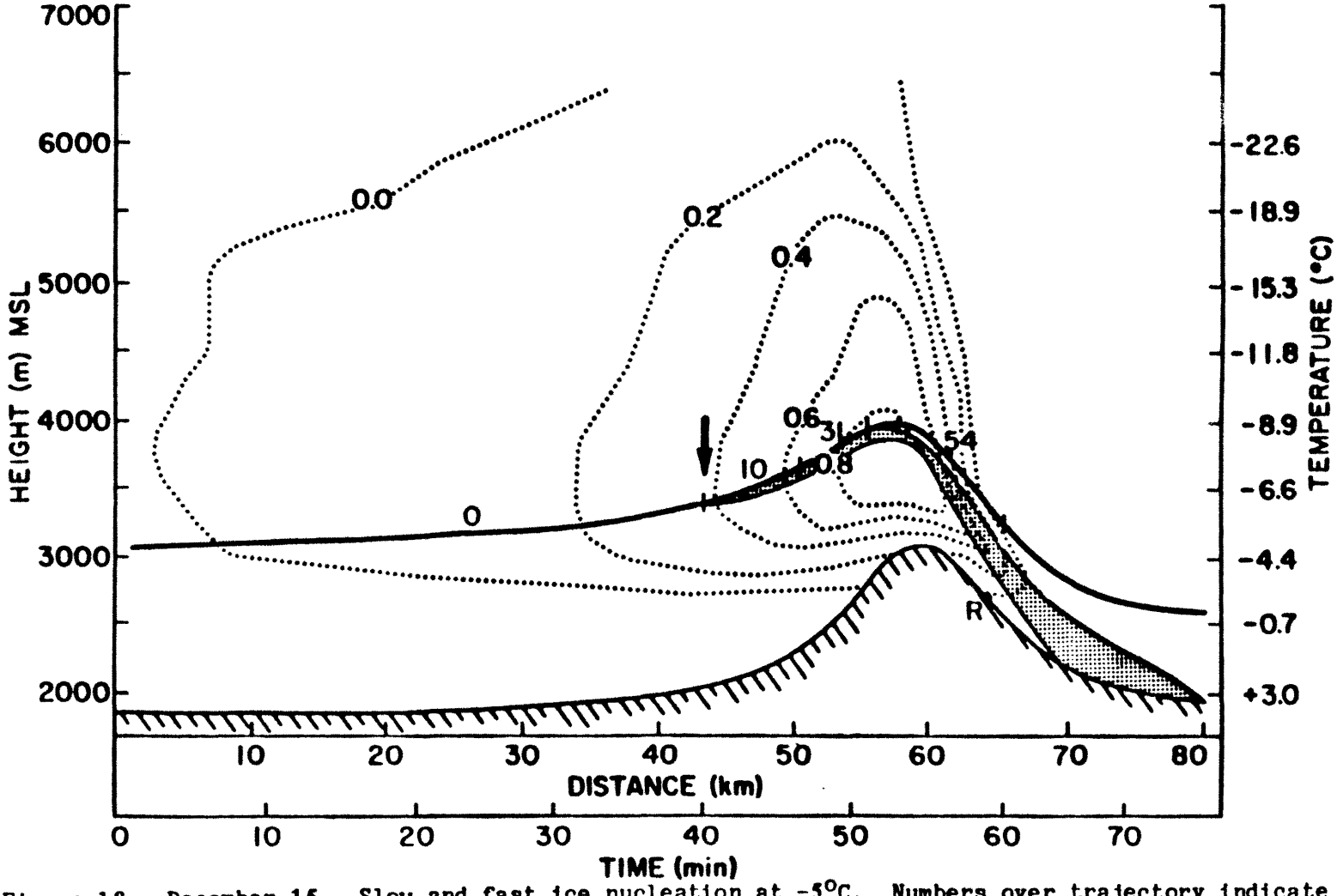

Figure 18: December 15. Slow and fast ice nucleation at -5°C. Numbers over trajectory indicate cumulative number of nucleation events. Stipled area shows model predicted ice crystal fallout due to nucleation. R indicates location of precipitaion when riming is included.

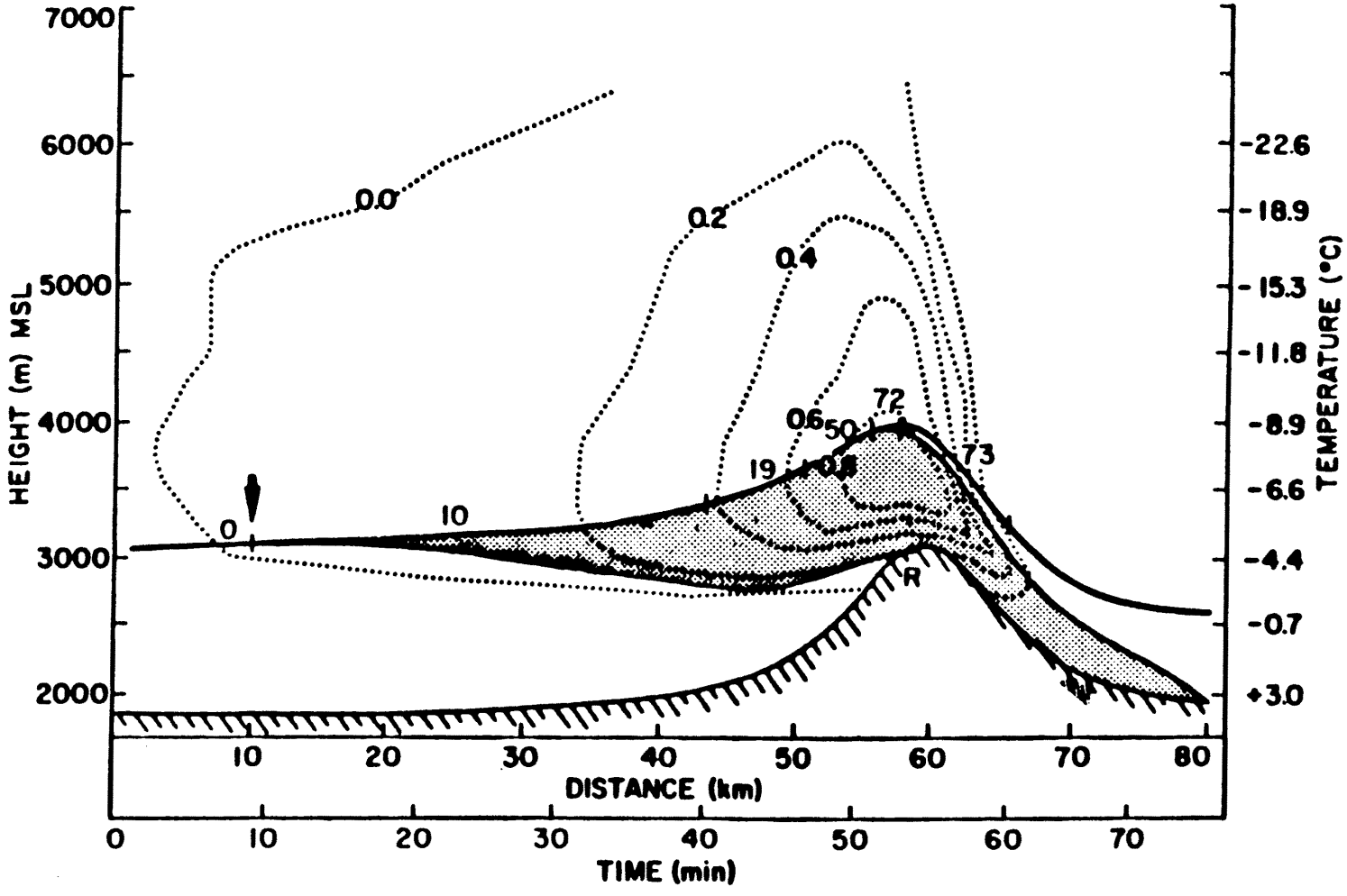

Figure 19: December 15. Fast ice nucleation at -5°C. Numbers over trajectory indicate cumulative number of nucleation events. Stipled area shows model predicted ice crystal fallout due to nucleation. R indictes location of precipitation when riming processes are included.

enough supersaturation for the fast nucleation mechanism to function exists at the location indicated by the arrow. This point was chosen because it is a location of primary orographic lift. The number of nucleation events increased by three percent. Fig. 19 shows the case where the supersaturation at cloud edge is large enough for fast nucleation. Ice formation becomes observable a few kilometers beyond cloud edge so that resulting precipitation begins further upwind at the barrier crest. The number of nucleation events is still low. Seven percent of the ice nuclei form crystals and five percent of the seeding material reaches the surface. The temperature in the trajectory ranges from -5 to -9°C. Warm temperatures, which reduces the yield of ice nucleation, can account for the loss of large numbers of ice nuclei which do not form precipitation.

The air parcel trajectory initiated at -10°C is shown in figs. 20-22. Fig. 20 shows only the slow nucleation process. A majority of ice nuclei, 83.4% do not form ice and exit the area. When it is assumed that supersaturation is large enough for fast nucleation near the barrier (fig. 21), 61% of the ice nuclei form ice. Ninety five percent of these form directly over the barrier. If fast nucleation commences at cloud edge (fig. 22), 84% of the ice nuclei form crystals, uniformly distributed in cloud. Ice crystal trajectory calculations indicate that precipitation at the surface from ice nucleation by 2AgI·NaI at this temperature occurs only if riming (or perhaps aggregation) occurs which significantly increases the ice particle fall velocities. Model results show that nucleation at the -10°C level in this case is at an elevation to far above the mountain barrier to permit growth and fallout of pristine ice crystals when nucleation is observed at cloud edge.

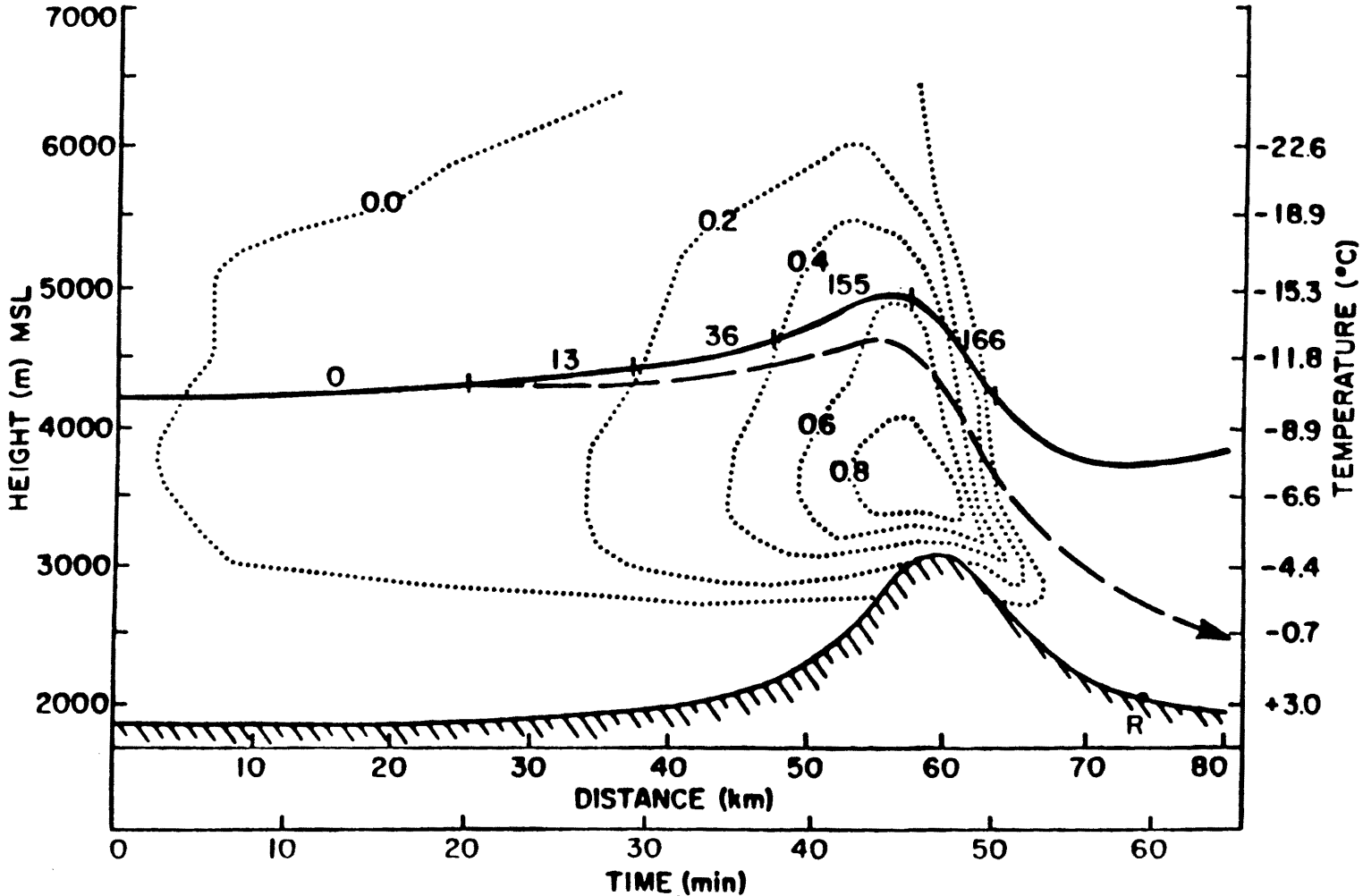

Figure 20: December 15. Slow ice nucleation at $-10^{o}C$. Numbers over trajectory indicate cumulative number of nucleation events. Dashed line shows model predicted ice crystal trajectory of the first ice nucleation event in the air parcel trajectory. R indicates location of precipitation when riming processes are included.

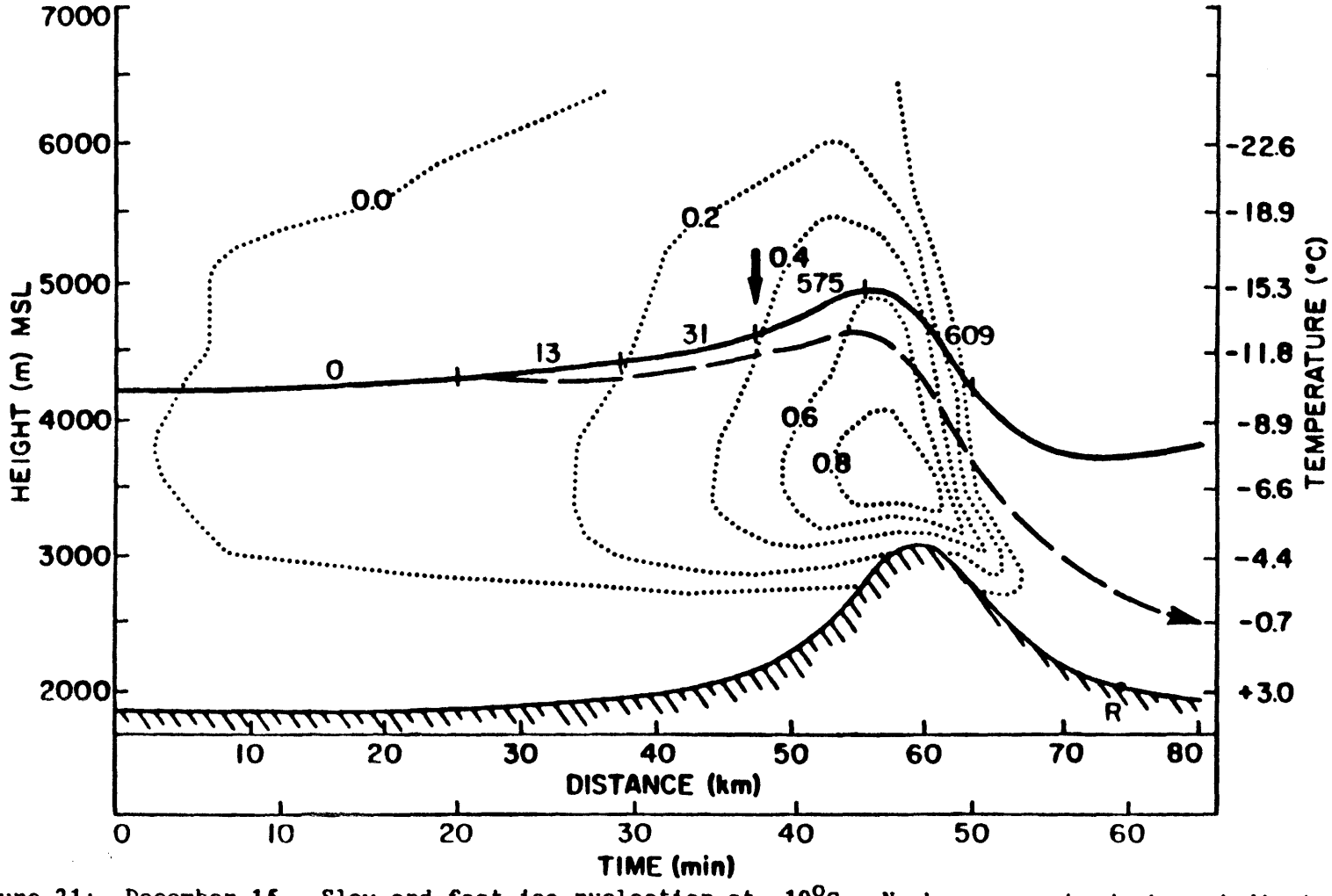

Figure 21: December 15. Slow and fast ice nucleation at $-10^{o}C$. Numbers over trajectory indicate cumulative number of nucleation events. Dashed line shows ice crystal trajectory of the first ice nucleation event. R indicates the location of precipitaion when riming is included. Arrow indicates transition between mechanisms.

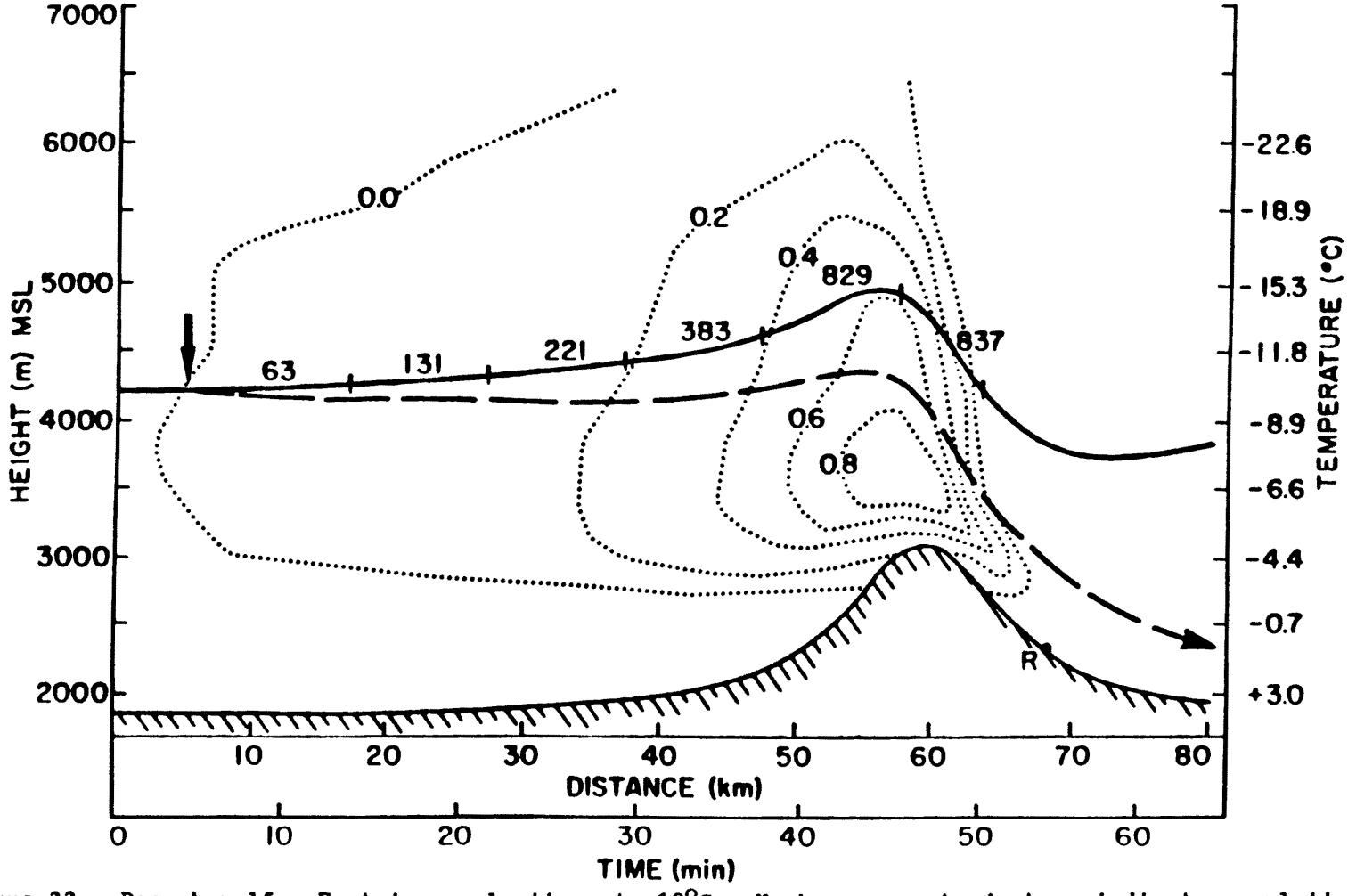

Figure 22: December 15. Fast ice nucleation at -10°C. Numbers over trajectory indicate cumulative number of nucleation events. Dashed line shows model predicted ice crystal trajectory of the first ice nucleation event. R indicates location of precipitation when riming processes are included.

Seeding at -15°C is shown in figs. 23-24. For the slow nucleation mechanism, fig. 23, nearly all the ice nuclei function uniformly through the cloud. For fast nucleation commencing at cloud edge, fig. 24, all the nuclei form ice within 30 minutes after seeding in the first 28 km of cloud. Again, precipitation at the surface is predicted only for rimed crystals with substaintially greater fall velocities than those of pristine ice crystals.

An experiment was made where rates were not used to determine ice nucleation. Only the temperature effect on yield was modeled with the assumption that nucleation was instantaneous. This is the same assumption used by Hobbs, et al. (1973), Young (1974a), and Plooster and Fukuta (1975) in models of cloud seeding with artificial ice nuclei. Results of runs without kinetics were identical to those in which the fast mechanism was initiated at cloud edge. The time resolution at each step of calculation was approximately 50 seconds. Ice crystal production was observed in the laboratory to be 80-90% complete within one minute. Thus, it can be assumed within the time resolution of the model that the fast mechanism is instantaneous.

Seeding this cloud system with 2AgI·NaI ice nuclei would not be beneficial. Wind speeds are such that seeding would have to be done less than 1500 m above ground for ice crystals to reach the surface. Warm temperatures at this level greatly inhibit the yield of ice nucleation. Most of the seeding material would exit the lee side of the cloud unaffected.

6.2.2 5 January Case Study

The 5 January case study is again an example where wind speeds are high, reducing the transit time of the air parcel and the time available

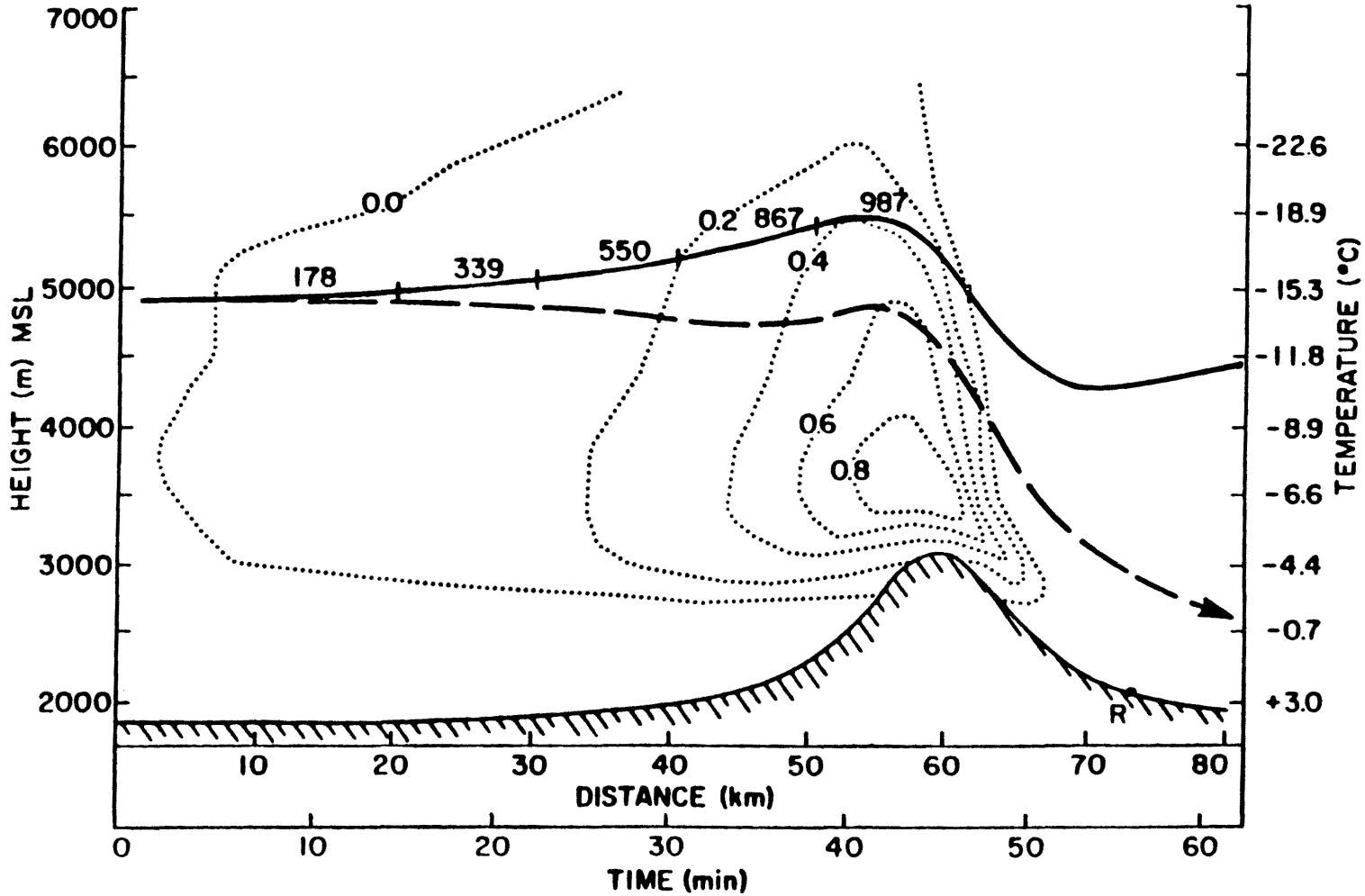

Figure 23: December 15. Slow ice nucleation at -15°C. Numbers over trajectory indicate cumulative number of nucleation events. Dashed line shows model predicted ice crystal trajectory of the first ice nucleation event. R indicates location of precipitation when riming processes are included.

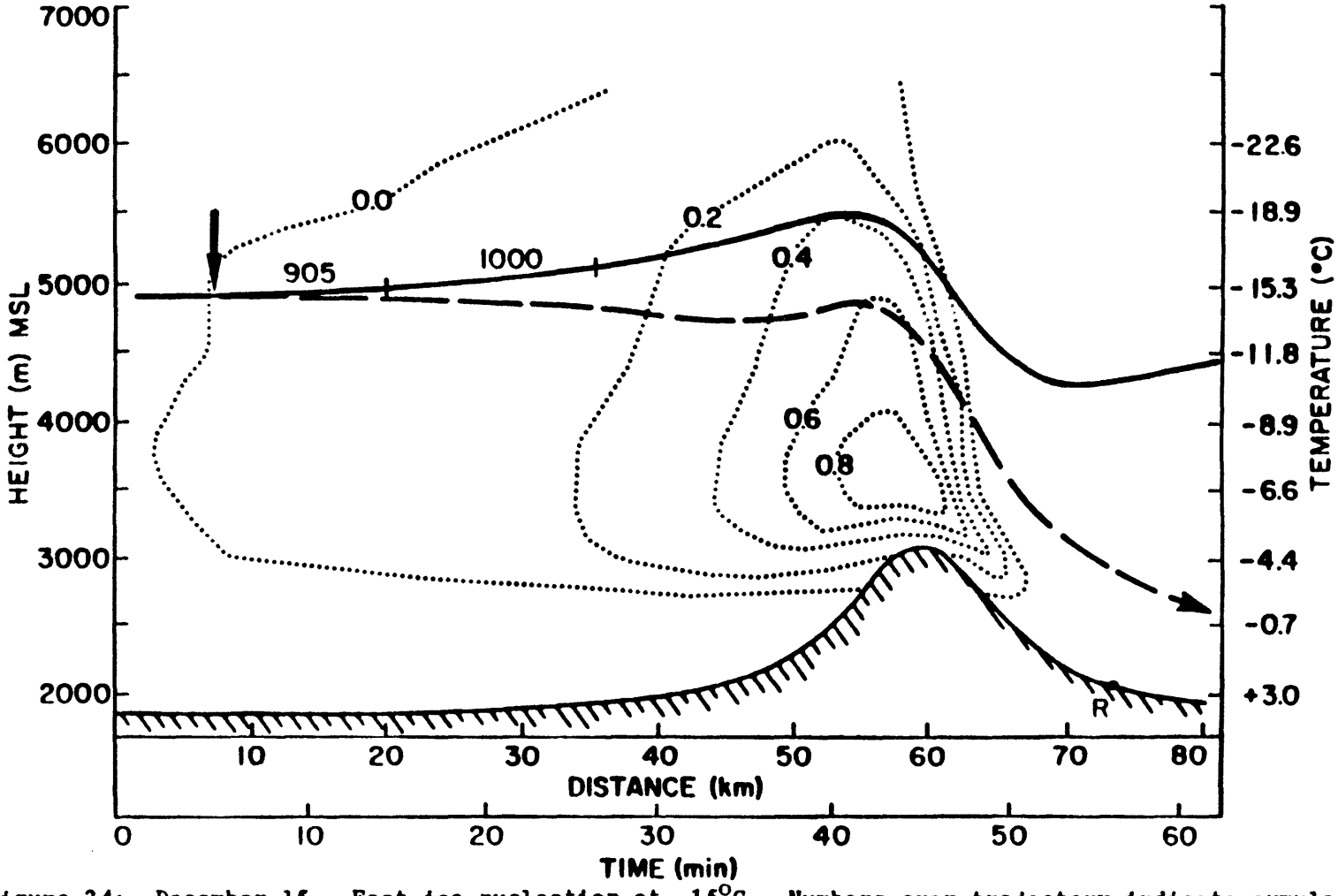

Figure 24: December 15. Fast ice nucleation at -15°C. Numbers over trajectory indicate cumulative number of nucleation events. Dashed line shows model predicted ice crystal trajectory of the first ice nucleation event. R indicates location of precipitation when riming processes are included.

for nucleation. Results are shown in figs. 25-32. Air parcel trajectories were initiated at -10, -15, and -20°C. These are shown in fig. 25. The trajectory nearest cloud base is 5°C colder than that of the cloud base trajectory of 15 December. Figs. 26-28 show that nucleation is more efficient for the colder case with the same height and wind conditions as 15 December. The slow mechanism of ice nucleation is shown in fig. 26. Nucleation commences 20 minutes after seeding, 12 km downwind of the cloud edge and 29% of the ice nuclei form ice. Precipitation, on the lee side of the barrier, results from 14% of the nuclei. Fig. 27 shows the case where supersaturation large enough for fast nucleation would occur near the barrier. Eighty five percent of the ice nuclei function, increasing the amount resulting in precipitation to 72%. Because much of the nucleation occurs near the barrier crest, 95% of the precipitation reaches the ground downwind of point T. Fig. 28 shows the case where the fast nucleation mechanism is initiated at cloud edge. Few ice nuclei exit the cloud. Precipitation begins at the mountain top and continues to the lee side because ice nucleation commences further upwind. Eighty three percent of the ice nuclei form precipitation.

Ice nucleation along the -15°C trajectory is shown in figs. 29-31. The high wind speed, approximately 30 ms^{-1}, reduces the transit time of the ice nuclei in cloud by 20 to 40 minutes. The low temperatures allow for efficient nucleation. The slow mechanism, fig. 29, results in ice nucleation through the length of the trajectory in cloud. Only one percent of the nuclei exits the lee side. Supersaturation near the barrier, fig. 30, results in the completion of nucleation within 3 km. For fast nucleation commencing at cloud edge, fig. 31, nucleation is

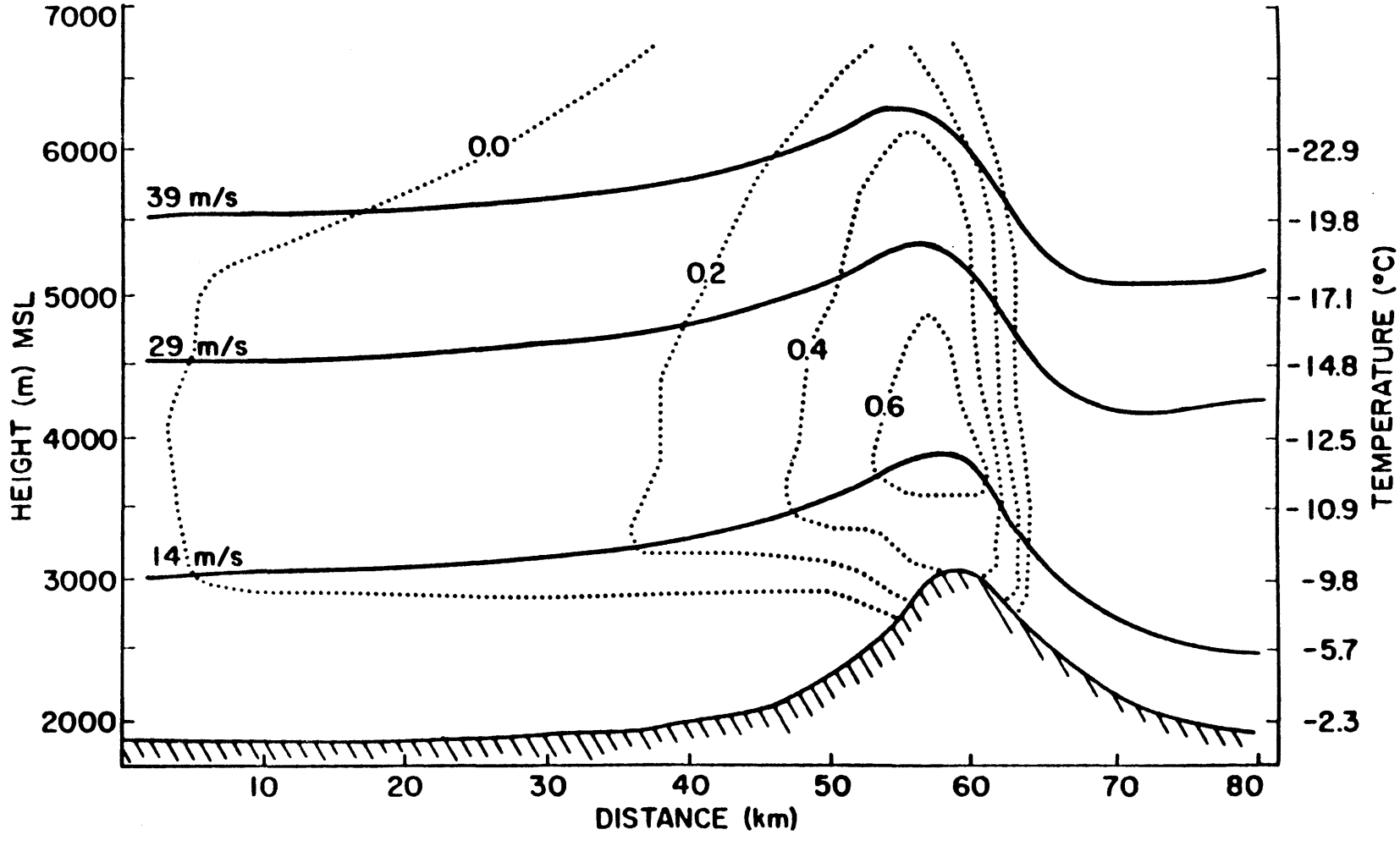

Figure 25: January 5 air parcel trajectories (heavy solid lines) and cloud water contents in gm^{-3} (dotted lines) as predicted by the orographic cloud model. Initial wind speeds are indicated on the upwind (left) side of the trajectories.

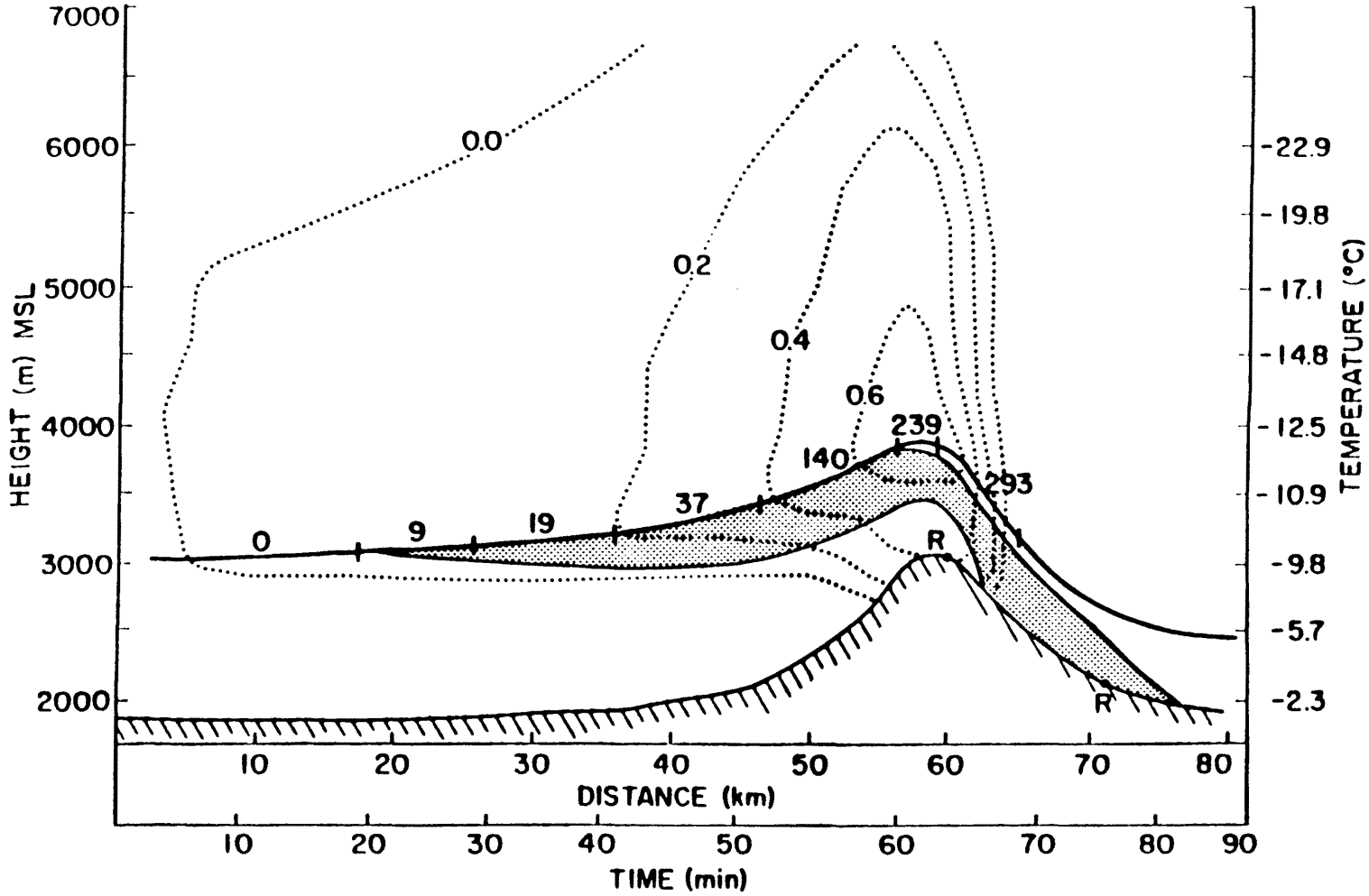

Figure 26: January 5. Slow ice nucleation at $-10^{o}C$. Numbers over trajectory indicate cumulative number of nucleation events. Stipled area shows model predicted ice crystal fallout due to nucleation. R indictes location of precipitation when riming processes are included.

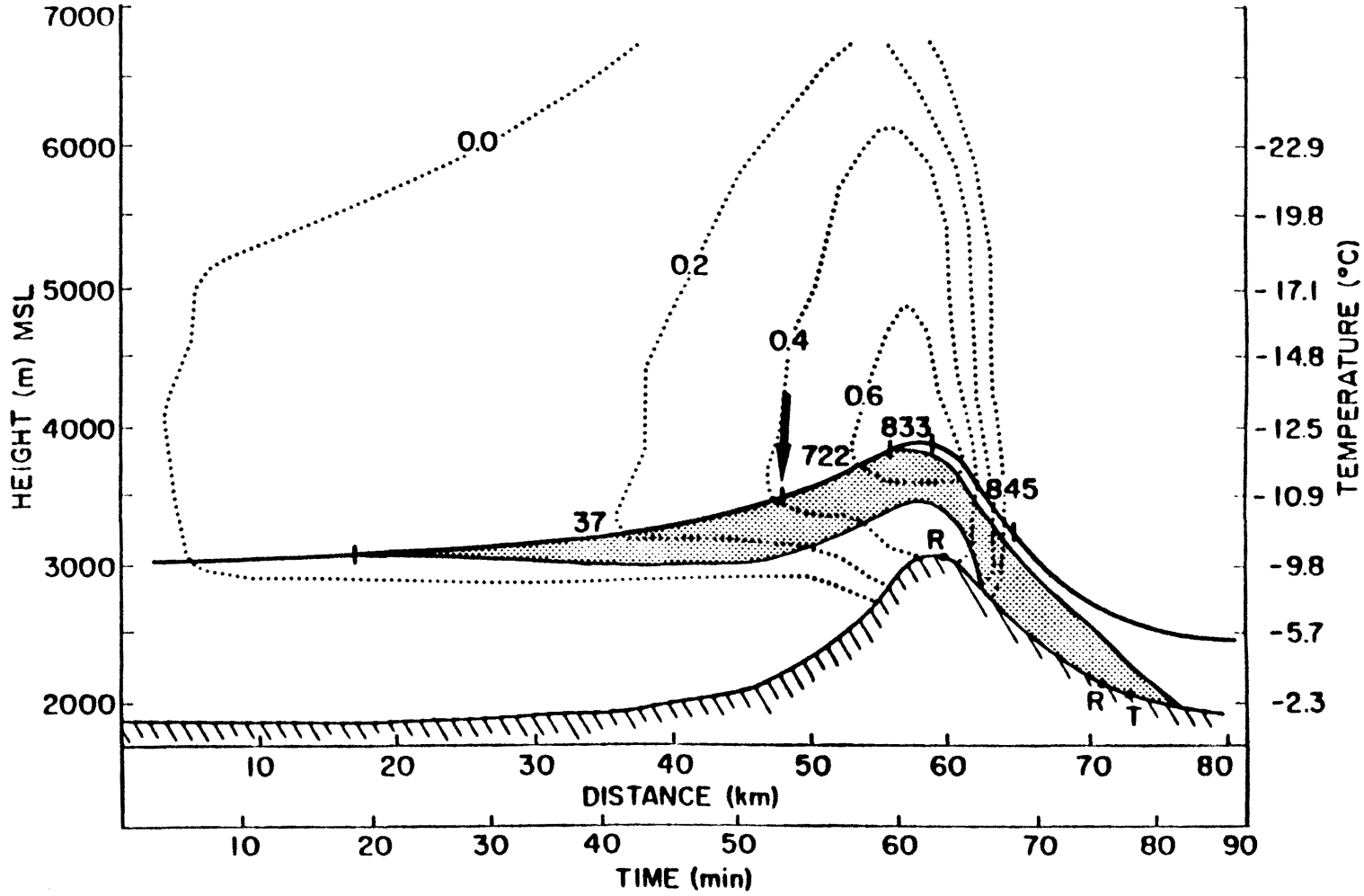

Figure 27: January 5. Slow and fast ice nucleation at -10°C. Numbers over trajectory indicate cumulative number of nucleation events. Arrow indicates location of transition between mechanisms. Stipled area shows model predicted ice crystal fallout due to nucleation. R indicates location of precipitaion when riming processes are included.

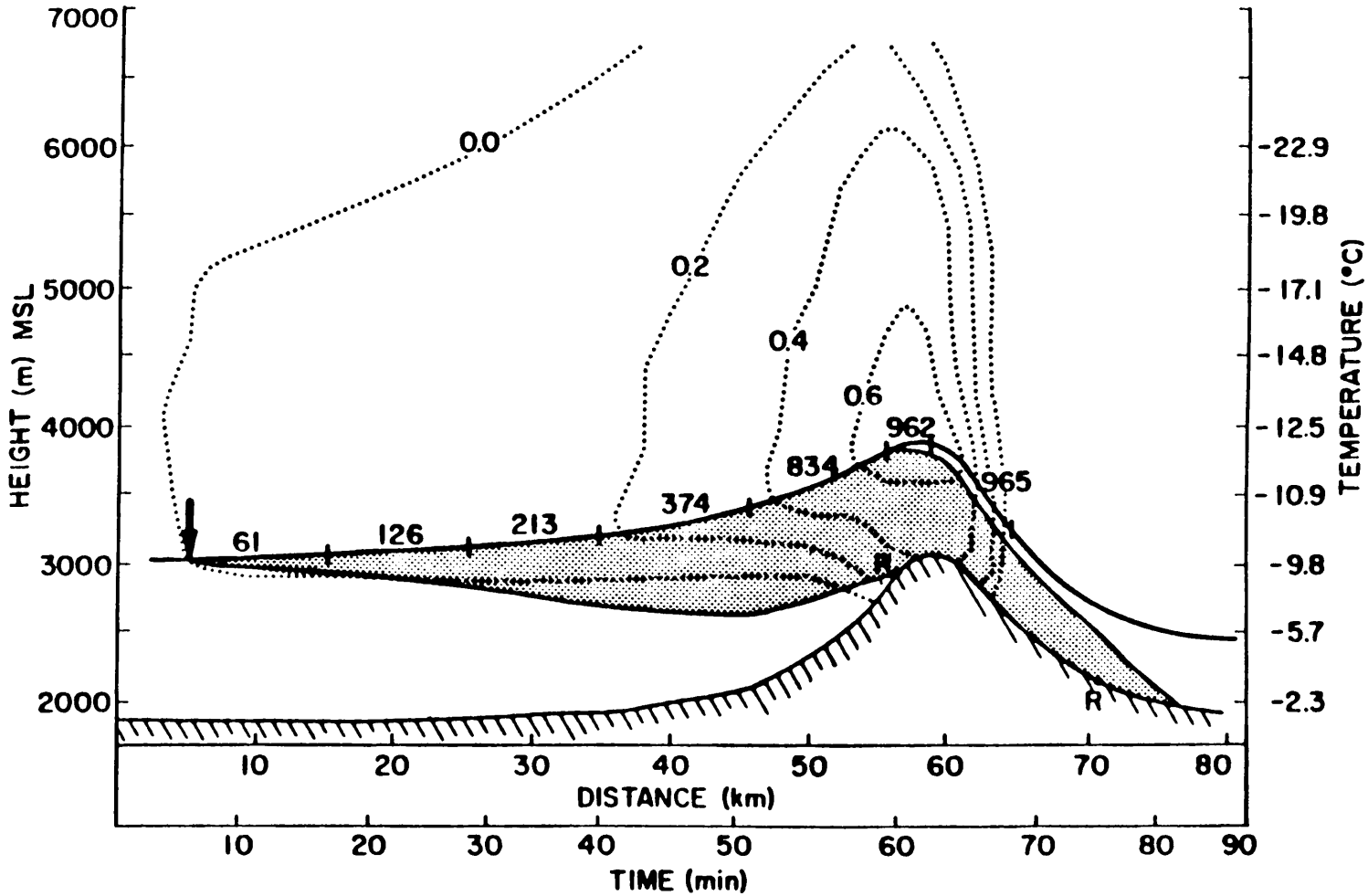

Figure 28: January 5. Fast ice nucleation at -10°C. Numbers over trajectory indicate cumulative number of nucleation events. Stipled area shows model predicted ice crystal fallout due to nucleation. R indictes location of precipitation when riming processes are included.

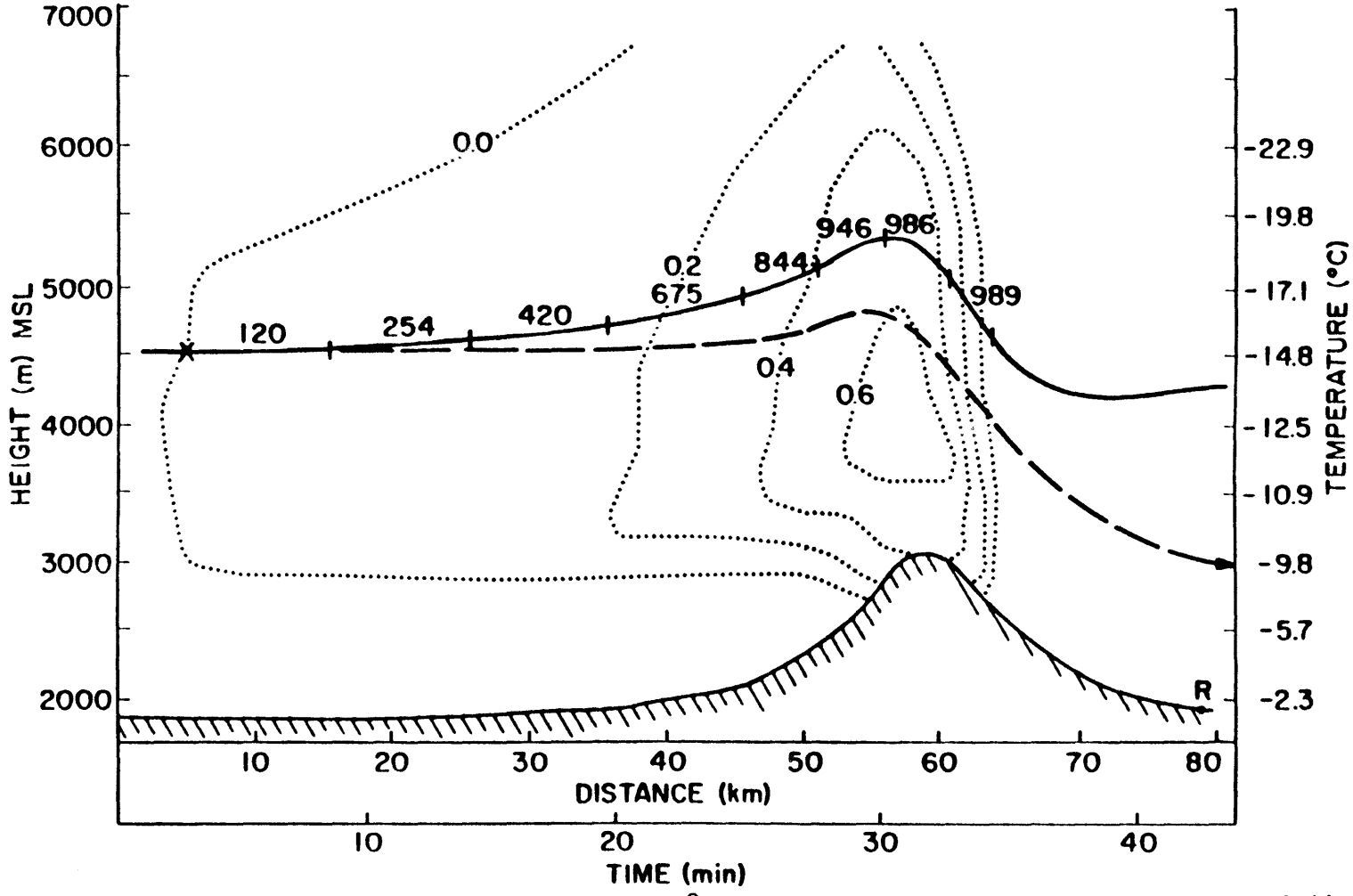

Figure 29: January 5. Slow ice nucleation at -15°C. Numbers over trajectory indicate cumulative number of nucleation events. Dashed line shows model predicted ice crystal trajectory of the first ice nucleation event. R indicates location of precipitation when riming processes are included.

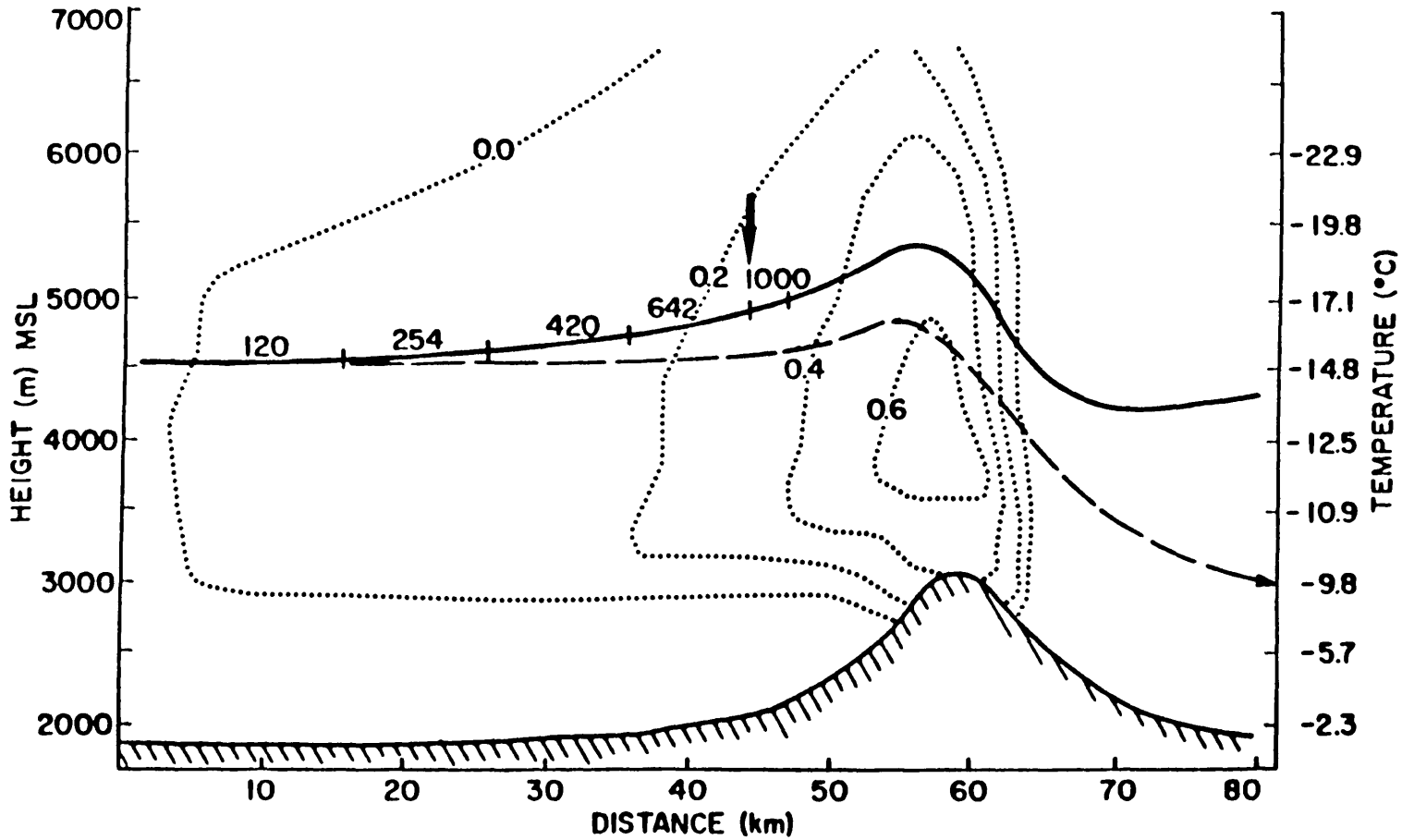

Figure 30: January 5. Slow and fast ice nucleation at -15°C. Numbers over trajectory indicate cumulative number of nucleation events. Dashed line shows ice crystal trajectory of the first ice nucleation event. Arrow indicates transition between mechanisms.

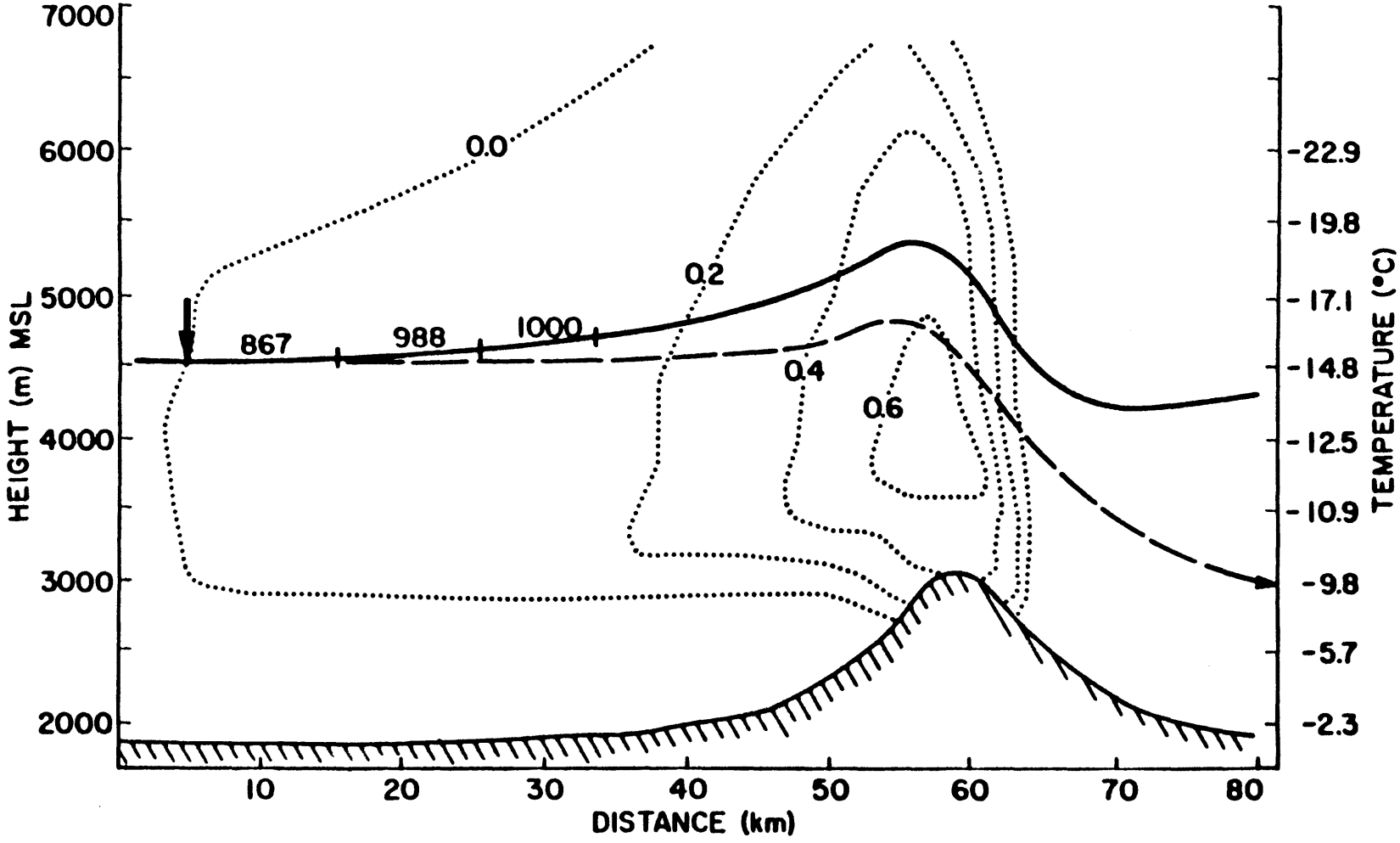

Figure 31: January 5. Fast ice nucleation at -15°C. Numbers over trajectory indicate cumulative number of nucleation events. Dashed line shows model predicted ice crystal trajectory of the first ice nucleation event.

complete within 35 minutes, or 28 km downwind of the cloud edge. No precipitation results because of the height of the trajectory and high wind speed. Results for the -20°C trajectory indicate that nucleation is complete 27 and 4 km downwind of cloud edge for the slow and fast nucleation mechanisms respectively. Strong winds prevent any precipitation from reaching the ground.

As with the case study of 15 Decemeber of the previous section, seeding of this cloud system with 2AgI·NaI would have to be done at the lower cloud levels. The colder temperatures allow for higher yield of nucleation. The critical parameter for this case is mechanism of nucleation. The slow mechanism results in most of the seeding material exiting the cloud on the lee side. If water vapor conditions are such that the fast nucleation mechanism can be assured to occur at cloud edge, seeding would be more effective (fig. 28).

Another important concept is exemplified in fig. 27. The system of detection of precipitation enhancement is related to the rate and mechanism of ice nucleation in orographic clouds. Point T on fig. 27 marks the transition between the slow mechanism upwind of the zone of supersaturation in cloud and the fast mechanism which is proposed to function over the barrier. Upwind of point T, approximately 5% of the precipitation resulting from seeding falls 10 km along the cross section. Downwind of point T, the remaining 95% of the precipitation is predicted to fall in 5 km. The location of precipitation gages in the zone of high precipitation is critical for the detection of a seeding effect as well as an accurate assesment of the transition to fast nucleation within the cloud.

6.2.3 12 January Case Study

A very shallow cloud system with moderate wind speeds was modeled and is shown in figs. 32-38. The cloud is about 900 m thick. The average wind speed of 6.5 ms^{-1} allows for 180 minute transit times for the air parcels. Two trajectories, -10 and -15°C, were calculated and are shown in fig. 32. The lower trajectory enters cloud 28 km upwind of the barrier crest. Figs. 33-36 shows nucleation for the cloud base trajectory. For the slow nucleation mechanism, 66.6% of the ice nuclei form ice (fig. 33). All of the nucleated crystals result in precipitation on the windward and lee side of the barrier because of the low level of the trajectory and moderate wind speed. When supersaturation is such that the fast mechanism follows the slow mechanism, the fast mechanism commences 8 km upwind of the barrier (fig. 34), nucleation increases to 87% of the nuclei. The transition between nucleation mechanisms results in 14% of the precipitation falling on the upwind side of the barrier and the remaining 86% on the lee side. If the fast mechanism is initiated 21 km from the barrier, 13 km further upwind than the previous example, fig. 35, 98% of the ice nuclei form crystals. Less than two percent of the precipitation reaches the ground upwind of point T and 48% falls on the windward side of the crest. When fast nucleation is initiated as the parcel enters cloud, fig. 36, essentially all of the ice nuclei function and precipitate. About half the precipitation falls on the windward side of the barrier.

Ice nucleation along the -15°C trajectory is shown in fig. 37-38. The slow nucleation mechanism, fig. 37, allows for 99% of the nuclei to form ice because of large transient times and cold temperatures. Precipitation results from all nucleated ice crystals. Wind speeds are

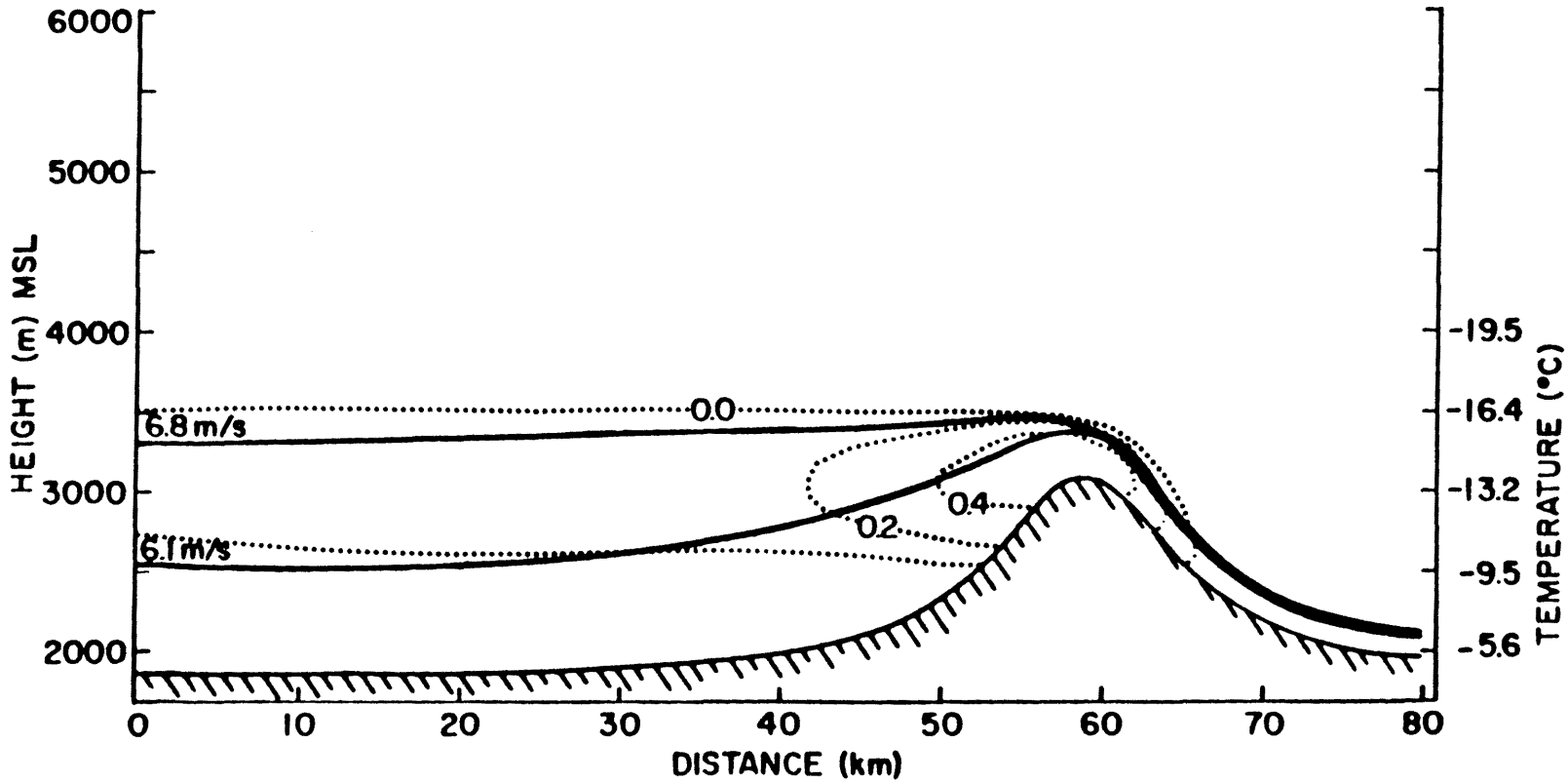

Figure 32: January 12 air parcel trajectories (heavy solid lines) and cloud water contents in gm^{-3} (dotted lines) as predicted by the orographic cloud model. Initial wind speeds are indicated on the upwind (left) side of the trajectories.

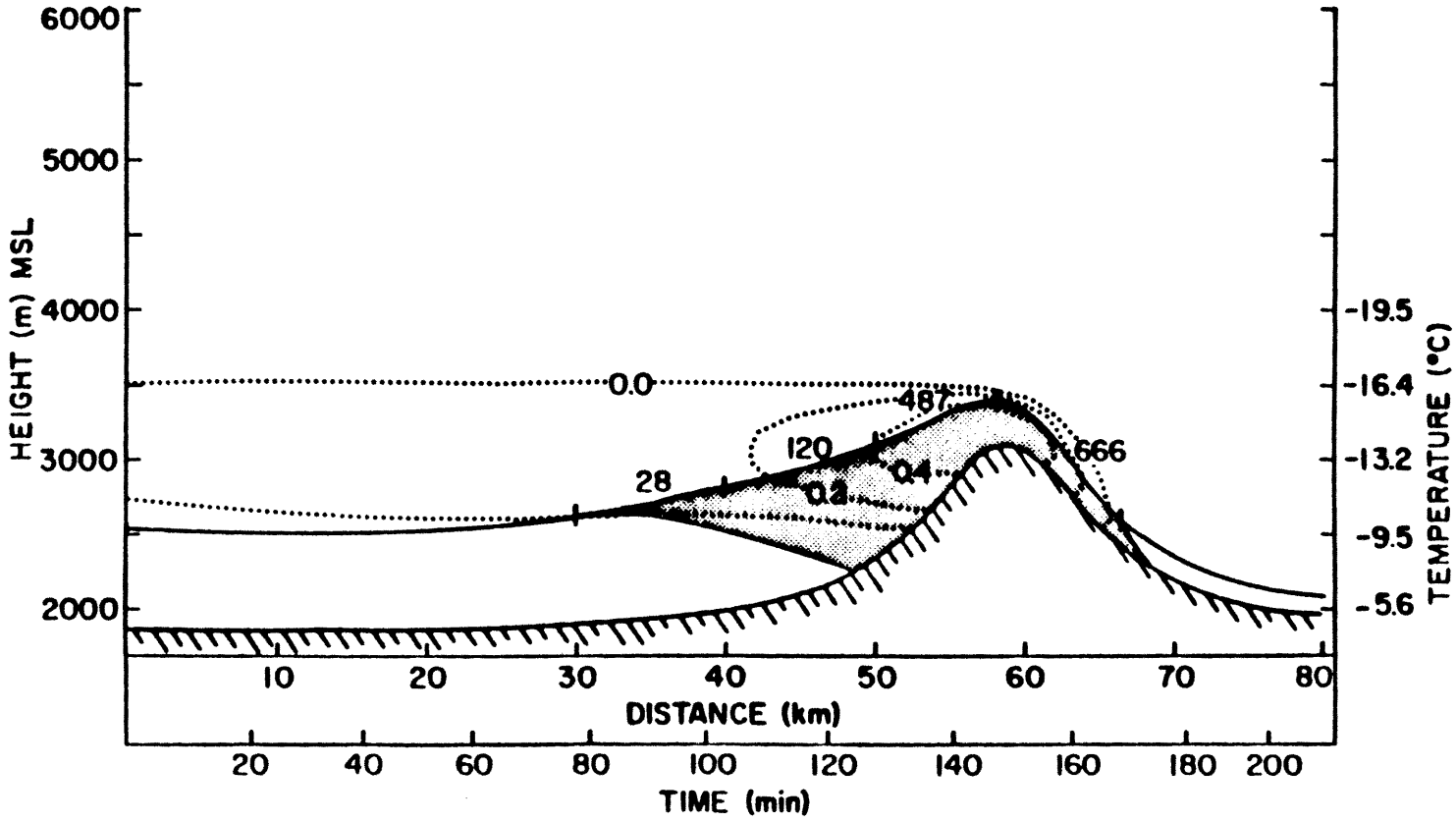

Figure 33: January 12. Slow ice nucleation at -10°C. Numbers over trajectory indicate cumulative number of nucleation events. Stipled area shows model predicted ice crystal fallout due to nucleation.

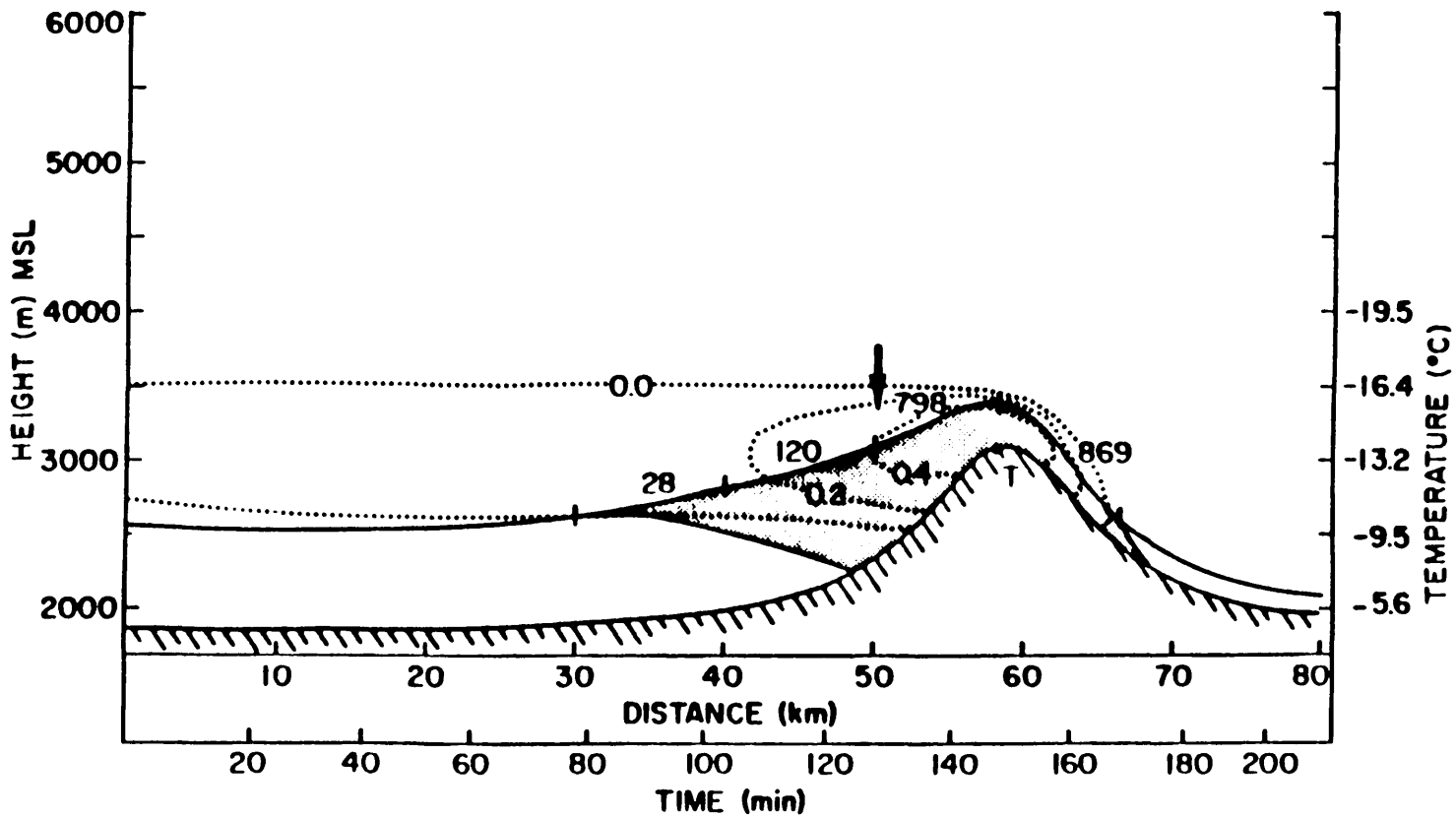

Figure 34: January 12. Slow and fast ice nucleation at -10°C. Numbers over trajectory indicate cumulative number of nucleation events. Arrow and T indicates location of transition between mechanisms. Stipled area shows model predicted ice crystal fallout due to nucleations.

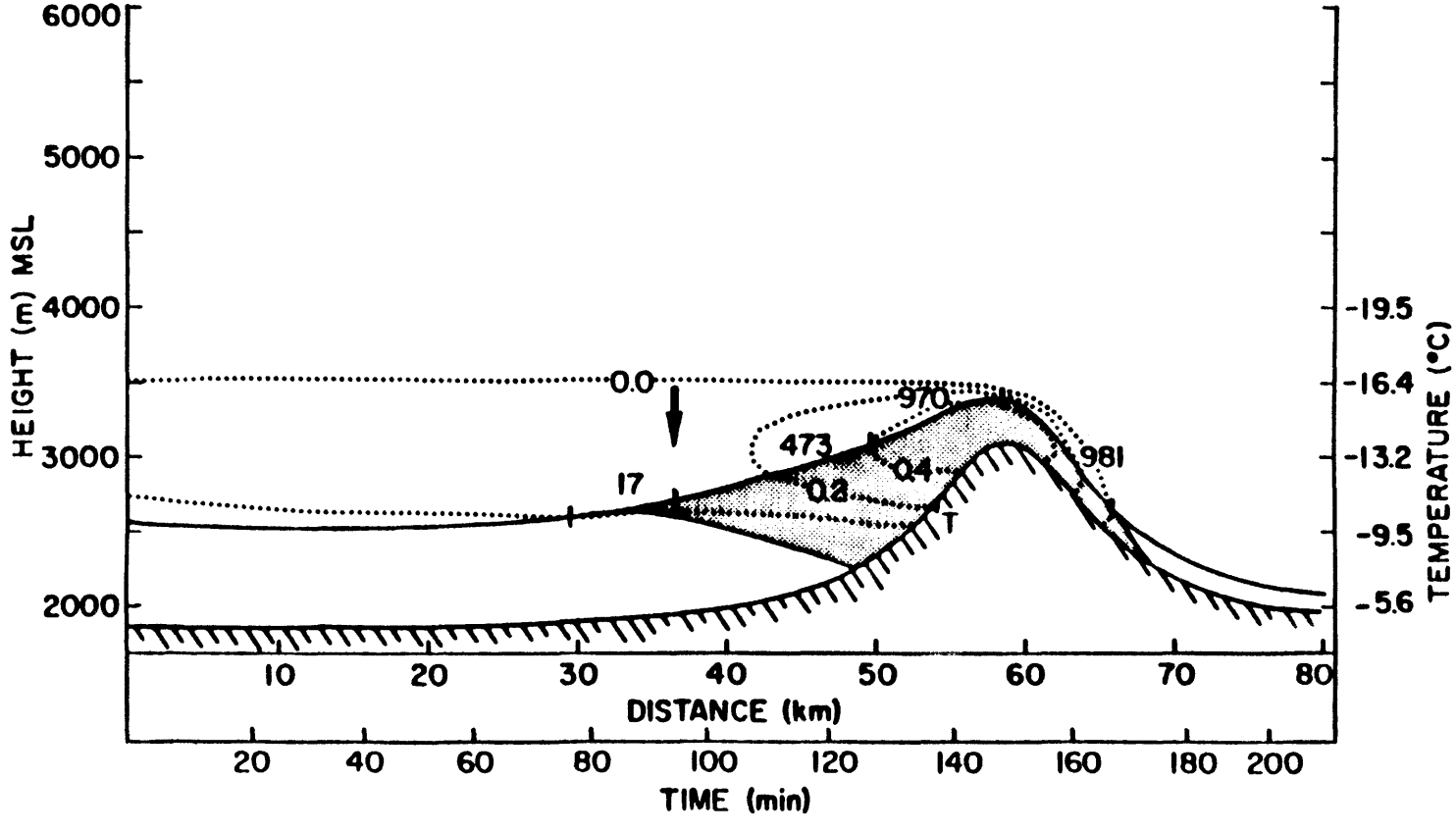

Figure 35: January 12. Slow and fast ice nucleation at -10°C. Numbers over trajectory indicate cumulative number of nucleation events. Arrow and T indicates location of transition between mechanisms. Stipled area shows model predicted ice crystal fallout due to nucleations.

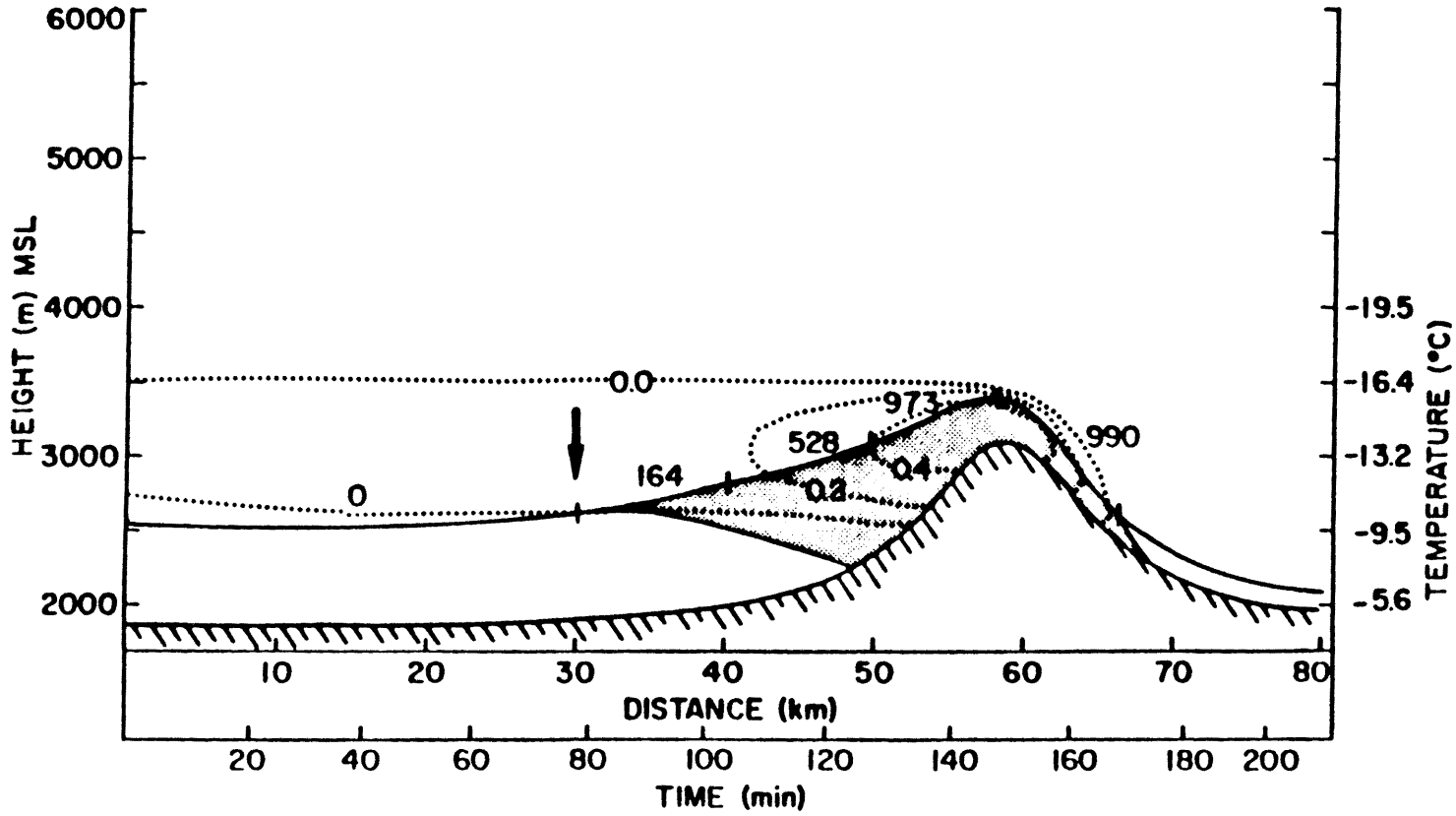

Figure 36: January 12. Fast ice nucleation at $-10^{o}C$. Numbers over trajectory indicate cumulative number of nucleation events. Stipled area shows model predicted ice crystal fallout due to nucleation.

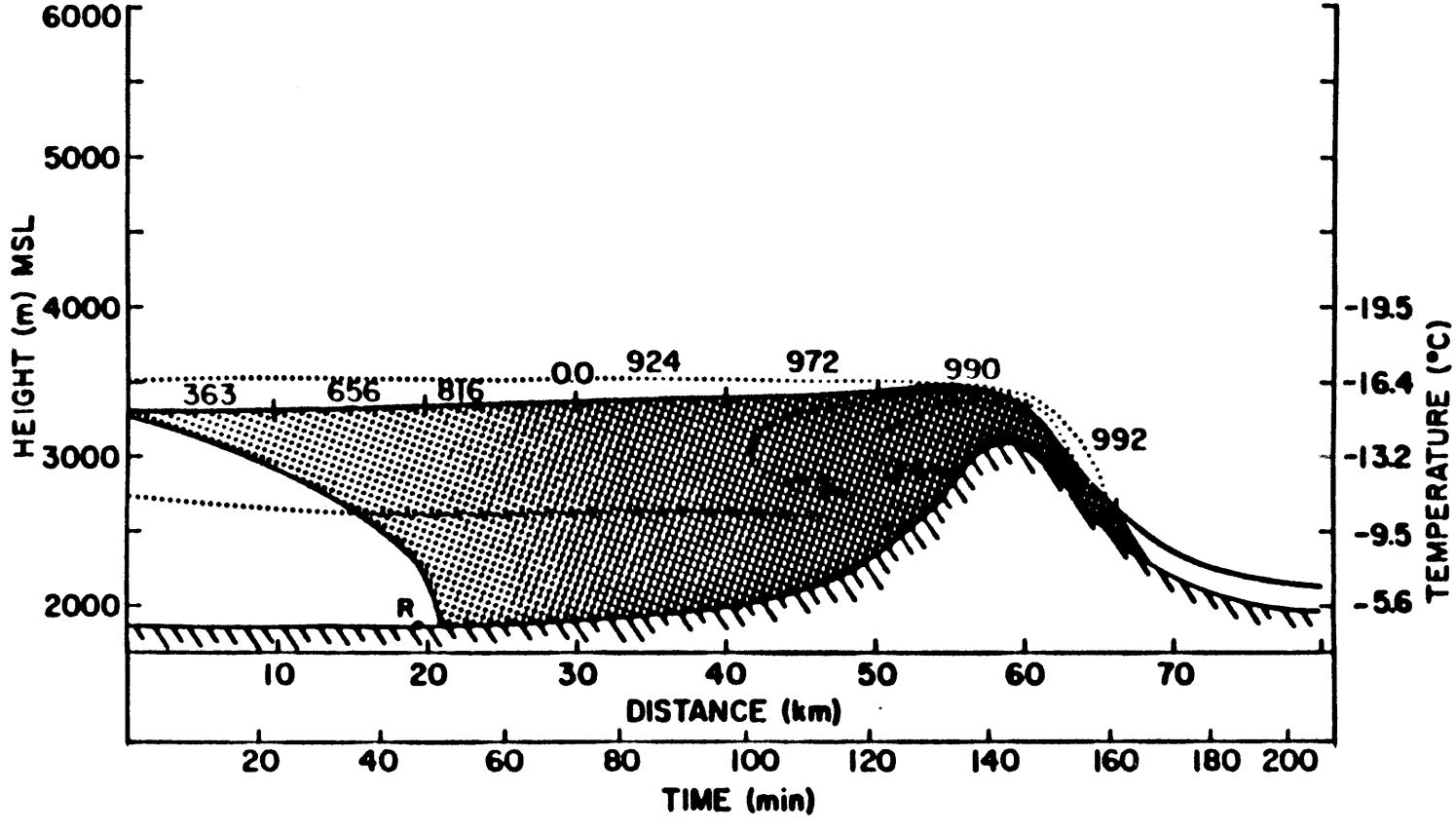

Figure 37: January 12. Slow ice nucleation at -15°C. Numbers over trajectory indicate cumulative number of nucleation events. Stipled area shows model predicted ice crystal fallout due to nucleation. R indicates location of precipitation when riming processes are included.

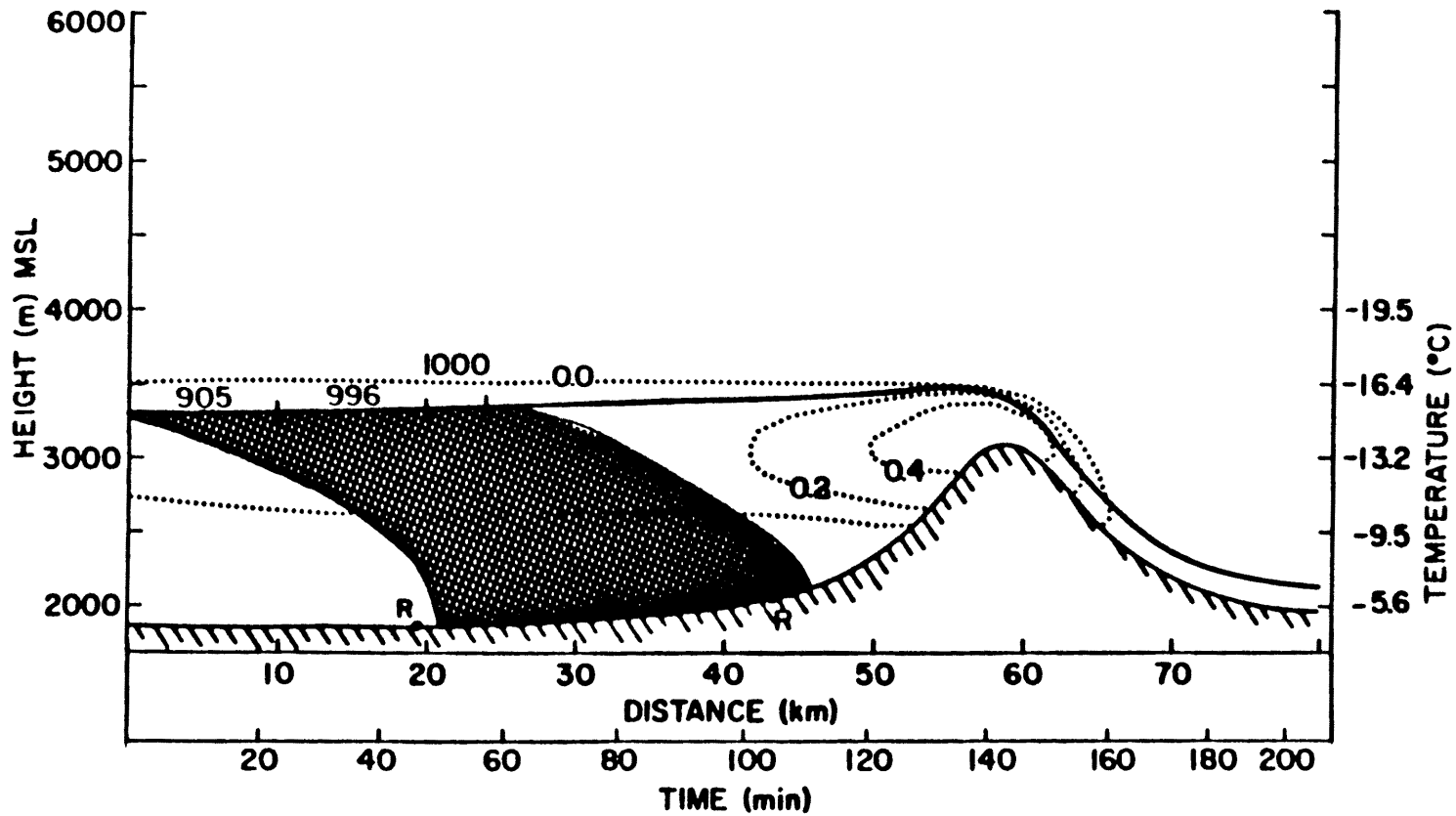

Figure 38: January 12. Fast ice nucleation at -15°C. Numbers over trajectory indicate cumulative number of nucleation events. Stipled area shows model predicted ice crystal fallout due to nucleation. R indicates location of precipitation when riming processes are included.

moderate, so precipitation from seeding is predicted to occur far upwind of the barrier. If supersaturation is large enough to induce the fast mechanism at the point of seeding, fig. 38, nucleation of the entire nucleus population is complete within 24 km. The resulting precipitation from the relatively small zone of nucleation falls well upwind of the barrier.

The shallow cloud system with moderate wind speeds appears to produce the best opportunity for seeding with 2AgI·NaI. Although yield is normally low at -10°C, cloud base seeding is effective because of the low wind speeds which allow sufficient time for nucleation by any mechanism. The mechanism is an important consideration in decisions regarding detection of precipitation enhancement. Comparison of figs. 37 and 38 shows a striking example of how water vapor conditions can alter the rate of nucleation and thus affect the targeting of increased precipitation.

6.2.4 Discussion of Model Experimentation

The extent and location of ice nucleation is controlled by three parameters: 1) nucleation mechanism, 2) cloud temperature, and 3) wind speed. The mechanism of nucleation determines the temporal rate of nucleation which in turn will influence whether ice crystal production occurs for large distances along the seeding trajectory or in a limited location near the barrier crest (compare figs. 37 and 38). The temperature strongly influences yield. For a fast mechanism, yield dominates the extent of nucleation (compare figs. 19, 22, and 24). Wind speed determines the time available for nucleation and thus the distribution of nucleation events along the seeding path (compare figs. 2[illegible] and 37).

VII. SUMMARY AND CONCLUSIONS

7.1 Summary and Conlusions

Ice nucleation by aerosol particles containing 2AgI·NaI has been characterized in a large, isothermal cloud chamber. The methodology of chemical kinetics has been successfully used in the analysis of the laboratory data. The mechanisms by which 2AgI·NaI nucleates the ice phase have been identified. Rates and yield of ice nucleation have been determined as a function of temperature, cloud liquid water content, and cloud water vapor content. Information about the mechanism and kinetics of ice nucleation by 2AgI·NaI has been applied to a theoretical orographic cloud model. The role of nucleation mechanism, rate, and yield on the location and time of nucleation in orographic clouds has been demonstrated. The major results and conclusions which can be drawn concerning ice nucleation by 2AgI·NaI are as follows:

Mechanisms of Ice Nucleation

1) Ice nucleation by 2AgI·NaI aerosol particles at water saturation has been identified as condensation to form dilute solution droplets followed by freezing. The rate of ice crystal production was found to be an exponential, first order rate process with respect to ice nuclei. Corrected nucleation rate constants are on the order of 0.01 min^{-1}. It is proposed that dilute solution droplets form prior to phase change for three reasons:

a) Ice crystal production is characteristically 'slow'. Complete nucleation of the aerosol in the ICC required 20 to 40 minutes. The hygroscopic particles are thus given sufficient time to grow to equilibrium size.

b) The rate of this mechansim is dependent only on temperature. A water vapor concentration dependence was not shown as would be expected of the droplet condensation process.

c) The energy of activation was determined to be $-130 kJmol^{-1}$. A large energy of activation associated with insoluble particles indicates chemical adsorption processes. Chemical reactions of this sort can be expected to occur within the pre-formed droplet containing AgI-NaI.

2) When water vapor is supersaturated with respect to liquid water the mechanism of ice nucleation by 2AgI·NaI is very fast and is believed to be sorption or condensation to aqueous embryos followed by freezing nucleation. The rate of ice crystal production in the ICC by this mechanism was observed to correspond to the rate of ice crystal fallout of naturally settling ice crystals. Fallout is a linear, zero order process. Rate constants are on the order of 10 crystals min^{-1}. Ice crystal fallout is complete within one to four minutes. Nucleation of the crystals must occur before this time. The fast process of aqueous embryo formation for hygroscopic particles may be the controlling, rate determining step for this nucleation process. More information about the mechanism could not be elucidated from the research because it could not

be observed. It is probable the mechanism is first order with respect to nuclei and is dependent on temperature and/or water vapor concentration. An aerosol particle size dependence is suggested by yield increase with increased extent of water supersaturation.

3) Contact ice nucleation was observed to occur for 2AgI·NaI aerosol particles at high cloud droplet concentrations. Contact ice nucleation occurs simultaneously with condensation to droplets followed by freezing. The rate of contact nucleation observed for 2AgI·NaI particles is considerably slower than that for AgI particles. The hygroscopic nature of 2AgI·NaI causes the particles to grow in the saturated environment of the cloud chamber, thus slowing the rate of contact. Also, 2AgI·NaI aerosol particles, too small to nucleate droplets, can contact droplets by Brownian motion. The low concentration of these particles has the effect of slowing the rate of contact.

Application of Ice Nucleation Kinetics to a Theoretical Cloud Model

1) The extent and location of ice nucleation by 2AgI·NaI aerosol particles in modeled orographic clouds is controlled by three parameters: a) nucleation mechanism, b) cloud temperature, and c) wind speed.

   a) The mechanism of ice nucleation determines the temporal rate of ice crystal production. For the case of the condensation to dilute solution droplets followed by freezing mechanism, the temporal rate of ice nucleation is slow. Ice nucelation along an air parcel trajectory may

be prolonged in time and space. In some cases, especially at warmer temperatures, it is possible for a proportion of the aerosol particles to exit the cloud before nucleation can occur because of the slow rate of the mechanism and the limited time available for nucleation. The faster mechanism of sorption or condensation to aqueous embryos followed by freezing generally occurs within shorter times and areas of the cloud.

b) Cloud temperature strongly influences yield or effectivity of ice nucleation. The fast mechanism is dominated by the temperature effect on yield. Ice nucleation by this mechanism most closely resembles past modelling efforts where only yield was considered.

c) Wind speed determines the time available for ice nucleation. Large amounts of the seeding material may be lost from the cloud when high wind speeds reduce the transit time of the nucleant in cloud.

2) The spatial pattern of precipitation has been shown to be affected by the mechanism of ice nucleation. When nucleation is prolonged over large distances, precipitation will also extend over large distances. The location in cloud where ice nucleation may change from the slow to fast mechanism due to an increase in water supersaturation is critical in determining the location of the resultant precipitation. Precipitation may fall in limited locations due to short bursts of nucleation by the fast mechanism. Care must be taken in designing and targeting precipitation enhancement programs.

7.2 Implication for Weather Modification

The kinetic characterization of 2AgI·NaI ice nuclei and particularly the definition of two mechanims of condensation-freezing at water saturation and supersaturation is an important aspect in the physical interpretation of weather modification programs which have utilized the nucleant. The demonstration that kinetic rates and mechanisms can be incorporated into a theoretical cloud model can be an important tool for the physical interpretation of programs that fail or succeed to induce enhanced precipitation.

Many programs have utilized 2AgI·NaI aerosol particles generated from acetone burners for purposes of enhancing precipitaion. The most well known of these are the CLIMAX and Israeli programs, in which statistically significant increases in precipitation were obtained (Mielke, et al., 1981, and Gagin and Neumann, 1981). The CLIMAX progam was a wintertime orographic seeding project. The Israeli program is a wintertime cumulus seeding project. A common factor in both programs is they utilized 2AgI·NaI ice nuclei. An understanding of the exact manner in which the ice nuclei functioned in these clouds, spatially and temporally, may provide an explanation for the observed results.

Another successful weather modification program was the Bridger Range Experiment, conducted in southwestern Montana during the winters of 1969-72 (Super and Heimbach, 1983). During the first year of this program, 2AgI·NaI ice nuclei generated by combustion of acetone solutions was utilized. For the remaining two winters of the program, AgI from acetone solution combustion was used. The program was evaluated statistically for precipitation increases in three concentric zones downwind from the seeding generators. Data obtained from the

'69-'70, 2AgI·NaI season was analyzed separately from data from the '70-'72, AgI season. Precipitation increases were found in all three zones when AgI contact ice nuclei was used. In contrast, increased precipitation was found only in the zone closest to the generators when 2AgI·NaI condensation-freezing ice nuclei were used. It is possible that the air, uplifted by the topography, became supersaturated with respect to water and provided favorable conditions for the fast ice nucleation mechanism to occur. In this case, most of the seeding material would function within a short distance from the mountain range and the resulting precipitation would fall in a zone close to the generators. Further analysis of this program using ice nucleation kinetics specific to the nucleant used may provide information about the physical processes that have caused the observed precipitation increases.

One way of assessing the effect of the ice nucleant on the results of a weather modification program is by incorporating the ice nucleation kinetics of the nucleant into a theoretical model of the clouds that are seeded. The model results presented in this study can be qualitatively related to the CLIMAX experiments. For instance, the model results indicate that when water supersaturations occur near the mountain barrier at relatively warm temperatures near cloud base, a switch in mechanism of 2AgI·NaI ice nucleation can cause an increase in precipitation due to seeding. Applying this concept to the more complex terrain of the Climax area, ice nuclei can travel long distances until they reach zones of high supersaturation associated with the mountain peaks. The fast nucleation process would then produce high concentrations of ice crystals in zones of increased liquid water

content. Subsequent riming and possibly aggregation processes could enduce higher precipitation rates in the CLIMAX target area. It is probably significant that the statistically significant differences in precipitation were obtained only with cases of warm cloud temperatures and moderate winds, conditions that are consistent with the modeling results presentedd here. Similar modeling and incorporation of the kinetics of 2AgI·NaI ice nucleation in cumulus clouds could reveal a physical reason for the effectiveness of the nucleant in the Israeli program.

The modeling of ice nucleation kineitcs can be an important tool in the design of weather modification projects. The mechanisms of other nucleants can be similarly modeled. This type of model can be used to determine the most effective nucleant to use for the particular cloud type and the specific cloud conditions that would be most conducive for nucleation. Also, the system used for detection of precipitation can be better designed if the appoximate location and intensity of seeding effects can be targeted.

7.3 Suggestions for Further Research

The major result of the laboratory work in this study was the delineation of two distinct mechanisms of condensation-freezing ice nucleation by 2AgI·NaI aerosol particles as they occur in water saturated and supersaturated environments. The major result of the theoretical work was the determination of the effect of nucleation rate on ice crystal formation and precipitation due to seeding. Two avenues of further research are needed for a more comprehensive understanding of these results. One is a more thorough characterization of the 2AgI·NaI aerosol system, particularly at water supersaturation. Quantitative

values of supersaturation which are required to induce the fast nucleation mechanism to occur are necessary for a complete characterization of 2AgI·NaI ice nuclei. Secondly, the effect of rates and mechanisms on the nucleation and precipitation patterns of seeded clouds should be investigated, both theoretically and observationally in field experiments.

The mechanism of condensation to droplets followed by freezing has been extensively characterized in this research. Determination of rates at temperatures colder than $-14^{o}C$ would provide useful information. Future research efforts should be concentrated on the characterization of the sorption or condensation to liquid embryos followed by freezing mechanism. An instrument that appears to be well suited for the determination of rates of fast nucleation is the thermal diffusion flow chamber (eg. Rogers, 1982). By operating the flow chamber with varying flow rates, the residence time of the nuclei can be varied, allowing rates to be determined. Additionally, water supersaturation can be accurately controlled to provide information on the order of the rate with respect to water vapor concentration.

The incorporation of rates and mechanisms of nucleation is necessary in both theoretical and field work involving ice crystal production in clouds. Careful consideration of the chemical species will lead to the proper assumption of mechanism. The subsequent use of rate appropriate to the mechanism will elucidate the spatial and temporal nature of the nucleation process. Theoretical modelling work should be done for all mechanisms and seeding materials for which rate information is available including contact, vapor deposition, and condensation-freezing ice nucleation. Various types of cloud systems

should be compared for the effect each mechanism has on it. For instance, a model of ice nucleation by 2AgI·NaI in a cumulus cloud would provide useful information that would aid in the interpretation of results of the Israeli program. Diffusion and entrainment of air parcels contaning seeding material would influence the concentration of the ice nucleant in cumulus cloud models. Knowing the concentration of ice nuclei and the age of the parcel, rates can be established in these models.

Observational work in the field is a vital link between the laboratory characterization and application of the nucleant in weather modification. Laboratory determined rates of ice nucleation must be confirmed in natural cloud. Comparative work, where several nucleants (ie. AgI, 2AgI·NaI, dry ice) are tested in the same cloud or cloud type, would be an excellent method to confirm laboratory determined rates. Both theoretical and observational research of ice nucleation mechanisms is necessasary for accurate design, prediction, and assesment of weather modification results.

VIII. REFERENCES

Atkins, P. W., 1982: Physical Chemistry, 2nd edition, W. H. Freeman, San Francisco, Calif., 1002-1037.

Berry, R. S., S. A. Rice, and J. Ross, 1980: Physical Chemistry, John Wiley and Sons, New York, N. Y., 1117-1260.

Blair, D. N., B. L. Davis, and A. S. Dennis, 1973: Cloud Chamber Tests of Generators Using Acetone Solutions of AgI-NaI, AgI-KI, and AgI-NH_4I. J. Appl. Meteor., 12, 1012-1017.

Burkardt, L. A. and W. G. Finnegan, 1970: Complex Ice Nuclei: The Silver Silver Iodide-Sodium Iodide System. Preprints of the 2nd National Conference on Weather Modification, Santa Barbara, California, April 6-9, 1970, 325-328.

Burkardt, L. A., W. G. Finnegan, and F. K. Odencrantz, 1968: Compositional Effects on Ice Nuclei Activity. Proc. Third Skywater Conf., Feb. 14-16, 1968, 29-38.

Chen, Y., B. L. Davis, and L. R. Johnson, 1972: Simulated Aerosol-Cloud Interaction in the AgI-NaI-H_2O Complexing System. J. Rech. Atmos., 6, 63-77.

Cheng, R. J., 1984: Ice Nucleation of Single Water Droplet by Silver Iodide - A Laboratory Observation. Preprints, Vol. II, 11th International Conference on Atmospheric Aerosols, Condensation, and Ice Nuclei, Budapest, Hungary, Sept. 3-8, 1984, 187.

Davis, B. L., 1969: Chemical Complexing of AgI-NaI Aerosols. J. Atmos. Sci., 26, 1042-1048.

Davis, B. L., 1972: Solubility of Small AgI Paticles in NaI and KI Solutions: Significance to Cloud Seeding. J. Appl. Meteor., 11, 366-369.

Davis, B. L. and R. L. Steele, 1968: Performance Characteristics of Various Artificial Ice Nuclei Sources. J. Appl. Meteor., 7, 667-673.

DeMott, P. J., 1982: A Characterization of Mixed Silver Iodide-Silver Chloride Ice Nuclei. Atmos. Science Paper #349, Colorado State Univerisity, Fort Collins, Colorado.

DeMott, P. J., W. G. Finnegan, and L. O. Grant, 1983: An Application of Chemical Kinetic Theory and Methodology to Characterize the Ice Nucleating Properties of Aerosols Used for Weather Modification. J. Climate Appl. Meteor., 22, 1190-1203.

DeMott, P. J., R. M. Rauber, and L. O. Grant, 1985: Ice Nucleation in Wintertime Orographic Cloud Systems. J. Atmos. Sci., accepted for publication.

Dennis, A. S., 1980: Weather Modification by Cloud Seeding. Academic Press, New York, N. Y., pp. 267.

dePena, R. G. and E. A. Caimi, 1967: Hygroscopisity and Chemical Composition of Silver Iodide Smoke Used in Cloud Seeding Experiments. J. Atmos. Sci., 24, 383-386.

Donnan, J. A., D. N. Blair, W. G. Finnegan, and P. St.-Amand, 1970: Nucleation Efficiencies of AgI-NH_4I and AgI-NaI Acetone Solutions and Pyrotechnic Generators as a Function of LWC and Generator Flame Temperature, A Preliminary Report. J. Wea. Mod., 2, 155-164.

Dundon, M. L. and E. Mack, Jr., 1923: The Solubility and Surface Energy of Calcium Sulfate. J. Amer. Chem. Soc., 45, 2479-2485.

Edwards, G. R. and L. F. Evans, 1960: Ice Nucleation by Silver Iodide: I. Freezing vs. Sublimation. J. Meteor., 17, 627-634.

Edwards, G. R., L. F. Evans, and V. K. LaMer, 1962: Ice Nucleation by Monodisperse Silver Iodide Prticles. J. Colloid Sci., 17, 749-758.

Esperson, J. H., 1981: Chemical Kinetics and Reaction Mechanisms. McGraw-Hill, New York, N. Y., pp. 218.

Fletcher, N. H., 1958: Time Lag in Ice Crystal Nucleation in the Atmosphere. Bull. Obs. Puy de Dome, 1, 11-18.

Fletcher, N. H., 1959: On Ice-Crystal Production by Aerosol Particles. J. Meteor., 16, 173-180.

Fletcher, N. H., 1968: Ice Nucleation Behavior of Silver Iodide Smokes Containing a Soluble Component. J. Atmos. Sci., 25, 1058-1060.

Fletcher, N. H., 1969: Active Sites and Ice Crystal Nucleation. J. Atmos. Sci., 26, 1266-1271.

Fukuta, N., 1969: Experimental Studies on the Growth of Small Ice Crystals. J. Atmos. Sci., 26, 522-531.

Fukuta, N. and R. C. Schaller, 1982: Ice Nucleation by Aerosol Particles: Theory of Condensation-Freezing Nucleation. J. Atmos. Sci., 39, 648-655.

Fukuta, N. and L. A. Walter, 1970: Kinetics of Hydrometeor Growth from a Vapor-Spherical Model. J. Atmos. Sci., 27, 1160-1172.

Gagin, A. and J. Neumann, 1981: The Second Israeli Randomized Cloud Seeding Experiment: Evaluation of the Results. J. Appl. Meteor., 20, 1301-1311.

Garvey, D. M., 1975: Testing of Cloud Seeding Materials at the Cloud Simulation and Aerosol Laboratory, 1971-1973. J. Appl. Meteor., 14, 883-890.

Garvey, D. M., L. E. Lilie, T. C. Grove, and L. O. Grant, 1976: Determination of the Rates of Ice Crystal Formation in Two Large Cloud Chambers. Preprints, International Conference on Cloud Physics, Boulder, CO, Amer. Meteor. Soc., 121-125.

Grant, L. O., J. O. Rhea, G. T. Maltesen, G. J. Mulvey, and P. W. Mielke, Jr., 1979: Continuing Analysis of the Climax Weather Modification Experiments. Preprints of the Seventh Conference on Inadvertent and Planned Weather Modification, Banff, Alberta, October 8-12, 1979, J43-J45.

Grant, L. O. and R. L. Steele, 1966: The Calibration of Silver Iodide Generators. Bull. Amer. Meteor. Soc., 47, 713-717.

Hobbs, P. V., R. C. Easter, and A. B. Fraser, 1973: A Theoretical Study of Air and Fallout of Solid Precipitation Over Mountainous Terrain: Part II. Microphysics. J. Atmos. Sci., 30, 813-823.

Horn, R. D., W. G. Finnegan, and P. J. DeMott, 1982: Experimental Studies of Nucleation by Dry Ice. J. Appl. Meteor., 21, 1567-1570.

Johnson, L. R. and B. L. Davis, 1972: Examination of the Solid Phase in the System AgI-NaI-H_2O. J. Appl. Crystall., 5, 194-200.

Langer, G., G. Cooper, C. T. Nagamota, and J. Rosinski, 1978: Ice Nucleation Mechanisms of Submicron Monodispersed Silver Iodide, 1,5-Dihydroxynaphtalene and Phloroglucinol Aerosol Particles. J. Appl. Meteor., 17, 1039-1048.

Mason, B. J. and J. Hallett, 1956: Artificial Ice-forming Nuclei. Nature, 177, 681-683.

Mielke, P. W., Jr., G. W. Brier, L. O. Grant, G. J. Mulvey, and P. N. Rosenzweig, 1981: A Statistical Reanalysis of the Replicated Climax I and II Wintertime Orographic Cloud Seeding Experiments. J. Appl. Meteor., 20, 643-659.

Moore, W. J., 1972: Physical Chemistry. Prentice Hall, Inc., Englewood Cliffs, N. J., 324-347.

Morrison, B. J., W. G. Finnegan, R. D. Horn, and L. O. Grant, 1983; CSU Sim Lab Dry Ice Pellet Experiments. Interim Report to Simpson Weather Associates, Charlottesville, Virginia, November, 31 pp.

Mossop, S. C., 1968: Silver Iodide as Nucleus for Water Condensation and Crystallization. J. Rech. Atmos., 3, 185-190.

Mossop, S. C. and K. O. L. F. Jayaweera, 1969: AgI-NaI Aerosols as Ice Nuclei. J. Appl. Meteor., 8, 241-248.

Mossop, S. C. and C. Tuck-Lee, 1968: The Composition and Size Distribution of Aerosols Produced by Burning Solutions of AgI and NaI in Acetone. J. Appl. Meteor., 7, 234-240.

Plooster, M. N. and N. Fukuta, 1975: A Numerical Model of Precipitation from Seeded and Unseeded Cold Orographic Clouds. J. Appl. Meteor., 14, 859-867.

Pruppacher, H. R. and J. D. Klett, 1978: Microphyics of Clouds and Precipitation. D. Reidel Publishing Co., Boston, Mass. pp 714.

Rauber, R. M., 1981: Microphysical Processes in Two Stably Stratified Orographic Cloud Systems. Atmos. Science Paper #337, Colorado State University, Fort Collins, Colorado.

Reiss, H., 1982: Common Problems in Nucleation and Growth, Chemical Kinetics, and Catalysis. Heterogeneous Atmospheric Chemistry, Geophys. Monogr. Ser., No. 26, Amer. Geophys. Union, 2-5.

Rilling, R. R., R. R. Blumenstein, W. G. Finnegan, and L. O. Grant, 1984: Characterization of Silver Iodide-Potassium Iodide Ice Nuclei: Rates and Mechanisms, and Comparison to the Silver Iodide-Sodium Iodide System. Preprints of the Ninth Conference on Weather Modification, Park City, Utah, May 21-23, 1984, 16-17.

Rogers, D. C., 1982: Field and Laboratory Studies of Ice Nucleation in Winter Orographic Clouds. Ph.D. Dissertation, Department of Atmospheric Science, University of Wyoming, Laramie, Wyoming.

Smith, E. J. and K. J. Heffernan, 1954: Airborne Measurements of the Concentration of Natural and Artificial Freezing Nuclei. Quart. J. R. Met. Soc., 80, 182-197.

Smith, E. J., J. A. Warburton, K. J. Heffenan, and W. J. Thompson, 1966: Performance Measurements of Silver Iodide Smoke Generators on Aircraft. J. Appl. Meteor., 5, 292-295.

St.-Amand, P., W. G. Finnegan, and L. Burkardt, 1971: Understanding of the Use of Simple and Complex Ice Nuclei Generated from Pyrotechnics and Acetone Burners. J. Wea. Mod., 3, 31-48.

St. Louis, P. T. and R. L. Steele, 1968: Certain Environmental Effects on Silver Iodide Ice Nuclei. Proc. International Conf. on Cloud Physics. Toronto, Aug. 26-30, 1968, 178-182.

Super, A. B. and J. A. Heimbach, Jr., 1983: Evaluation of the Bridger Range Winter Cloud Seeding Experiment Using Control Gages. J. Climate Appl. Meteor., 22, 1989-2011.

Tompkins, L. M., D. A. Muss, and T. Pearson, 1963: Water Adsorption in the System AgI-KI-H_2O. J. Geophs. Res., 68, 3537-3539.

Turnbull, D. and B. Vonnegut, 1952: Nucleation Catalysis. Ind. and Eng. Chem., 44, 1292-1298.

Vonnegut, B., 1947: The Nucleation of Ice Formation by Silver Iodide. J. Appl. Phys., 18, 593-595.

Vonnegut, B., 1949: Nucleation of Supercooled Water by Silver Iodide Smokes. Chem. Rev., 44, 277-289.

Vonnegut, B., 1950: Techniques for Generating Silver Iodide Smoke. J. Colloid Sci., 5, 37-48.

Vonnegut, B., 1957: Early Work on Silver Iodide Smokes for Cloud Seeding. Final Report of the Advisory Committee on Weather Modification, 2, 283-285.

Warburton, J. A. and K. J. Heffernan, 1964: Time Lag in Ice Crystal Nucleation by Silver Iodide. J. Appl. Meteor., 3, 788-791.

Warner, J., 1957: An Instrument for the Measurement of Freezing Nucleus Concentration. Bull. Obs. Puy de Dome, 2, 33-46.

Young, K. C., 1974a: A Numerical Simulation of Wintertime, Orographic Precipitation: Part I. Description of Model Microphysics and Numerical Techniques. J. Atmos. Sci., 31, 1735-1748.

Young, K. C., 1974b: A Numerical Simulation of Wintertime, Orographic Precipitation: Part II. Comparison of Natural and AgI-Seeded Conditions. J. Atmos. Sci., 31, 1749-1767.